Precipitation of nickel and cobalt sulphides using different reactor configurations

Ashton Mark Swartbooi

A thesis submitted for the degree of MSc (Chemical Engineering) to the University of Cape Town

"I know the meaning of plagiarism and declare that all the work in the document, save for that which is properly acknowledged, is my own".

Executive summary

The nickel reduction process produces a stream containing unreacted dissolved nickel and cobalt. Removal of these metals to optimum levels is desired, however, the product should also be easy to handle and the process easy to incorporate into the current system.

There are various precipitation agents that can be used to remove metals from solution, these being hydroxide, carbonates or sulphides. Sulphide precipitation has been gaining increased attention because of the advantages it holds above the other methods. These include:

- attainment of high degree of metal removal over a broad pH range
- effective removal of metals such as As, Cu and Hg even at low pH
- low retention time required in the reaction tank because of high reactivity
- feasibility of selective metal recovery

There are various methods of introducing the sulphide into the system as well, with a soluble sulphide source most commonly used. The problem with this, and coupled to the high reactivity of the sulphide ion, is the creation of high local supersaturation.

The supersaturation governs all precipitation and crystallisation processes in the way that it features in nucleation and growth rates. In crystallisation processes, the supersaturation can easily be controlled by thermal methods of evaporation or cooling. However, in precipitation, the creation of supersaturation is by a reaction, which commonly leads to high supersaturation. Thus, to obtain a product that has good filterability and settling ability, methods for controlling the supersaturation in precipitation reactions needs to be investigated.

Apart from investigating metal removal in this thesis, investigations into the methods of sulphide addition were also looked at, as well as reactor configurations.

The addition of a gaseous sulphide source adds a limiting factor to the reaction kinetics, that of gas diffusion into the liquid medium. The control of the pH of said liquid media provides a method of controlling the supersaturation for a precipitation reaction, due to the sulphide chemistry and speciation (both well understood) involved. The end result is a sulphide product of good quality.

Reactor configurations were also investigated and tested. Batch experiments provided a means for characterising the system. The use of a fluidised bed reactor has been successfully tested for the removal of $NiCO_3$ previously at the university (Guillard (2001)) as well as copper using a sulphide stream (Peterson (2002)). However, both of these tests were conducted at low concentrations.

Testing in the fluidised bed reactor proved not to be successful for this investigation. The high metal concentrations encountered lead to the formation of particulate fines that could not be removed from solution. This was also one of the reasons for using an alternative sulphide source.

Methods for using gaseous hydrogen sulphide exist in literature, mostly for systems in the biological treatment of AMD. Sulphate reducing bacteria produce soluble sulphide that performs two functions in treating AMD: sulphate removal as well as metal removal through sulphide precipitation. SRB treatment however treats an effluent stream and is also not useful inline or under process conditions.

The method was thus adapted to treat high concentrations using a cylinder containing a mixture of H_2S and N_2. This proved successful in both removal efficiency as well as settling rates.

Results

Batch testing was done using a soluble sulphide source. The results indicated that high metal removal rates were possible. However, it could not be understood why, at a sulphide:metal ratio of 1:1, higher removals could not be achieved.

The first assumption was the loss of sulphide to the open air just above the vessels in which the experiments were conducted. However, no real sulphide was smelt during the experiments.

A second test using 20% excess sulphide provided a better insight. Again no sulphide was detected above the reaction vessel, and testing of the aqueous media showed no real significant sulphide in solution. This lead to the hypothesis that a poly-sulphide species (aqueous or solid) was formed. Such a poly-sulphide species has been reported by van Hille (2005) in his work on copper sulphide precipitation. However, no real comparative study could be found for nickel and/or cobalt.

Testing in a fluidised bed reactor again showed that effective metal removal could be achieved, however, particulate fines were formed and could not be removed from the solution. Result for one test is shown in the figure below:

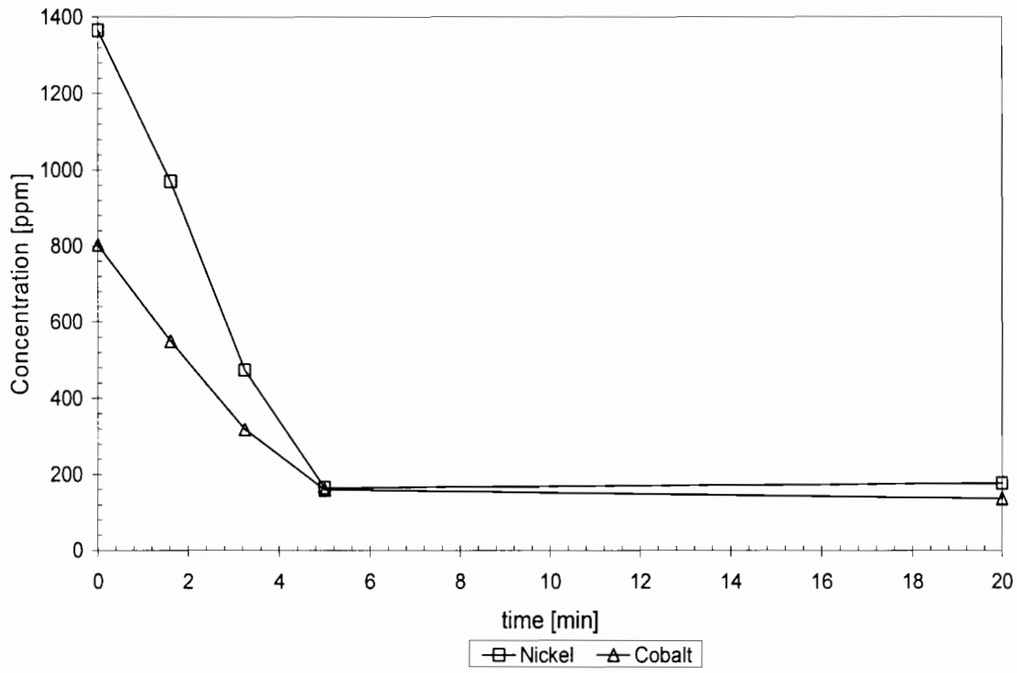

Figure 1: Metal conversion vs. time in a fluidised bed reactor

Further testing to remove the fines from solution proved fruitless, and it was hypothesised that attrition played the biggest role in the fines formation due to the rigorous mixing inside the reactor. This has also been the case for nickel carbonate precipitation in a fluidised bed (Taty-Costodes et al, 2004).

Tests using biologically produced H_2S were conducted to prove that a system using H_2S could be more efficient than the liquid sulphide system. Initial test were conducted at low initial concentrations because of the limitation on the size of the SRB and the H_2S produced. Results are shown below:

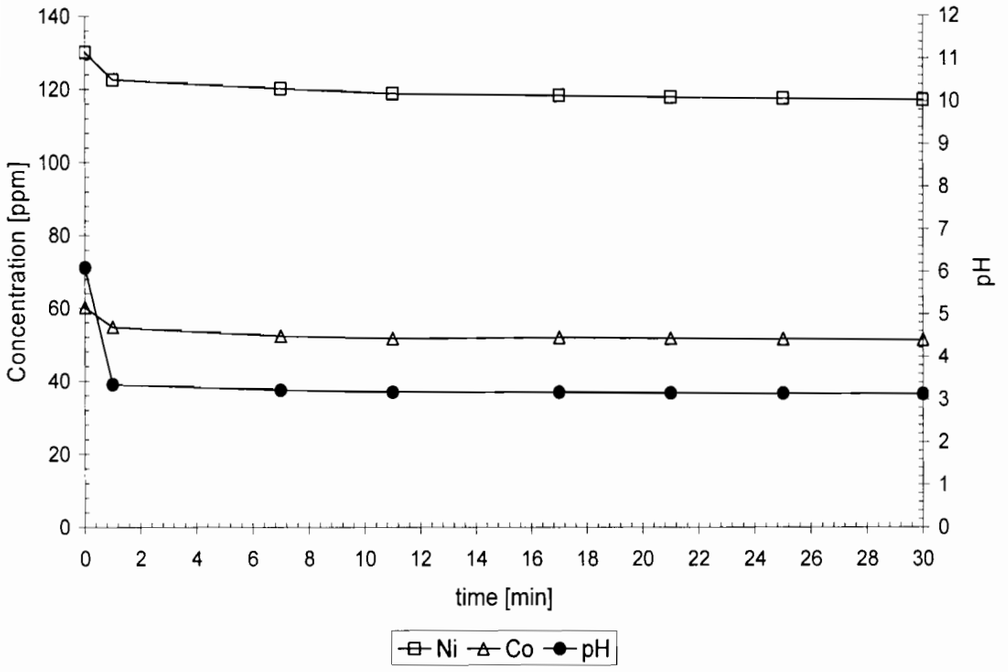

Figure 2: Experimental results using SRB (low pH)

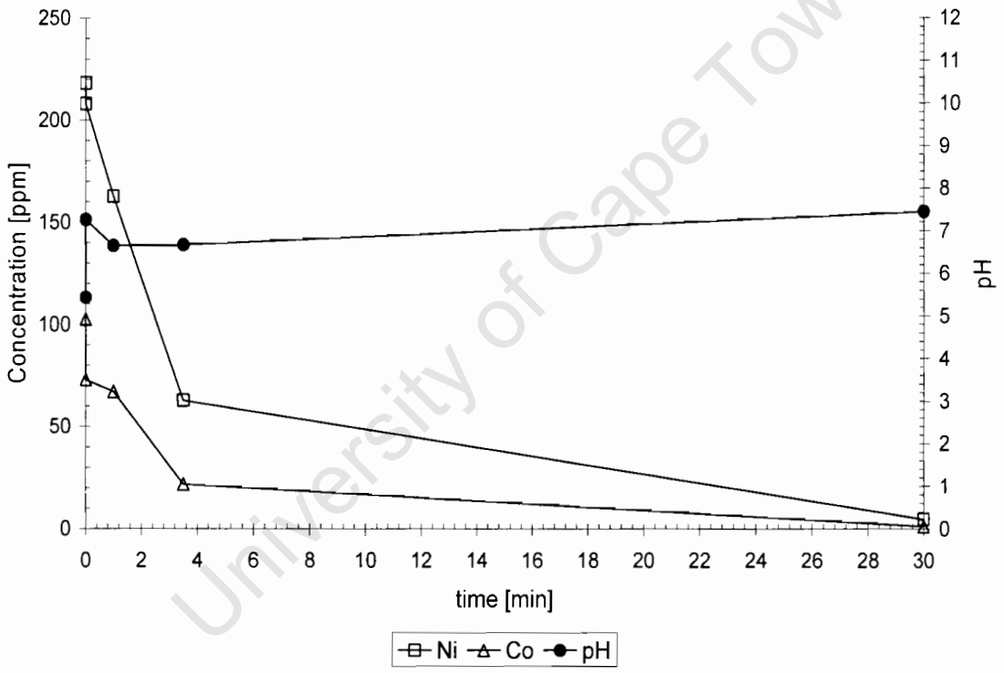

Figure 3: Experimental results using SRB (neutral pH)

From the figures, it was observed that pH was an important factor and for subsequent tests, a pH control was installed for the tests conducted using the gas mixture from the cylinder.

From the figure below it is observed that the removal of metals exceed the target limits within 30 minutes of operation.

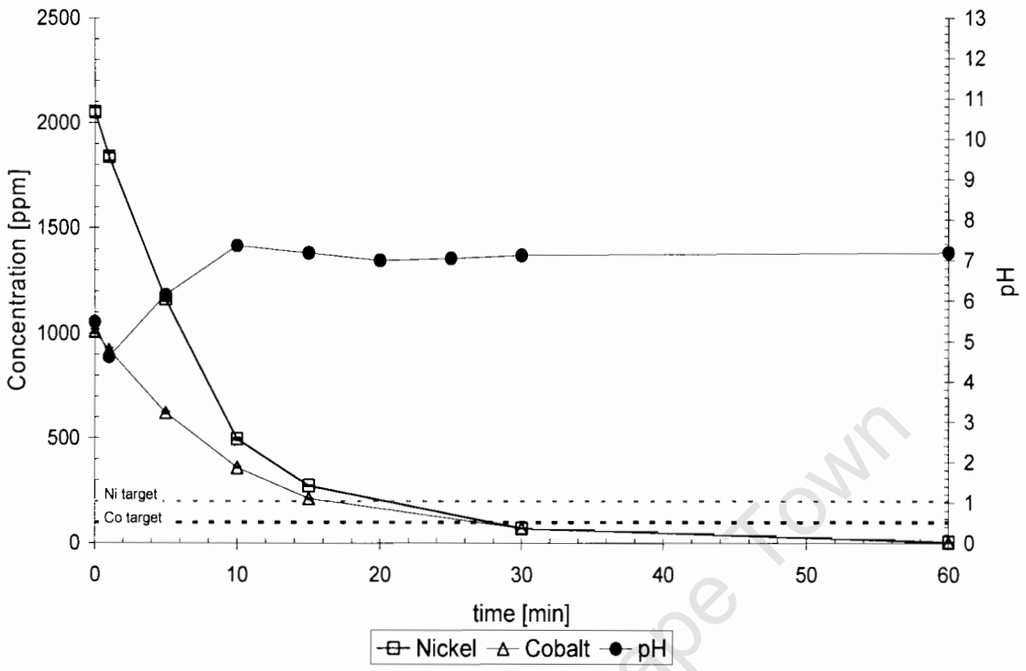

Figure 4: Results using a 10% H_2S mixture

Using the data obtained the kinetics of the precipitation reactions were calculated. It was discovered that the kinetics of nickel precipitation were significantly higher than that of cobalt, even though the cobalt sulphide has a lower solubility product than nickel sulphide. This could be explained by the findings of Bryson and Bijsterveld (1991) in their study of a manganese and cobalt system.

They discovered that cobalt exhibited an induction time before precipitation and that the precipitation was also catalysed by previously formed sulphides. Thus for

the case of the nickel-cobalt system, it would be expected that the nickel sulphide would act as the catalyst for the cobalt sulphide precipitation.

Conclusions

- Sulphide precipitation have very high nucleation rates and fines formation
- Sulphide precipitation fairs better than hydroxide or carbonate precipitation
- The use of a fluidised bed reactor is limited
- The sulphide source is important for supersaturation
- Gaseous sulphide is better for sulphide precipitation

From the results obtained and conclusions drawn, recommendations for any future work are also included:

- Future testing should include measurements of the PSD to quantify the aggregation rate for the fluidised bed reactor
- A reactor configuration could be tested that allows enough time for particle settling when using the gaseous system (e.g. a tapered reactor) or an alternative system that has a settling tank following the reactor.

Table of Contents

List of Figures

List of Tables

Chapter 5

Chapter 6

Nomenclature

α	Geometric factor that depends on the shape of the crystal
β_0	size-independent part of the aggregation kernel (m^{-3}/s)
$\bar{\gamma}$	Interfacial energy (assumed to be independent of cluster size) (J/m^2)
σ	Absolute or relative supersaturation
ν	Number of moles of ions in 1 mole of salt (mol)
γ	Activity coefficient
$\Delta\mu$	Driving force (J/mol)
μ_1	Chemical potential in crystal state (J/mol)
μ_2	Chemical potential in supersaturated state (J/mol)
δ	Length of the diffusion path (m)
η	Absolute viscosity (m^2/s)
ΔC	Concentration driving force (mol/l)
ΔG_{bulk}	bulk excess free energy (J)
ΔG_{surf}	surface excess free energy (J)
$[Me^{2+}]$	metal concentration at time t (mol/l)
$[Me^{2+}]_0$	initial metal concentration (mol/l)
$[S^{2-}]$	sulphide concentration at time t (mol/l)
$[S^{2-}]_0$	initial sulphide concentration (mol/l)
A	factor related to the efficiency of collisions of ions or molecules
a	Activity (mol/l)
A	concentration of species A (mol/l)
A	surface area of the crystal (m^2)
a^*	activity of a saturated solution (mol/l)
A_b	gas-liquid interfacial area (m^2)
B	concentration of species B (mol/l)
B_u	Source function ($m^{-3}.s^{-1}$)

c solute concentration in the solution (supersaturated)

C Solution concentration (mol/l)

C^* Equilibrium concentration (mol/l)

c^* equilibrium saturation concentration (mol/l)

C^0_{H2S} interfacial concentration of H_2S in the liquid (kg/m)

C^0_{MeSO4} initial concentration of $MeSO_4$ (kg/m)

c_i solute concentration in the solution at the crystal-solution interface (mol/l)

C_{MeSO4} concentration of $MeSO_4$ at time t (kg/m)

D Brownian diffusion coefficient (cm^2/s)

D coefficient of diffusion of the solute

d particle diameter (cm)

D_A diffusion coefficient of species A (m^2/s)

D_{H2S} diffusion coefficient of hydrogen sulphide (m^2/s)

g acceleration due to gravity (m/s)

G gas-flow rate (l/s)

G mean velocity gradient ($time^{-1}$)

G growth rate (m/s)

h height of the liquid phase (m)

IAP Ion activity product (mol/l)

j number of molecular units in the nucleus (-)

J number of nuclei formed per unit time per unit volume ($\#s^{-1}m^{-3}$)

k Boltzmann constant ($1.3805x10^{-23}$ JK^{-1})

k_2 second order rate constant

K_a Activity solubility product of the salt (mol/l)

k_d coefficient of mass transfer by diffusion

k_L gas-liquid mass transfer coefficient ($m.s^{-1}$)

k_m coefficient of mass transfer

k_r a rate constant for the surface reaction (integration)

m mass of solid deposited in time t (kg)

n number of bubbles per second ($\#.s^{-1}$)

N_A Avogadro number ($6x10^{23}mol^{-1}$)

r	equivalent radius of bubbles (m)
R	Gas constant (J/mol.K)
S	Supersaturation ratio
T	Temperature (K)
t_c	surface renewal time (s)
V	volume of liquid phase (m^3)
v_∞	rising velocity of the bubbles (m/s)
V_M	molar volume of the solid phase (m^3)

Abbreviations used in this text

AAS	Atomic Absorption Spectrometry
AMD	Acid Mine Drainage
PSD	Particle Size Distribution
SRB	Sulphate Reducing Bacteria

Chapter 1

Introduction

Industrially it is desired to operate processes at conditions that maximise yield and recovery. Most process optimisation controls the operating conditions at which the reactions occur, e.g. temperature and pressure for catalytic processes. For processes like crystallisation and especially precipitation however, primary focus is on growing particles that could easily be separated from solution; this involves particles that are easy to filter.

Chemical reactions require a driving force which exploits certain characteristics of the desired product. For processes like precipitation, the driving force is the difference between the theoretical solubility and that of the actual species in solution. This is termed supersaturation. For crystallisation processes, supersaturation is usually achieved by a change in temperature, i.e. heating or cooling. Precipitation processes, however, achieve supersaturation by the chemical reaction of two or more species. Because of the usually very low solubility and almost instantaneous reaction supersaturations are usually high, and control in precipitation processes is very difficult. The importance of supersaturation to precipitation is discussed in chapters that follow.

The nickel reduction process produces a stream containing unreacted dissolved nickel and cobalt. Removal of these metals to optimum levels is desired, however, the product should also be easy to handle and the process easy to incorporate into the current system. In general, in precipitation processes, optimisation of the product in terms of particle size is difficult to achieve.

Focus on metal precipitation

Although various methods exist for metal recovery/removal, this thesis will focus on metal precipitation, and especially sulphide precipitation. The use of sulphide as a precipitant has been receiving increased attention, because of the reactivity of the sulphide ion.

Peters *et al* (1998) suggested the use of sulphide precipitation as a viable method for the removal of heavy metals from waste water as it is a more effective process compared to hydroxide precipitation. Sulphide precipitation achieves a high degree of metal removal due to low solubilities of the product over a broad pH range as well as fast reaction times. Sulphide precipitates exhibit less of an amphoteric nature than hydroxide precipitates and have less of a tendency to re-dissolve (McAnally *et al*, 1983). Bhattacharyya (1981) also showed that sulphide precipitates produced denser sludges than hydroxides. The attractive feature of using sulphide precipitation for heavy metal removal is also in the fact that the precipitated metal can be recovered in common smelters.

Different methods of sulphide addition exist, with a liquid, soluble sulphide, e.g. sodium sulphide, used most commonly. However, because of the low solubility of the sulphide precipitate coupled with the high reactivity of the sulphide ion, instantly high local supersaturation is encountered. Although high supersaturation favours a large driving force, product quality is usually negatively affected.

Apart from investigating base metal removal through sulphide, this thesis also discusses the importance of the sulphide source, especially for high concentration process streams. The initial processes by the authors mentioned previously have been proven to effectively remove heavy metals, usually for process waste streams and thus at lower concentrations.

Many of the researchers used an aqueous sulphide stream for precipitation. Other methods of sulphide introduction are not widely reported in literature, apart from biological systems. Oktaybas *et al.* (1994) used gaseous hydrogen

sulphide to study the kinetics of copper removal through sulphide precipitation.

Passive treatment of aqueous waste streams, especially ones high in sulphates, usually involves biological treatment. Sulphate reducing bacteria (SRB), in reducing sulphates to sulphides, effectively introduce sulphide into the system thus precipitating the metals from solution. This system also works well for waste streams where metal concentrations are moderately low. At process conditions however, metal inhibition occurs and the bacteria become ineffective.

Objectives

This thesis investigates the factors that optimise the removal of nickel and cobalt from a synthetic aqueous steam. In the removal of the base metals, the following key questions will be addressed:

i. What are the factors affecting base metal removal?
ii. How does supersaturation affect the product quality?
iii. Does a gaseous sulphide source greatly affect the removal efficiency and quality?

Removal efficiency will be determined from the aqueous concentrations of the metals remaining in solution, while the product quality will be assessed by particle size and filterability.

Scope

The main discussion in this thesis focuses on the removal of nickel and cobalt from a synthetic aqueous stream by precipitation. However, the chapters preceding the results focus on the theory of precipitation and mechanisms involved in particle growth. *Chapter 2* introduces supersaturation and how it affects nucleation, particle growth and agglomeration.

Chapter 3 will discuss the sulphide chemistry, as well as the speciation of the sulphide and metal species. It will also discuss the advantages of the sulphide precipitates over the more common hydroxide precipitates.

Chapter 4 will discuss the transport phenomena of diffusion and gas-liquid mass transfer and its rate-limitation on the precipitation reaction.

Chapter 5 discusses the experimental set-up used in this research. It also focuses on each set-up investigated and discusses some of the problems experienced with each.

Chapter 6 presents results and discussions, with relevant conclusions and or recommendations following in *chapter 7*.

Chapter 2

Theory

2. Introduction to precipitation theory

Precipitation has been defined as fast crystallisation (Söhnel and Garside, 1992). Whilst crystallisation occurs by controlled cooling or evaporation when the solute exceeds its solubility; in precipitation, however, the product is formed by a chemical reaction and the precipitate is generally sparingly soluble in the solvent (Kind, 1999).

Once the concentration of a solute exceeds its solubility, the solution is deemed to be supersaturated. With controlled cooling or evaporation for crystallisation, a controlled supersaturation can be achieved. For precipitation processes, controlling the generation of supersaturation is often a challenge.

The following chapter discusses, in detail, the concepts of supersaturation and the particle rate processes that it influences regarding particle formation, i.e. nucleation, crystal growth and agglomeration.

2.1 Defining supersaturation

Like all reactions, a thermodynamic driving force is required, supersaturation being the driving force for precipitation processes. Supersaturation can be described as the distance, or departure from the more favoured equilibrium concentrations. Literature reports different definitions of supersaturation, with each derived from the other. These terms are the supersaturation ratio, S, or a quantity referred to as the relative supersaturation, σ.

$$\Delta C = C - C^{*} \qquad (2\text{-}1)$$

$$S = C / C^{*} \qquad (2\text{-}2)$$

$$\sigma = \Delta C / C^* = S - 1 \quad (2\text{-}3)$$

ΔC = Concentration driving force (mol/l)

C = Solution concentration (mol/l)

C^* = Equilibrium concentration (mol/l)

S = Supersaturation ratio

σ = Absolute or relative supersaturation

The supersaturation ratio can be linked to the chemical potential as derived below. For crystallisation, the chemical potential, as a driving force, can be written as:

$$\Delta\mu = \mu_2 - \mu_1 \quad (2\text{-}4)$$

$\Delta\mu$ = Driving force (J/mol)

μ_1 = Chemical potential in crystal state (J/mol)

μ_2 = Chemical potential in supersaturated state (J/mol)

The chemical potential in each state can be defined as:

$$\mu = \mu_0 + RT \ln a \quad (2\text{-}5)$$

R = Gas constant (J/mol.K)

T = Temperature (K)

a = Activity (mol/l)

The activity of each species can be redefined in terms of the product of its concentration and a dimensionless activity coefficient

$$a = \gamma C \text{ (mol/l)} \quad (2\text{-}6)$$

γ =Activity coefficient

Rewriting equation (2-5) and introducing a ratio between the activities of the supersaturated solution to that of a saturated solution (equilibrium):

$$\Delta\mu / RT = \ln(a / a^{*}) = \ln S \qquad (2\text{-}7)$$

a^{*} = activity of a saturated solution (mol/l)

More commonly, researchers tend to normalise the definition of the supersaturation. Mullin (2001) defines the supersaturation for a sparingly soluble electrolyte in terms of its ion activity product and solubility product

$$S = (IAP / K_a)^{(1/\nu)} \qquad (2\text{-}8)$$

IAP = Ion activity product (mol/l)
K_a = Activity solubility product of the salt (mol/l)
ν = Number of moles of ions in 1 mole of salt (mol)

This definition relates directly to that of equation (2-7) in that the ion activity product can be defined as

$$IAP = a_{+}a_{-} = \gamma_{+}C_{+}\gamma_{-}C_{-} \qquad (2\text{-}9)$$

The K_a is defined similarly, but with equilibrium concentrations. For crystallites and commonly found precipitates, K_a is termed the solubility product, K_{sp}, and values for this equilibrium constant can be found in numerous literature tables.

According to Söhnel and Garside (1992), the crystallisation of sparingly soluble substances is usually the result of three kinetic processes:

(i) crystal nucleation
(ii) crystal growth
(iii) secondary changes in the resulting crystal suspension by, for example, agglomeration and ageing.

They have found that, depending on reaction conditions, these processes can proceed either in series or simultaneously (in parallel). Each of these processes will be discussed in the following chapters.

2.2 The Kinetics of Precipitation

2.2.1 Nucleation

Nucleation can be described as the kinetic step that allows a solid to be formed from the bulk liquid.

Nucleation corresponds to the formation of the new centres from which spontaneous growth can occur. The nucleation process determines the size and the size distribution of the crystals produced (Elving and Kolthoff, 1979).

Nucleation can usually be divided into two mechanisms, i.e. primary and secondary nucleation. Primary nucleation in itself is subdivided into two additional categories, depending on whether the nuclei formed spontaneously or if a foreign substance was present. The following representation highlights this point (Mullin, 1992 in Söhnel and Garside, 1992):

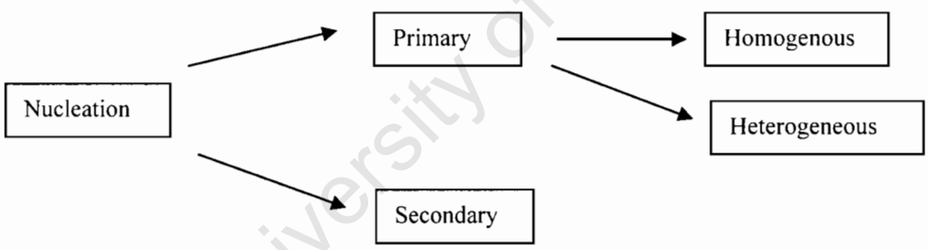

Figure 2.1 Nucleation mechanisms

Primary nucleation can be defined as the formation of a new phase. Homogenous primary nucleation is when this formation is not initiated by the presence of any solid phase. Heterogeneous nucleation forms a new solid phase which is usually catalysed by the presence of a foreign solid.

Secondary nucleation is the formation of new crystals on pre-existing crystal surfaces of their own species.

These mechanisms can occur individually or simultaneously in a reactor vessel. Where high local supersaturation occurs (like the feed inlet points), homogenous primary nucleation tends to dominate, with very high nucleation rates. In regions where the homogenous nucleation rate is negligible, but the system remains supersaturated, heterogeneous nucleation or secondary nucleation are the dominating mechanisms (Franke and Mersmann, 1995).

2.2.1.1 Homogenous Primary Nucleation

The classical theory of nucleation was found to describe homogenous nucleation best, in that it fitted experimental data obtained (Söhnel and Garside, 1992).

As with most chemical reactions, an activation energy barrier has to be overcome first. This barrier creates the need for a degree of supersaturation before spontaneous crystallisation may occur (Elving and Kolthoff, 1979). Stable nuclei can only be formed after this activation energy barrier has been surmounted.

The free energy of the formation of a nucleus, ΔG_j, consists essentially of energy gained from making bonds and of work required to create a surface:

$$\Delta G_j = \Delta G_{bulk} + \Delta G_{surf} \qquad (2\text{-}10)$$

ΔG_{bulk} = bulk excess free energy (J)
ΔG_{surf} = surface excess free energy (J)

For a nucleus, ΔG_{bulk} is always negative in a supersaturated solution. This quantity can more commonly be expressed as:

$$\Delta G_{bulk} = -jkT \ln \frac{a}{a^*} = -jkT \ln S \qquad (2\text{-}11)$$

j = number of molecular units in the nucleus (-)

($j = \frac{4\pi r^3}{3V}$ for a spherical particle of radius r, and "molecular" volume V)

k = Boltzmann constant (1.3805×10^{-23} JK^{-1})

T = Temperature (K)

The second quantity in equation (2-10) is given (for a spherical nucleus) by:

$$\Delta G_{surf} = 4\pi r^2 \bar{\gamma} \qquad (2\text{-}12)$$

$\bar{\gamma}$ = interfacial energy (assumed to be independent of cluster size) (Jm^{-2})

Hence equation (2-10) can be rewritten as

$$\Delta G_j = -\frac{4\pi r^3}{3V} kT \ln S + 4\pi r^2 \bar{\gamma} \qquad (2\text{-}13)$$

As can be seen from the equation above, the volume free energy is proportional to r^3, while the surface free energy is only proportional to r^2. Thus with increasing cluster size, the first term on the right outweighs the second term; for large crystals the second term becomes negligible.

Equation (2-13) is represented in figure 2.2 below. As r increases from a value of zero, the overall excess free energy ΔG_j reaches a maximum value when the nucleus achieves a critical size. This critical radius is maximised when $d\Delta G_j / dr = 0$, i.e.

$$\frac{d\Delta G_j}{dr} = -\frac{4\pi r^2 kT}{V} \ln S + 8\pi r \bar{\gamma} \qquad (2\text{-}14)$$

which upon solving, yields a critical radius, r*

$$r^* = \frac{2\bar{\gamma}V}{kT\ln S} \qquad (2\text{-}15)$$

The critical nucleus represents the minimum nucleus size which, if exceeded, produces stable crystals under the average conditions of supersaturation obtained in the bulk fluid. Below this critical nucleus, particles tend to redissolve because they are unstable and hence do not reach maturity.

Using equations (2-15) and substituting into equation (2-13), the critical energy barrier that needs to be overcome can be calculated.

$$\Delta G^* = \frac{16\pi\bar{\gamma}^3 V^2}{3[kT\ln S]^2} = \frac{4\pi\bar{\gamma}}{3}(r^*)^2 \qquad (2\text{-}16)$$

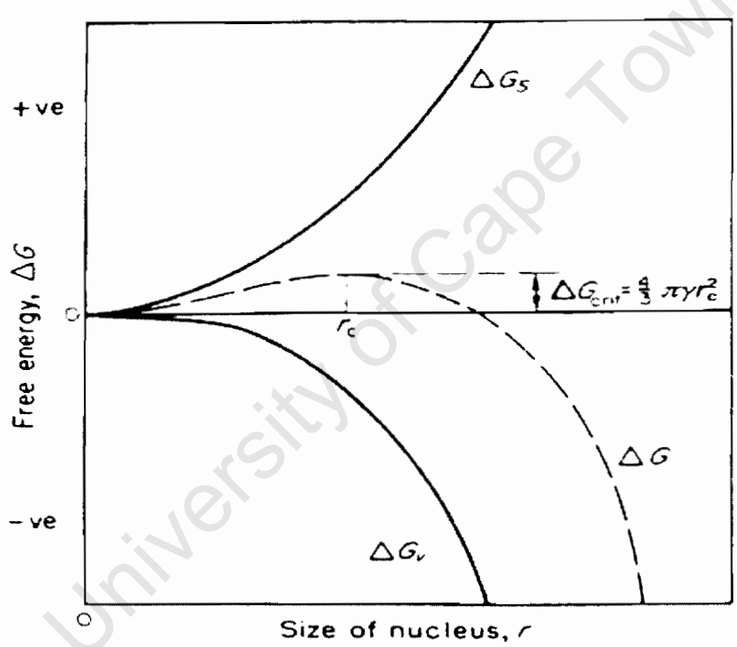

Figure 2.2 Free energy diagram for nucleation, explaining the existence of a "critical nucleus size" (Mullin, 2001).

Mullin (2001) explains the critical energy produced to form a stable nucleus as follows: "because there will be a statistical distribution of energy in the

molecules constituting the system, in supersaturated regions where energy levels rises temporarily, nucleation will be favoured".

The rate of nucleation can be expressed in the form of an Arrhenius reaction velocity equation:

$$J = A\exp\left[\frac{-\Delta G^*}{kT}\right] \qquad (2\text{-}17)$$

J = number of nuclei formed per unit time per unit volume (#$s^{-1}m^{-3}$)
A = factor related to the efficiency of collisions of ions or molecules

If equation (2-16) is substituted into (2-17):

$$J = A\exp\left[\frac{-16\pi\overline{\gamma^3}V^2}{3k^3T^3(\ln S)^2}\right] \qquad (2\text{-}18)$$

This equation shows that the rate of nucleation is controlled by three main variables: the interfacial energy $\overline{\gamma}$, the temperature T and the supersaturation S. At high degrees of supersaturation, the nucleation rate is so high that the precipitate formed, consists mostly of extremely small crystallites. If the nucleus is smaller than a one-unit cell, the growing crystallite produced initially is most likely to be amorphous (Elving and Kolthoff, 1979).

2.2.1.2 Heterogeneous Primary Nucleation

Particles of a foreign solid phase that can act as a catalyst for nucleation are present in all systems that have not been cleaned properly. In a similar way as a catalyst reduces the activation energy of chemical reactions, foreign solids catalyse the nucleation process by reducing the energy barrier.
Qualitatively, if the surface of the solid matches well with the crystal, the interfacial energy barrier between the two solids is smaller than the interfacial

energy barrier between the crystal and the solution, and nucleation may take place at a lower saturation on a solid surface than in solution.

In a similar way as homogenous nucleation, the overall free energy change associated with heterogeneous nucleation is written as

$$\Delta G_{het} = -mkT \ln \frac{IAP}{K_{sp}} + \bar{\gamma} A \qquad (2\text{-}19)$$

m = number of formula units of the mineral in the crystal, i.e. $m = j / \nu$

A is the surface area of the crystal, and can be expressed as

$$A = \alpha \left(\frac{V_M}{\eta N_A} \right)^{2/3} j^{2/3} \qquad (2\text{-}20)$$

V_M = molar volume of the solid phase

N_A = Avogadro number (6×10^{23} mol^{-1})

α = geometric factor that depends on the shape of the crystal

The mean ionic radius can be given by

$$\bar{r} = \frac{1}{2} \left(\frac{V_M}{\eta N_A} \right)^{1/3} \qquad (2\text{-}21)$$

Rewriting equation (2-19) into a more general form

$$\Delta G_{het} = -mkT \ln S + 4\alpha \bar{\gamma} \overline{r^2} j^{2/3} \qquad (2\text{-}22)$$

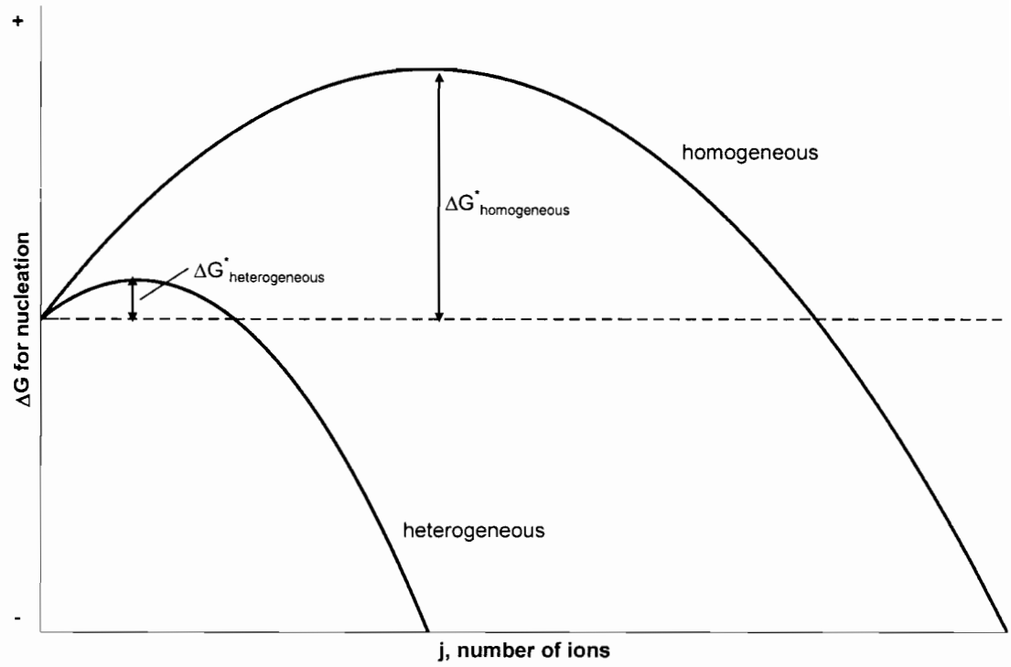

Figure 2.3 Activation energy comparison for heterogeneous vs. homogenous energy (replicated from Stumm and Morgan, 1981)

In the case of heterogeneous nucleation, the interfacial energy needs some redefinition because the nucleus is now formed in part in contact with the solution and in part with the surface of a solid substrate. For homogenous nucleation $\Delta G_{surf} = \bar{\gamma}_{CL} A$, whereas Van Cappellen (1991) (as reported in Elving and Kolthoff) stated that

$$\Delta G_{\text{int}erface} = \bar{\gamma}_{CL} A_{CL} + (\bar{\gamma}_{CS} - \bar{\gamma}_{SL}) A_{CS} \qquad (2\text{-}24)$$

The subscripts CL, CS, SL refer to crystal-liquid, crystal-solid and solid-liquid respectively.

In ideal cases, $\bar{\gamma}_{CS}$ becomes very small and the solid-liquid interfacial energy of the substrate is similar to that of the cluster. As a consequence, a "good" substrate would have

$$\Delta G_{\text{int}erface} = \gamma_{CL} (A_{CL} - A_{CS}) \qquad (2\text{-}25)$$

Mullin (2001) discusses the interfacial energy as part of a contact angle between the crystal and the solid matter. With three phases in contact, interfacial energy balances in any direction could be made as follows (see figure 2.4):

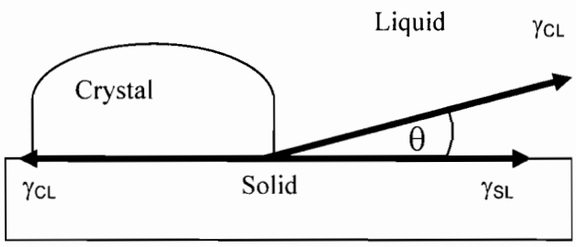

Figure 2.4 Interfacial tensions at the boundaries between three phases

$$\gamma_{SL} = \gamma_{CS} + \gamma_{CL}\cos\theta \qquad (2\text{-}26)$$

or $$\cos\theta = \frac{\gamma_{SL} - \gamma_{CS}}{\gamma_{CL}} \qquad (2\text{-}27)$$

The angle of contact between the two solids corresponds to the angle of wetting in liquid-solid systems.

Mullin also states that the overall free energy required for heterogeneous nucleation should be lower than that for homogenous nucleation, i.e.

$$\Delta G_{het} = \phi \Delta G_{\text{hom}} \qquad (2\text{-}28)$$

The factor Φ is less than unity. It can also be expressed in terms of the contact angle as

$$\phi = \frac{(2+\cos\theta)(1-\cos\theta)^2}{4} \qquad (2\text{-}29)$$

Figure 2.5 below indicates the relationship between Φ and Θ.

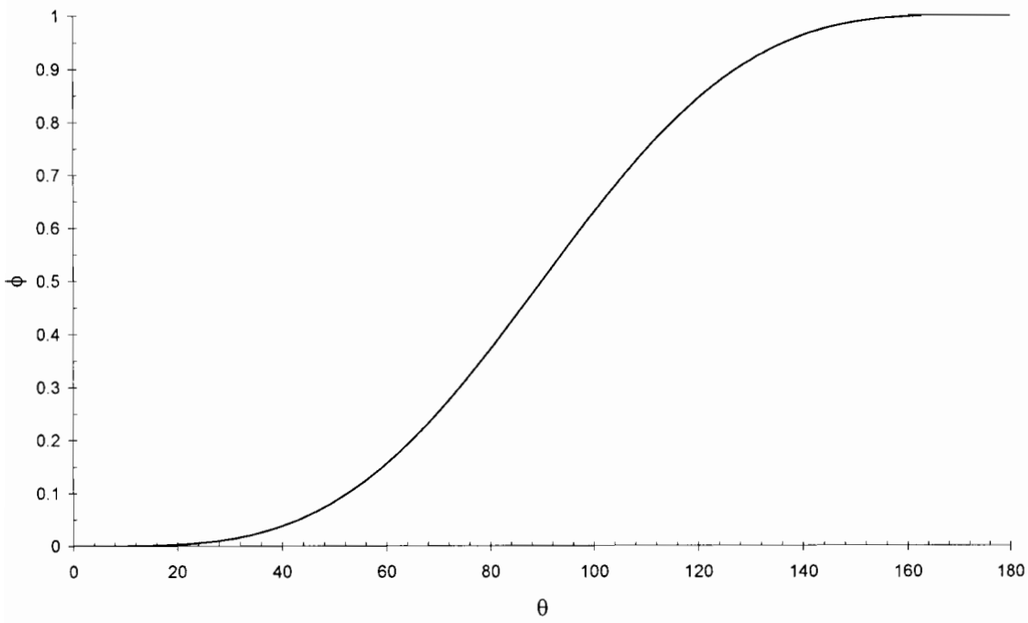

Figure 2.5 Ratio of free energies of homogenous and heterogeneous nucleation as a function of contact angle

2.2.1.3 Secondary Nucleation

Secondary nucleation occurs when a new nucleus is formed at the interface of a pre-existing precipitate of its own species. As this definition has a very close resemblance to heterogeneous nucleation, the two can easily be confused. The only difference would be that secondary nucleation occurs on existing crystals, whereas heterogeneous nucleation occurs on a foreign particle.

There are different types of secondary nucleation, e.g. initial breeding, dendritic breeding, fracture breeding, contact nucleation and fluid shear breeding (Söhnel and Garside, 1992). In crystallisation processes however, contact nucleation is usually the most important, largely because the nuclei are produced by contact with the agitator, pump, flow lines or other crystals.

Precipitation and crystallisation processes are usually focussed on producing particles of a large size and narrow size distribution to minimise filtration costs. Secondary nucleation usually helps in this regard by allowing an

effective control over product size and size distribution. This is commonly achieved by deliberate seeding to initiate crystallisation.

2.2.2 Crystal Growth

As soon as stable nuclei have been formed in a supersaturated system, they begin to grow into crystals of visible size (Mullin, 2001). However, there are many proposed mechanisms of crystal growth:

- *Surface energy theories*: Although this theory has not been completely abandoned, it has largely fallen into disuse. It postulates that the shape of a growing crystal assumes that of minimum surface energy.
- *Diffusion theories*: Presumes that matter is deposited continuously on a crystal face at a rate proportional to the difference in concentration between the point of deposition and the bulk solution.
- *Adsorption theories*: Some researchers suggested that crystal growth was a discontinuous process, taking place by adsorption, layer by layer, on the crystal surface.

Because of the high process concentrations that will be employed in this investigation, it is hypothesised that very little crystal growth would occur, and that particle enlargement would be dominated by secondary processes like agglomeration.

The sparingly soluble nature of the precipitates formed leads to high supersaturation, resulting in rapid and significant primary nucleation. The nucleation consumes most of the supersaturation so that very little supersaturation is left for further growth of the precipitates. Precipitation processes are usually dominated by nucleation (because of the high supersaturation) and agglomeration (because of the abundance of particles).

2.2.2.1 Diffusion-reaction theories

It was assumed that the deposition of solid on the face of a growing crystal is a diffusion dominated process (Noyes and Whitney, in Mullin, 2001). It was further assumed that crystallisation was the reverse of dissolution and that both rates were controlled by the difference between the concentration at the solid surface and that of the bulk solution.

Crystal growth can be seen as a succession of events:

1. Transport of reactive species through the solution (the diffusion step)
2. Adsorption at crystal/solution interface
3. Surface diffusion
4. Reaction at the interface
5. Incorporation of the reaction products into the crystal lattice

Generally, the rate of all processes is controlled by the slowest of these events, usually step 1 in the above paragraph.

For surface diffusion, an equation was proposed of the following form:

$$\frac{dm}{dt} = k_m A(c - c^*) \qquad (2\text{-}30)$$

m = mass of solid deposited in time t (kg)
A = surface area of the crystal (m^2)
c = solute concentration in the solution (supersaturated) (mol/l)
c^* = equilibrium saturation concentration (mol/l)
k_m = coefficient of mass transfer (kg.m/mol.s)

A revised form of this equation was proposed by Nernst in Mullin (2001), on the assumption that there would be a thin stagnant film of liquid adjacent to the growing crystal faces:

$$\frac{dm}{dt} = \frac{D}{\delta} A(c - c^*) \qquad (2\text{-}31)$$

D = coefficient of diffusion of the solute (kg.m^2/s)

δ = length of the diffusion path (m)

Studies done by Miers (1904) led to the conclusion that the solution in contact with a growing crystal face is not saturated, but supersaturated. This lead some researchers to propose the idea that although a diffusion process transport solute molecules to the solid surface from the bulk phase, a first-order "reaction" takes place when the solute molecules arrange themselves into the crystal lattice (Berthoud, 1912 and Valeton, 1924 in Mullin, 2001). Thus

$$\frac{dm}{dt} = k_d A(c - c_i) \quad \text{(diffusion)} \qquad (2\text{-}32)$$

$$\frac{dm}{dt} = k_r A(c_i - c^*) \quad \text{(reaction)} \qquad (2\text{-}33)$$

k_d = coefficient of mass transfer by diffusion (kg.m.mol^{-1}.s^{-1})

k_r = a rate constant for the surface reaction (integration) (kg.m/mol.s)

c_i = solute concentration in the solution at the crystal-solution interface (mol/l)

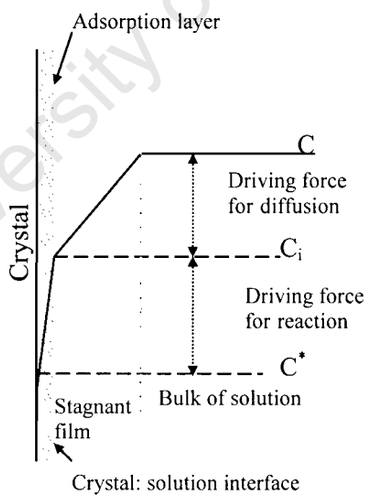

Figure 2.6 Concentration driving forces in crystallisation from solution according to the simple diffusion-reaction model

2.2.3 Agglomeration

Larger crystals are usually formed when smaller ones cluster together. This is termed aggregation or agglomeration, and is the result of a number of mechanisms, with smaller particles held together by several different forces.

The rate of particle agglomeration depends on the frequency of collisions and on the efficiency of particle contacts. Particle collisions are the consequence of at least three mechanisms:

1. Particles move because of their thermal energy (Brownian motion).
2. If colloids are sufficiently large or the fluid shear rate high, the relative motion from velocity gradients exceeds that caused by Brownian effects (orthokinetic agglomeration).
3. In settling, particles of different gravitational settling velocities may collide.

For a simplistic system, with no growth, the following discussions hold true.

The time-dependant decrease in concentration of particles (N = number of particles per cubic centimetre) due to Brownian motion can be expressed as a second-order rate law

$$-\frac{dN}{dt} = k_p N^2 \qquad (2\text{-}34)$$

or

$$\frac{1}{N} - \frac{1}{N_0} = k_p t \qquad (2\text{-}35)$$

where k_p is the rate constant [$cm^3.s^{-1}$].

K_p can also be expressed as

$$k_p = 4D\pi d \qquad (2\text{-}36)$$

D = Brownian diffusion coefficient [$cm^2.s^{-1}$]

d = particle diameter [cm]

The diffusion coefficient can also be expressed with the Einsteiin-Stokes:

$$D = \frac{kT}{3\pi\eta d} \tag{2-37}$$

η = absolute viscosity (m^2/s)

Multiplying the right hand side of equation (2-34) by a factor α_p which is the fraction of collisions leading to permanent agglomeration, and substituting into equation (2-37):

$$-\frac{dN}{dt} = \alpha_p \frac{4kT}{3\eta} N^2 \tag{2-38}$$

This relates to agglomeration of particles due to Brownian motion alone and is usually for particles with d < 1μm.

Orthokinetic agglomeration is usually enhanced by agitation in the system, as agitation may accelerate aggregation of larger particles. Because particles follow the fluid motion (where spatial velocity gradients may exist), opportunities for interparticle contact are created.

The rate of decrease in particle number due to agglomeration of particles (having uniform size) under the influence of a mean velocity gradient G can be described as

$$-\frac{dN}{dt} = \frac{2}{3}\alpha_o G d^3 N^2 \tag{2-39}$$

α_o is defined similarly to α_p

G = mean velocity gradient [$time^{-1}$]

d = particle diameter [cm]

If the volume of solid particles is conserved during agglomeration, the volume fraction of colloidal particles, i.e. the volume of colloids per unit volume of suspension, can be expressed as

$$\phi = \frac{\pi}{6} d_o^3 N_o \qquad (2\text{-}40)$$

where N_o and d_o are the initial number of particles and initial particle diameter respectively.

Equation (2-39) can then be rewritten as

$$-\frac{dN}{dt} = \frac{4}{\pi} \alpha_o \phi G N \qquad (2\text{-}41)$$

Assuming then that separate mechanisms are additive, the overall rate of decrease in particle concentration can be written as

$$-\frac{dN}{dt} = \alpha_p \frac{4kT}{3\eta} N^2 + \alpha_o \frac{4\phi G}{\pi} N \qquad (2\text{-}42)$$

The first term usually becomes negligible for particles with a diameter d > 1μm, whereas the second term is less important for particles with a diameter d < 1μm.

The above equations all assumed that no growth occurs at the same time in the system. However, it can be seen from equation (2-40) that the assumptions are based on the particle diameter. Where growth occurs, the particle diameter would also be a dynamic factor in that it changes with time.

Because most systems would have growth and agglomeration occurring simultaneously as size enlargement mechanisms, it is usually difficult to determine the rates of each individually (Bramley et al, 1996). They also proposed a method for determining aggregation rates from experimental data,

using experimentally obtained particle size distributions (PSD). A similar method is also proposed by Aoun et al (1999) in determining nucleation and growth rates.

Explanations and derivations of the equations below can be followed in the text as reported by Bramley.

For size-independent growth and agglomeration in a batch system, the zeroth and third moments can be calculated by:

$$\frac{dm_0}{dt} = -\frac{1}{2}\beta_0 m_0^2 \qquad (2\text{-}43)$$

$$\frac{dm_3}{dt} = 0 \qquad (2\text{-}44)$$

m_j = j^{th} moment ($m^j.m^{-3}$)
β_0 = aggregation kernel

The moments referred to above are the number density (zeroth moment) and the volume density (third moment).

If a size-independent growth rate is included, equation (2-43) remains unchanged, but (2-44) then becomes

$$\frac{dm_3}{dt} = 3Gm_2 \qquad (2\text{-}45)$$

G = growth rate ($m.s^{-1}$)

Thus, from experimentally obtained particle size distributions (PSDs), the values for the moments and thus the rates of change of the moment can be obtained and used in the above equations to determine β_0 and G.

The above only holds true for size-independent growth and agglomeration however, so the method was generalised for other systems.

Bramley and co-authors arrived at the following set of simultaneous equations that can be solved using data extracted from PSDs:

$$\dot{m}_0 = \beta_0 \phi_0 + B_u \quad (2\text{-}46)$$

$$\dot{m}_3 = G\phi_3 + B_u \overline{L_1^3} \quad (2\text{-}47)$$

$$\dot{N} = G\phi_2 + \beta_0 \phi_1 + B_u \quad (2\text{-}48)$$

$\dot{m}_j$ = rate of change of the j^{th} moment ($m^j.m^{-3}.s^{-1}$)

B_u = source function ($m^{-3}.s^{-1}$)

$\dot{N}_1$ = rate of change of particle number in the first size interval ($m^{-3}.s^{-1}$)

L_1 = average particle size in the first size interval (m)

The definitions for ϕ_0, ϕ_1, ϕ_2 and ϕ_3 can be found in the text and are not presented here. The unknowns in the above equation (β_0, G and B_u) can thus be solved with values for the other parameters obtained from a PSD.

The above method has been successfully applied to the batch precipitation of calcium oxalate monohydrate by Bramley *et al* (1996).

Chapter Summary

This chapter indicated the importance of nucleation or the factors leading to nuclei formation on the precipitation process. Supersaturation has been shown to be a dominant factor in all mechanisms and thus an important factor to either control or monitor in the precipitation reactions. For size enlargement mechanisms in the precipitation reaction, both growth and agglomeration play an important role, with a method described for obtaining rates of each mechanism using experimentally obtained PSDs.

Chapter 3

Sulphide Chemistry

This chapter briefly describes the sulphide chemistry that would most likely be encountered in the system under investigation. It also discusses the advantages of using sulphide as a precipitating agent, with comparisons made to the more commonly used hydroxide precipitation.

3.1 Advantages and Disadvantages

Although sulphide precipitation is used on hydrometallurgical plants, the use of sulphide as a precipitating agent only received increased attention since Bhattacharyya et al (1981) investigated the use of sodium sulphide to precipitate heavy metals from solution.

They found that the sulphide precipitation was an effective method for removing heavy metals to within acceptable legal limits (in the ppm range). According to the authors, the attractive features are

- attainment of high degree of metal removal over a broad pH range
- effective removal of metals such as As, Cu and Hg even at low pH
- low retention time required in the reaction tank because of high reactivity
- feasibility of selective metal recovery

These features were also noted by other authors (Peters et al, 1984 and Kamaru et al, 1991). These features make sulphide precipitation superior to hydroxide precipitation.

Mishra and Das (1992) also reported that the shortcomings of the hydroxide precipitates are their high solubilities, the amphoteric nature of the metal hydroxides and the ineffectiveness of metal removal in the presence of

chelating agents, commonly found in metal finishing operations. The metal sulphides have higher stability and metal can be removed even in the presence of chelating agents.

Peters et al (1984) also highlighted that sulphide precipitates exhibits better thickening and dewatering characteristics than hydroxide precipitates. Sulphide precipitates can also be processed by existing smelters for metal recovery (Veeken et al, 2003).

Sulphide precipitation does have some disadvantages associated with it. Depending on the dosage used, sulphide residual concentrations could be found in the treatment effluent. This could lead to emission of toxic hydrogen sulphide gas as well as odour problems.

Because of the low solubilities of metal sulphides, colloidal particles are often encountered. The metal sulphide precipitates also tend to be amorphous, suggesting improvement of the particulate properties as an important factor (Peters et al, 1984).

3.2 Aqueous speciation

Apart from the chemical reactions that need to be considered in the precipitation process, the sulphide equilibrium also needs to be investigated.

For the sulphide system, the following equilibrium reactions exist:

$$H_2S(g) \overset{K_H}{\Leftrightarrow} H_2S(aq) \qquad (3.1)$$

$$k_H = 8.7 \times 10^{-2}\, M.atm^{-1}$$

$$H_2S \overset{K_1}{\Leftrightarrow} H^+ + HS^- \qquad (3.2)$$

$$K_1 = 1.0 \times 10^{-7.05}$$

$$HS^- \overset{K_2}{\Leftrightarrow} H^+ + S^{2-} \qquad (3.3)$$

$$K_2 = 1.0 \times 10^{-12}$$

The Henry's constant reported in equation (3-1) was sourced from De Bruyn et al (1995) as reported by Sander (http://www.mpch-mainz.mpg.de/~sander/res/henry.html)

As can be seen, the equilibrium sulphide species are highly dependant on the pH of the solution. This can also be seen in figure 3-1. Figure 3-1 shows a generic plot for a total sulphide concentration of 0.1**M**. It was drawn using the equilibrium constants above as given by Su et al (1997) in their work of determining these constants using amplified potentiometric methods.

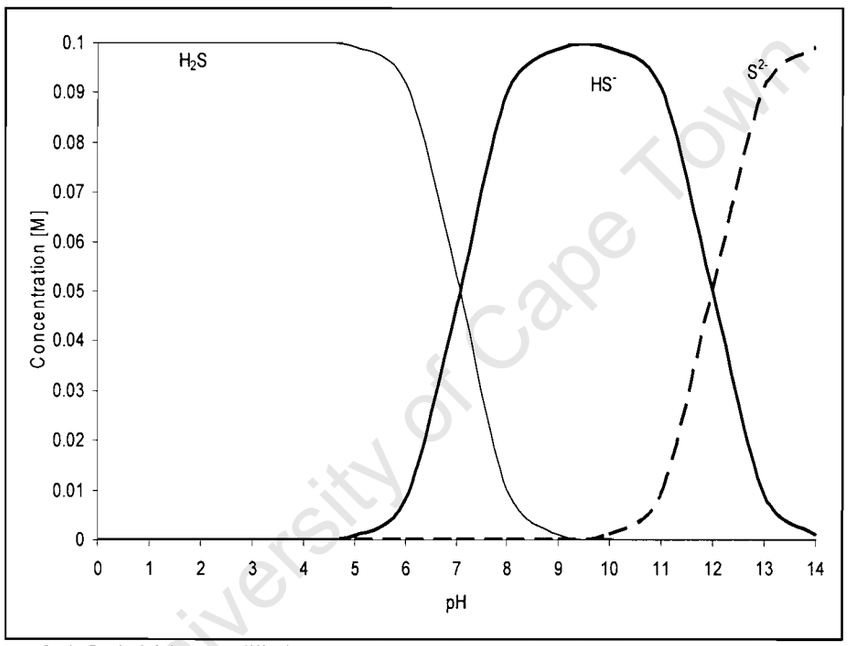

Figure 3.1 Sulphide equilibrium and speciation showing the dependence on pH

For a diprotic acid like H_2S the equations used to calculate the equilibrium concentrations are given by (Stumm and Morgan, 1996):

$$H_2S = \frac{[S]_{total}}{1 + \frac{K_1}{[H^+]} + \frac{K_1 K_2}{[H^+]^2}} \qquad (3.4)$$

$$HS^{-} = \frac{[S]_{total}}{\frac{[H^+]}{K_1} + 1 + \frac{K_2}{[H^+]}} \quad (3.5)$$

$$S^{2-} = \frac{[S]_{total}}{\frac{[H^+]^2}{K_1 K_2} + \frac{[H^+]}{K_2} + 1} \quad (3.6)$$

The dependence of the equilibrium species on the literature constants used are apparent in the equations above. Much debate has arisen over the value of K_2. In their work, Su et al (1997) scrutinised values reported by certain authors (values of pK_2 ranging from 13-19) with calculations based on mass-balances.

Chapter Summary

The chemistry of the sulphide system was discussed, highlighting the advantages and disadvantages of such a sulphide system. The sulphide species were also shown to be of importance, especially under operating conditions where hydroxide precipitation tends to be minimal (i.e. low to neutral pH). It is thus expected that under the planned conditions for this study, the main precipitation reaction would be

$$Me^{2+} + HS^{-} \rightarrow MeS + H^{+} \quad (3.7)$$

Chapter 4

Reaction kinetics: Gas-liquid reactions

The absorption of gases into liquids with which they react is an important aspect of multiphase processes. This chapter will be concerned with the chemical interaction of gases and liquids, especially linking gas absorption and the dissolution and reaction.

4.1 General overview

For precipitation using a gaseous reagent, there are usually a number of sub processes involved (Oktaybas et al, 1994):

1. absorption of gaseous component into the gas-liquid interface
2. **diffusion of gaseous component to the reaction zone**
3. **diffusion of the metal ion to the reaction zone**
4. reaction at the reaction zone
5. precipitation of reaction products from the reaction zone

The two steps highlighted are usually assumed to be the slowest and thus rate controlling (Mishra and Kapoor, 1978; Oktaybas, 1994).

4.1.1 General diffusion with reaction

The reactions referred to in this chapter can only take place to the extent that the gas is absorbed by the liquid, and the gas can only be absorbed by diffusing into the liquid from the interface. Diffusion is thus central to the discussion of gas-liquid reactions (Danckwerts, 1970).

Although the case of physical absorption without reaction will not be discussed in this chapter, it can be seen as a special case to the one given below, by simply setting all relevant reactions to zero.

If the dissolved gas reacts with a dissolved reagent in the liquid, the general equation for the concentration of a diffusing reagent at a distance x is:

$$-D\frac{\partial c}{\partial x}+D\left(\frac{\partial c}{\partial x}+dx\frac{\partial^2 c}{\partial x^2}\right)=dx\frac{\partial c}{\partial t}+rdx \qquad (4.1)$$

where r is the rate of reaction of diffusant (per unit volume of liquid)

For the general second order equation of the form

$$A+bB\rightarrow yP \qquad (4.2)$$

(A being the gaseous diffusing species), equation (4.2) can be reduced and rewritten as

$$D_A\frac{\partial^2 A}{dx^2}=\frac{\partial A}{\partial t}+k_2AB \qquad (4.3)$$

D_A = diffusion coefficient of species A
A = concentration of species A
B = concentration of species B
k_2 = second order rate constant

A similar equation can be written for species B. At this point it should be noted that the *b* in equation (4.2) refers to *b* moles of B reacting with one mole of A and does not imply that the rate expression must take the form $r=kAB^b$. This is because there is not necessarily any relationship between the stoichiometry of the reaction and its order.

Although the solution of equation (4.3) is not discussed in this chapter, a more detailed explanation can be found in Danckwerts (1970) using specified boundary conditions and enhancement factors for various conditions.

4.1.2 Kinetics using H_2S

Although the use of sulphide as a precipitating agent has received increased attention in hydrometallurgical processes, the use of hydrogen sulphide as a reagent is not widely covered in literature.

Oktaybas et al (1994) studied the kinetics of copper precipitation by H_2S from sulphate solutions. Their work was based on studies carried out by Mishra and Kapoor (1978) in their kinetic studies of liquid-gas reactions. They bubbled H_2S through a $CdCl_2$ solution to precipitate CdS. The discussions that follow are largely based on the work done by Oktaybas (1994), but could also be found in Mishra and Kapoor (1978).

For a generic equation for precipitation of a metal sulphide from a sulphate solution with hydrogen sulphide, the following chemical equation can be written:

$$MeSO_4(aq) + H_2S(g) \rightarrow MeS(s) + H_2SO_4 \qquad (4.4)$$

where Me is the metal species.

Both authors state that, according to "Higbie's theory", the precipitation rate can be expressed as

$$\frac{dC_{MeSO_4}}{dt} = -\frac{A_b}{V} k_L (C_{MeSO_4} + C^0_{H_2S}) \qquad (4.5)$$

C_{MeSO4} = concentration of $MeSO_4$ at time t ($kg.m^{-3}$)
A_b = gas-liquid interfacial area (m^2)
V = volume of liquid phase (m^3)
k_L = gas-liquid mass transfer coefficient ($m.s^{-1}$)
C^0_{H2S} = interfacial concentration of H_2S in the liquid ($kg.m^{-3}$)

Oktaybas et al (1994) reports a value of 18.18kg.m^{-3} for the interfacial concentration of H_2S(aq) as calculated from Perry's Chemical Engineering Handbook. Mishra and Kapoor (1978) report this value as 18.24 kg.m^{-3}. This report uses the value as reported by Oktaybas et al.

After integration of equation (4.5) and substituting the above value, the following equation is found:

$$\ln\left(\frac{18.18 + C_{MeSO_4}}{18.18 + C^0_{MeSO_4}}\right) = -\frac{A_b}{V} k_L t \qquad (4.6)$$

C^0_{MeSO4} = initial concentration of $MeSO_4$ (kg.m^{-3})

From this equation, a plot of the logarithmic of the term on the left versus time should yield a slope equal to the reaction rate constant k, and thus

$$slope = k = -\frac{A_b}{V} k_L \qquad (4.7)$$

The linear nature of this plot would indicate that the overall rate of reaction is controlled by diffusion, as previously assumed.

In order to calculate the mass transfer coefficient, the value of A_b is required. This can be calculated from:

$$A_b = \frac{\pi n r^2 h}{v_\infty} \qquad (4.8)$$

n = number of bubbles per second (#.s^{-1})
r = equivalent radius of bubbles (m)
h = height of the liquid phase (m)
v_∞ = rising velocity of the bubbles (m.s^{-1})

The rising velocity of the bubbles is given by

$$v_\infty = 1.02(gr)^{1/2} \quad (4.9)$$

g = acceleration due to gravity ($m.s^{-2}$)

The equivalent radius of the bubbles can also be calculated from

$$r = \left(\frac{3G}{4000\pi n}\right)^{1/3} \quad (4.10)$$

G = gas-flow rate ($l.s^{-1}$)

Rearranging for the number of bubbles per second, and after substituting equations (4.9) and (4.10) into (4.8):

$$A_b = \frac{Gh}{1360\sqrt{g}r^{3/2}} \quad (4.11)$$

and

$$k_{L,\exp} = \frac{1360kV\sqrt{g}r^{3/2}}{Gh} \quad (4.12)$$

The above equation has been termed $k_{L,exp}$ merely because all of the unknowns in the equation are dependent on the experimental conditions used.

The Higbie model also allows a theoretical prediction of k_L from the following equation

$$k_L = \frac{2}{\sqrt{\pi}}\left(\frac{D_{H_2S}}{t_c}\right)^{1/2} \quad (4.13)$$

D_{H2S} = diffusion coefficient of hydrogen sulphide ($m^2.s^{-1}$)

t_c = surface renewal time (s)

The surface renewal time can be calculated from

$$t_c = \frac{2r}{v_\infty} \tag{4.14}$$

and thus

$$k_{L,theo} = \frac{1.451\sqrt{D_{H_2S}}}{r^{1/4}} \tag{4.15}$$

This allows a basis to compare the accuracy of the experimental data obtained. However, it should be noted also that discrepancies have been noted by Mishra and Kapoor (1978) in the derivation of equation (4.13) in that turbulence of the rising bubbles was not taken into account. Since turbulence decreases the surface renewal time, k_L would increase.

Chapter Summary

This chapter highlighted the fact that diffusion of the reacting species is the rate limiting step. For a gas diffusing into an aqueous solution, the gas-liquid diffusion would be the slowest. Ways of calculating the mass transfer coefficient were also presented.

Chapter 5

Experimental Procedure

A description of each of the experimental set-ups investigated in this research follows in this chapter. The use of a fluidised bed reactor has been shown to be successful and was thus also investigated here. The limitations or shortcomings of the fluidised bed are highlighted here and efforts to control supersaturation in the reactor were employed. Gaseous sulphide systems were also investigated, looking at biologically produced hydrogen sulphide before employing a composite mixture from a gas cylinder.

All experiments were conducted with analytical grade $NiSO_4.6H_2O$ and $CoSO_4.7H_2O$ Merck chemicals. Solutions were made up to required concentrations using distilled water.

5.1 Batch testing

5.1.1 Precipitation reaction and settling rates

Batch experiments were conducted in 500ml beakers continuously stirred with a magnetic stirrer. Metal concentrations used were 250ppm (a diluted stream) and 2000ppm for nickel and 100ppm and 1000ppm for cobalt.

An aqueous source of sodium hydroxide, sodium carbonate or sodium sulphide (depending on the precipitate desired) was added rapidly to the beakers and samples were periodically withdrawn, filtered through 0.45μm cellulose nitrate syringe filters and analysed using atomic adsorption spectroscopy (AAS). The ratio of metal to precipitating agent was kept constant at 1:1.

At the end of each run, the precipitate samples were transferred to conical Imhoff cones to test their settling characteristics.

5.2 Continuous testing

5.2.1 Fluidised Bed Set-up

The fluidised bed reactor is shown in figure 5.1 below. The reactor consists of a cylindrical glass column which is 1.5m high and has a 25mm ID. The column was also filled to a height of 90cm with beach sand (SiO_2) (250-500μm) as a seeding material. The set-up is similar to those used by other authors like Zhou (1999), Seckler (1996), Peters (1984), Guillard and Lewis (2001a,2001b) and van Hille et al (2005).

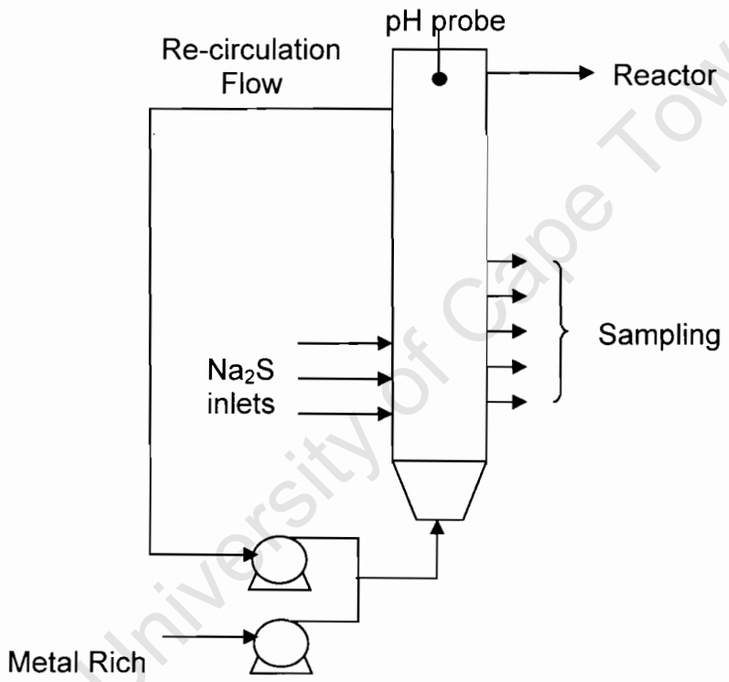

Figure 5.1 Schematic representation of the pellet reactor

Table 5.1 Experimental equipment

Re-circulation	Watson Marlow 505S; Marprene tubing #16
Metal rich stream	Watson Marlow 505S; Marprene tubing #16

Na_2S stream	Watson Marlow 505S; Marprene tubing #16
ph probe	Metrohm 6.0219.100 (pH 0-14) (temp. 0-70°C)
Reactor	1.5 m high custom-made fluidised bed glass column

The bottom of the reactor was fitted with a 25mm diameter plastic disk containing 2mm holes for flow distribution. A circular, 25mm diameter, wire gauze (180μm) was positioned above the disk to prevent sand clogging the inlet flow pipe. A 2cm bed of 5mm glass beads provided extra support for the sand (see figure 5.2).

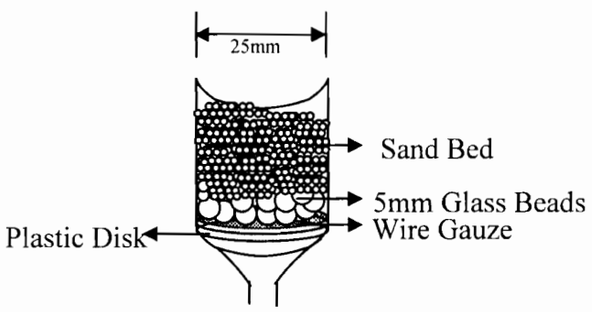

Figure 5.2 Inlet of the pellet reactor

An aqueous metal-rich stream together with the re-circulation stream entered via the bottom of the column. The re-circulation stream helped to fluidise the bed. Air was excluded from the column, as air bubbles ascending through the column could result in the loss of seed material to the re-circulation (these could lead to blockages in the pipes due to the peristaltic motion of the pumps) or effluent streams.

Sodium sulphide was introduced via three inlet points on the side of the reactor. They were equally spaced 10cm from each other.

Samples were taken from the reactor outlet and were analysed for metal concentrations using AAS. Filtered (filtered through 0.45μm cellulose nitrate syringe filters) and unfiltered samples were taken from the reactor outlet. Unfiltered samples were acidified by adding hydrochloric acid to the sample to redissolve the precipitate.

Because fluidised beds are usually characterised by their good mixing profiles, continuous contact between particles gives rise to high attrition rates. This leads to fines formation inside the fluidised bed as well as high nucleation rates due to supersaturation. Fines tend to persist throughout the column and they also tend not to settle very well.

Tests were also conducted in two fluidised beds (a similar set-up was also investigated by Zhou (1999)) in series to test whether these fines would adhere to the surface of the bed material. Sodium sulphide was added to the first reactor similar to the approach described above. The product stream from the first reactor (containing particulate fines) was then passed into the second reactor. Here no sulphide was added; the second reactor acted merely as a "scrubber" where the fines were allowed to adsorb onto the clean sand particles.

5.2.2 Biologically produced hydrogen sulphide

The reactor configuration is shown in figure 5.3 below.

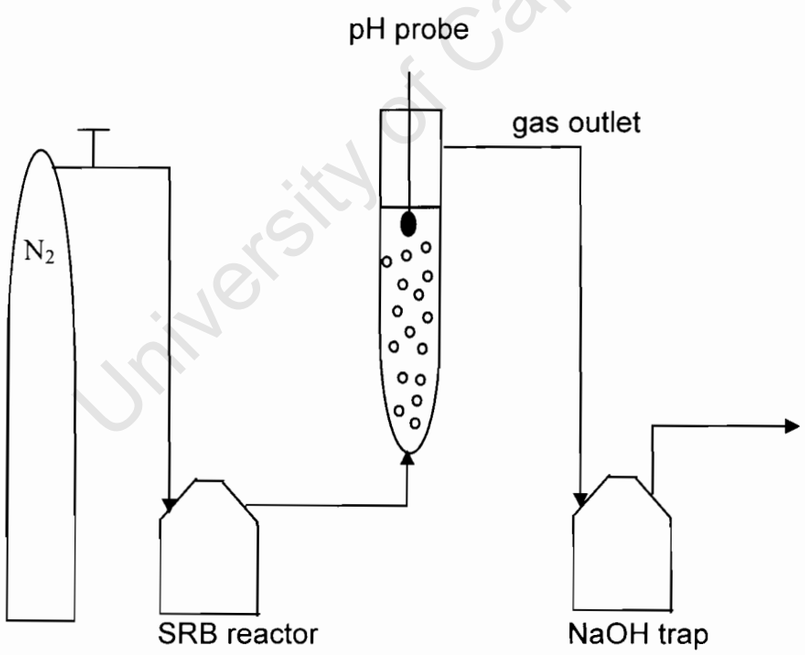

Figure 5.3 Schematic representation of biologically produced H_2S for precipitation

The precipitation reactor consists of a cylindrical glass column which is 1m high and has a 50mm ID.

Although the process was batch in terms of the metal stream, it has been included in this section as an introduction to the next set-up investigated. This experimental set-up allowed precipitation rate data to be determined using a gaseous source.

Nitrogen gas was sparged at a constant flowrate, through a reactor containing a mixed culture of sulphate reducing bacteria (SRB) producing a sulphide by-product. The SRB reactor was not part of the original plan of experiments but provided a means for quick H_2S generation when required.

Due to liquid-gas equilibrium, gaseous H_2S was formed in the SRB reactors. This generation was dependent on two predominant factors: 1) sulphide concentrations in the liquid phase and 2) the pH of the liquid media. High sulphide concentrations resulted in higher H_2S generation, whilst a high pH tends to lower the amount of H_2S released largely due to the speciation of the sulphide.

The N_2-H_2S mixture was passed through the precipitation reactor with gas distribution achieved by means of an airstone fitted to the bottom of the column. Unreacted H_2S was passed into a NaOH trap before releasing the scrubbed N_2 gas.

Because of the varying conditions inside the SRB reactor, tests were conducted by passing the generated H_2S directly into the NaOH trap. The NaOH trap had a concentration of 0.125**M**. The increase in the sulphide concentrations in the NaOH trap was measured by the methyl blue indicator test (standard analytical sulphide measurement), reading the absorbance (using a Ultrospec 1100pro) at 670nm.

Data from these runs were used to formulate a predictive mathematical model based on the pH and concentrations inside the SRB reactor. The model (see figure 5.4 below) was based on a best fit of 7 experimental runs under varying conditions. The model equation used was:

$$Y = a\exp(b * Conc + c * pH^2) \quad (5.1)$$

Y = Sulphide concentration in NaOH trap (mg/l)
Conc and pH are conditions measured inside the SRB reactor
a, b, c = time dependent constants

This relationship was used as a calibration for expected sulphide increases in the NaOH trap. Any differences could thus be attributed to the precipitation reactions.

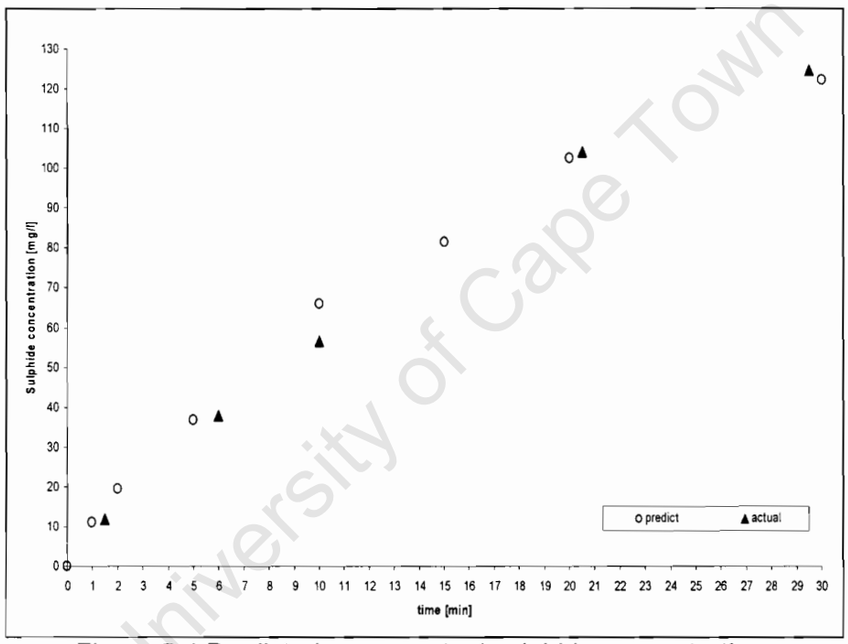

Figure 5.4 Predicted versus actual sulphide concentrations

For precipitation with the gaseous species, the following reactions could be written

$$NiSO_4 + H_2S \Rightarrow NiS + H_2SO_4 \quad (5.2)$$

$$CoSO_4 + H_2S \Rightarrow CoS + H_2SO_4 \quad (5.3)$$

Acid production from the above reactions would tend to decrease the pH of the precipitating solution, resulting in lower H_2S utilisation rates. At low pH values, sulphide equilibrium tends to the formation of $H_2S(aq)$, which can then be released through the gaseous phase (see chapter 3). Thus, under these conditions, little soluble sulphide would be available.

This necessitated the need for pH control in the precipitation reactor in order to ensure the availability of soluble sulphide species. Under batch operation, this was achieved with the addition of $CaCO_3$ which acted as a buffer during the acid formation.

5.2.3 Mixture of 10% H_2S and 90% N_2

The experimental set-up employed in this part of the research is similar to the previous set-up, however, the SRB reactor has been replaced by a gas cylinder comprising of 10% (± 3%) H_2S with N_2 making up the rest. The gas was dispersed using an airstone fitted to the bottom of the column, as with the previous set-up.

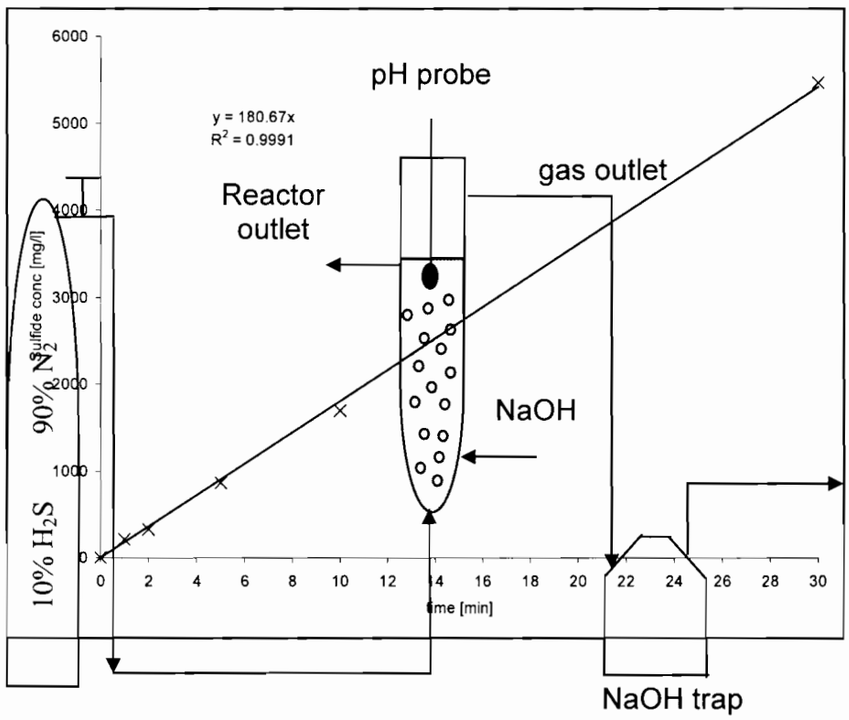

Figure 5.5 Schematic representation of final set-up investigated

Figure 5.6 Sulphide standard increase using a gas cylinder

Similar to the previous set-up, a sulphide standard curve was produced by passing the gas into a NaOH trap at a fixed flowrate, allowing a reference for any sulphide lost due to reaction. Because of a constant sulphide supply, the correlation shows a straight line (see figure 5.6).

Methodology used in the set-up is similar to the previously investigated set-up. The metal stream was operated in batch mode, as the reactor did not allow enough settling time for formed precipitates. The volume of liquid added to the reactor was 700ml. The precipitate product was thus transferred to Imhoff

settling cones once the experiment was stopped to determine the settling rates.

In contrast from the previous set-up, the pH was adjusted by means of the addition of NaOH at calculated rates depending on the acid production rates from preliminary experiments.

5.3 Experimental progress

Table 5.2 All planned experimental conditions investigated in this report

Experiment number	Objective	Method	Conditions
A1-A7	Reaction and settling kinetics	Batch (reaction) Imhoff cones (settling)	$[Ni^{2+}]$ = 200 & 2000ppm $[Co^{2+}]$ = 100 & 1000ppm $[S^{2-}]$ /$[Me^{2+}]$ = 1
B1	Maximise metal recovery Minimise fines formation (low concentrations)	Fluidised bed reactor	$[Me^{2+}]_{total}$ = 200ppm Q_{feed}= Q_{Na2S} = 50ml/min $[S^{2-}]$ /$[Me^{2+}]$ = 1 $Q_{recycle}$ = 50ml/min [**Recycle ratio** = 1]
B2	Maximise metal recovery Minimise fines formation (high concentrations)	Fluidised bed reactor	$[Me^{2+}]_{total}$ = 3000ppm Q_{feed}= Q_{Na2S} = 75ml/min $[S^{2-}]$ /$[Me^{2+}]$ = 1 $Q_{recycle}$ = 75ml/min [**Recycle ratio** = 1]
C1	Maximise metal recovery Minimise fines formation (high concentrations)	2 x Fluidised bed reactors in series	$[Me^{2+}]_{total}$ = 2000ppm Q_{feed} =Q_{Na2S} = 35ml/min $[S^{2-}]$ /$[Me^{2+}]$ = 1.5 $Q_{recycle}$ = 70ml/min [**Recycle Ratio** = 2]
D1 D2	Reduce S using biologically generated hydrogen sulphide	SRB reactor with precipitation column reactor	$[Me^{2+}]_{total}$ = 200ppm Q_{N2} = 1l/min No $CaCO_3$
D3	Reduce S using biologically generated hydrogen sulphide	SRB reactor with precipitation column reactor	$[Me^{2+}]_{total}$ = 200ppm Q_{N2} = 1l/min 15g $CaCO_3$
D4 – D6	Reduce S using gaseous hydrogen sulphide	Gas mixture from cylinder with column reactor	$[Me^{2+}]_{total}$ = 2000ppm Q_{gas} = 1l/min Q_{feed} = (variable depending on experiment) Q_{NaOH} = (variable depending on desired pH)

Chapter 6

Results and Discussion

This chapter discusses results that were obtained during this investigation. It follows discussions of metal removal for the various systems investigated, the kinetics of each system as well as the settling rates for different precipitates.

6.1 Batch Results

Batch experiments were conducted in order to investigate and understand the kinetics of the precipitation processes involved. In general, the kinetics of precipitation are almost instantaneous and not easy to calculate according to the integrated rate laws. This is largely because data acquisition is difficult over the short reaction times. Equilibrium is usually reached within the first few minutes (even seconds) of operation, especially for the sulphide system.

Conditions investigated are presented in Table 6.1 below:

Table 6.1 Experimental conditions investigated for batch experiments

Experiment number	$[Co^{2+}]$ (ppm)	$[Ni^{2+}]$ (ppm)	V_{Me2+} (ml)	$[S^{2-}]$ (**M**)	V_{S2-} (ml)	$Me^{2+}:S^{2-}$
A1	108	217	500	0.1	27.25	1:1
A2	109	216	500	0.05	54.50	1:1
A3	107	211	500	0.01	272.40	1:1
A4	1080	2170	100	0.1	54.50	1:1
A5	1090	2160	100	0.05	108.99	1:1
A6	1070	2110	100	0.01	544.97	1:1
A7	109.5	216.78	500	0.05	65	1:1.2

It should be noted that the reported concentrations are actual concentrations as measured by AAS and not the concentrations as reported in chapter 5, section 5.3.

The measured metal removal versus time for filtered samples for the various conditions above are given in Figures 6.1 and 6.2

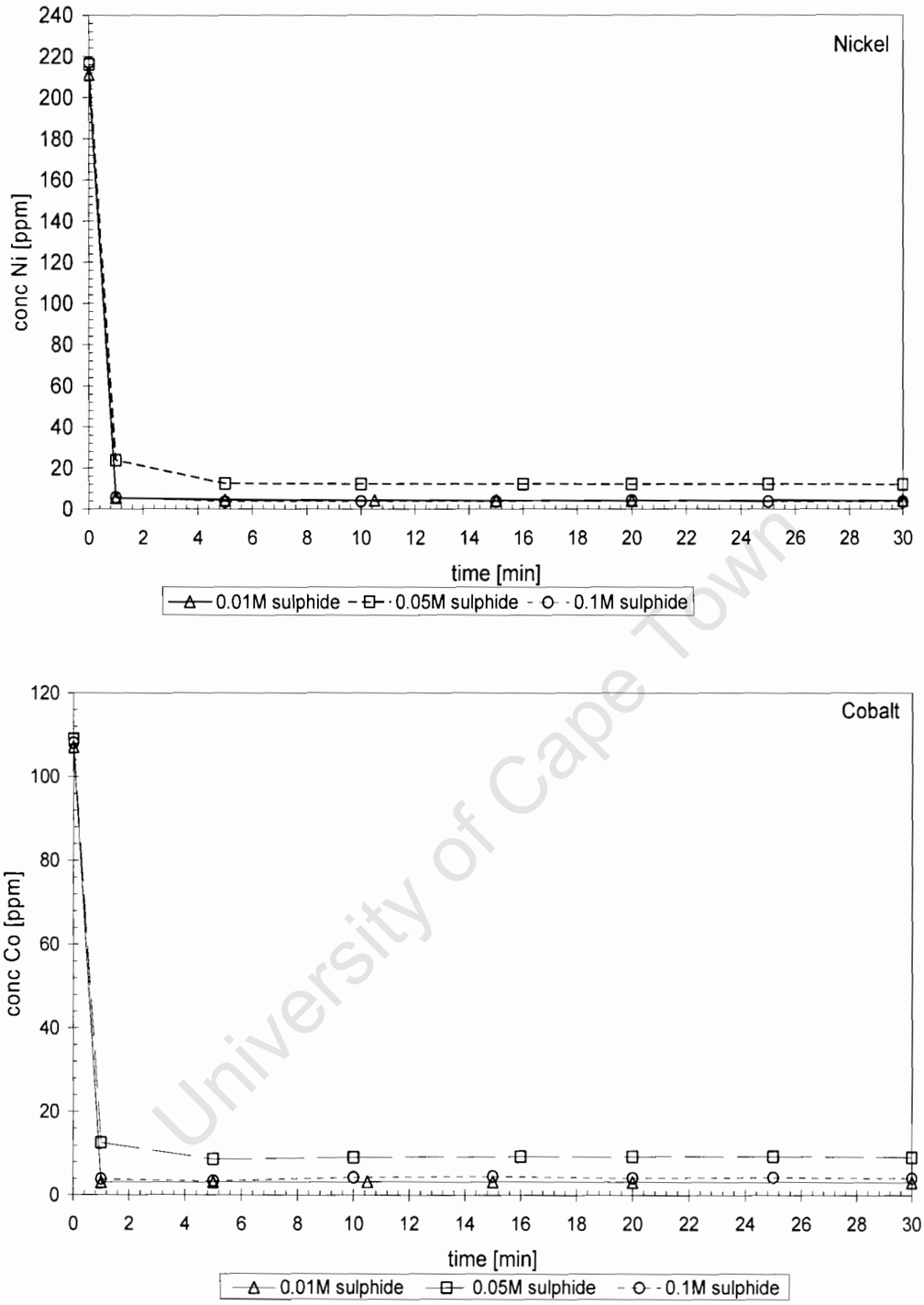

Figure 6.1 Metal removal versus time for experiments A1-A3

Characteristic of both figures is the rapid extent of the reaction within the first minute of sulphide addition with equilibrium being reached after 5 minutes for all experiments.

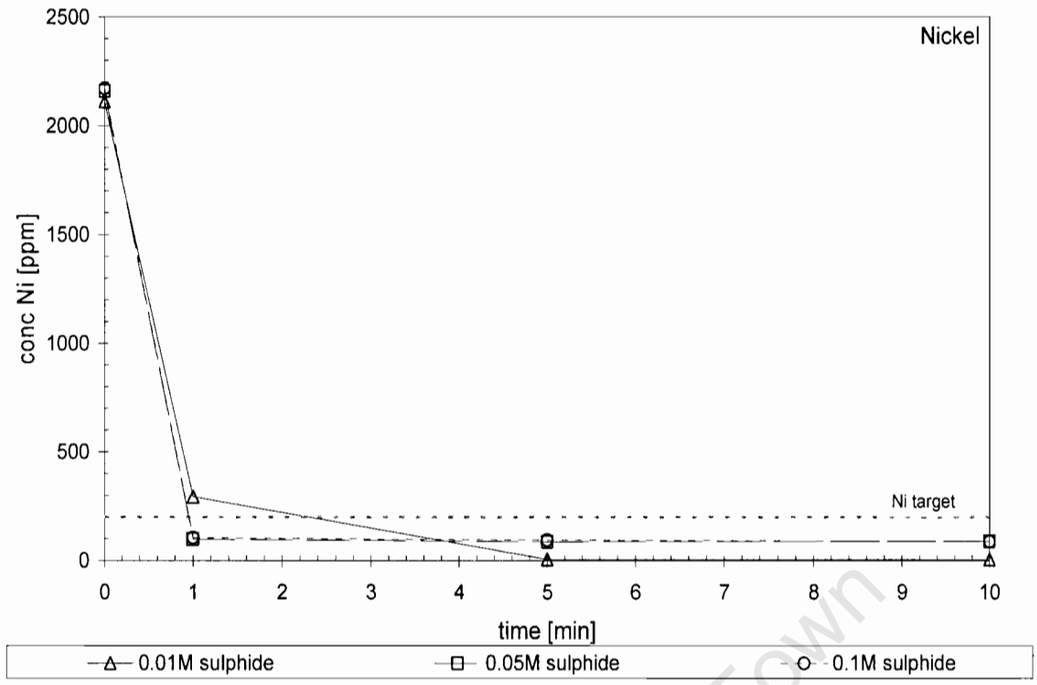

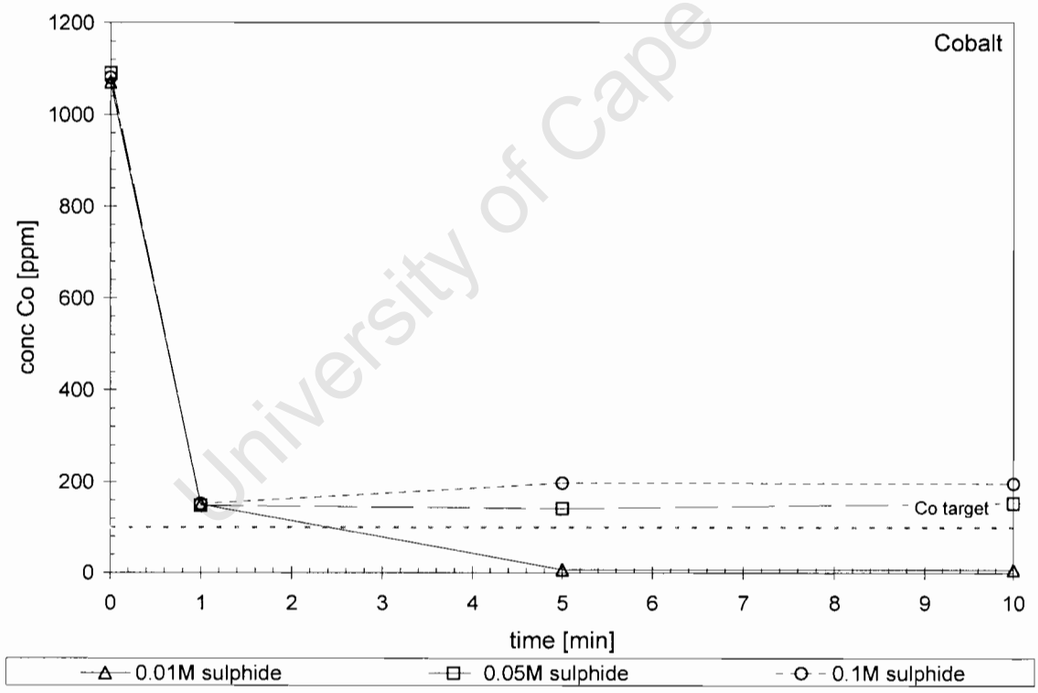

Figure 6.2 Metal removal versus time for experiments A4-A6

Removal of approximately 90% on average for both metals was achieved for all experiments. It is assumed that the reaction kinetics of metal to sulphide follow a stoichiometric reaction ratio of 1 mole metal reacting with 1 mole of sulphide. Thus all of the metal should theoretically have been removed in experiments A1-A6.

Possible discrepancies could arise from sulphide losses to gaseous H_2S that could have occurred at the top of the beakers used. This would have been detected by smelling sulphide during the experiments.

Experiment A7 was conducted to test if the sulphide concentration was limiting and if complete metal removal could be achieved. 20% excess sulphide was arbitrarily chosen and added to the metal mixture. Results are shown in Figure 6.3.

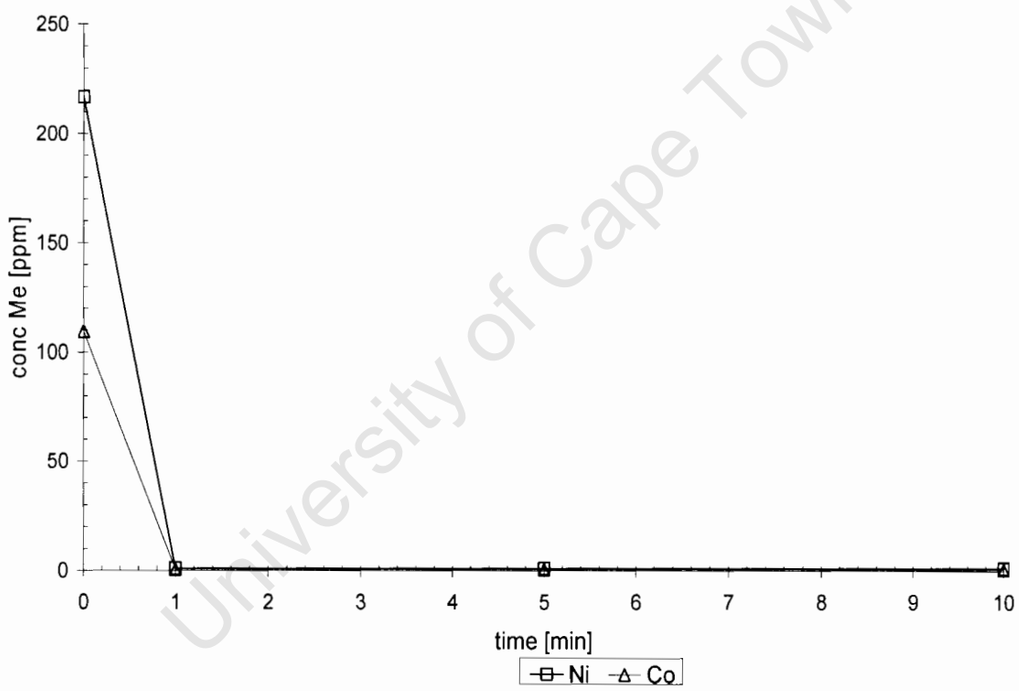

Figure 6.3 Metal removal with 20% excess sulphide (Experiment A7)

The concentrations of both metals are shown to decrease within the first minute of operation to less than 1ppm. This was also the detection limit of the analytical instrument.

Measurement of the sulphide content in the aqueous media showed that there was no significant sulphide remaining in solution ($1.92x10^{-5}$**M**) and this relates to approximately 99.67% sulphide conversion. Although this is similar to the metal conversion, the loss of the additional 20% added is not accounted for, indicating a loss of sulphide, the formation of an aqueous polysulfide species which could not be detected by the sulphide test or the formation of a polysulphide solid.

Aqueous polysulphide species have been identified by Shea and Heltz (1988) for the copper system, and described in van Hille et al (2005). However, there are no comparable studies for the nickel and cobalt sulphide system.

For a solid polysulphide species, and specifically a metal sulphide of the form Me_xS_y, the ratio $^x/_y$ does not equal unity. It is further hypothesised that the ratio might be less than unity, with a higher sulphide content than expected. The precipitated nickel (and cobalt) sulphides could also exist in various $^x/_y$ ratios such that the final precipitate mass contains a mixture of sulphides. A common case for nickel is the formation of NiS_2 during precipitation. Such sulphides would have led to the overall $^x/_y$ ratio being reduced from unity. NiS_2 is insoluble in HCl and this could also help to explain why fines in later experiments of the fluidised bed system could not be measured.

6.2 Fluidised bed Results

Nickel and cobalt concentrations were measured as filtered and unfiltered samples. Fines in the system indicate the inefficiency of the process, high concentration of fines indicating low process efficiency. Initial experiments were conducted in a seeded fluidised bed reactor to determine which parameters have the most significant effect on the process. These conditions are shown in table 6.2 below

Table 6.2 Initial experimental conditions for fluidised bed reactor (fresh feed to reactor)

Variable	value
$[Ni^{2+}]$	120 ppm
$[Co^{2+}]$	50 ppm
Metal stream feed flowrate	50 ml/min
$[Me^{2+}]:[S^{2-}]$	1:1.46
Sulphide feed rate ($[S^{2-}]$ = 136ppm)	50 ml/min
Recycle ratio (recycled flow/fresh feed)	1

Under these conditions though, a large quantity of fines were formed due to either homogenous nucleation or attrition. The supersaturation is calculated below using activity coefficients calculated using OLI (OLI Systems Inc, 2003) Software. Then, with reference to each metal, the calculated supersaturations were

$$S_{Ni} = \frac{\gamma_{Ni}[Ni^{2+}]\gamma_S[S^{2-}]}{K_{sp,NiS}} = \frac{0.807*(2.04*10^{-3})*0.807(4.25*10^{-3})}{1*10^{-19.4}} = 1.42x10^{14}$$

$$S_{Co} = \frac{\gamma_{Co}[Co^{2+}]\gamma_S[S^{2-}]}{K_{sp,CoS}} = \frac{0.870*(0.848*10^{-3})*0.869*(4.25*10^{-3})}{1*10^{-21.3}} = 5.44x10^{15}$$

Results are shown in Figure 6.4, where a difference in the dissolved and total metal concentrations indicating fines formation is clearly observed.

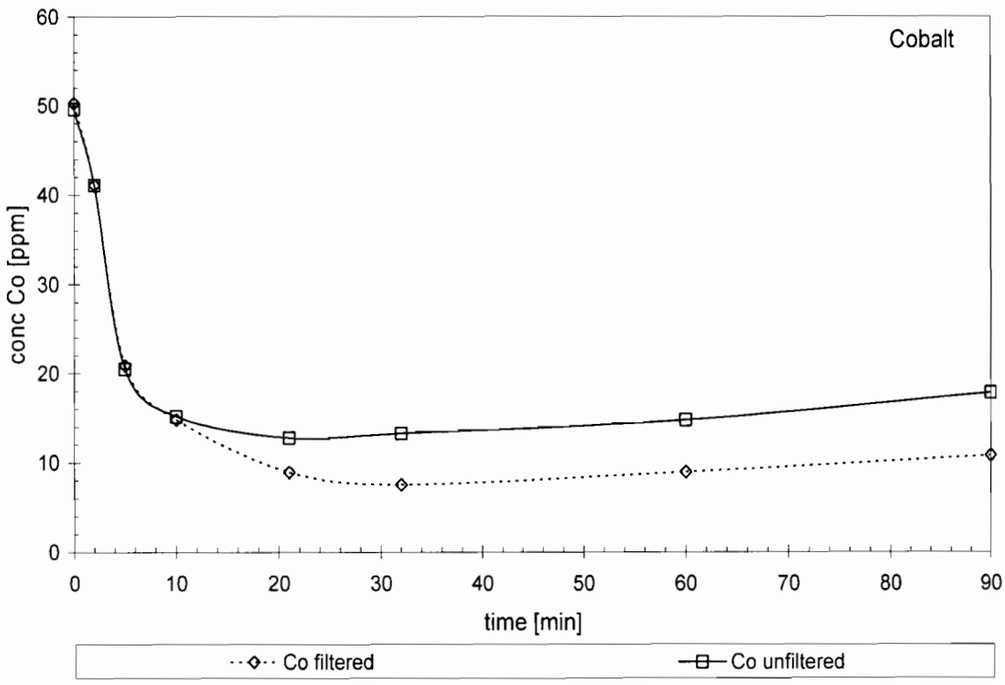

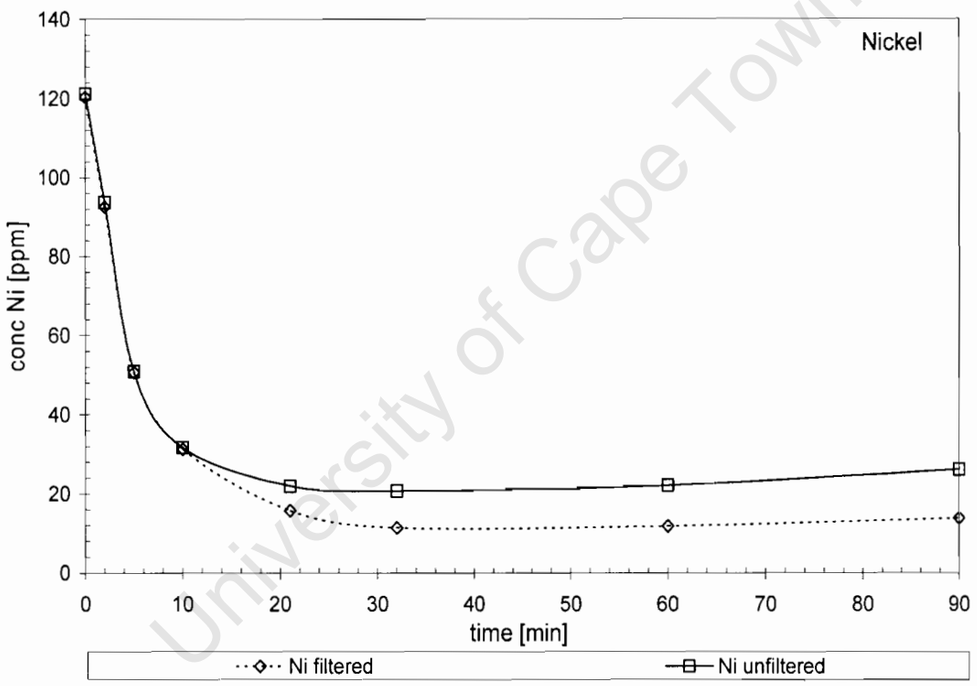

Figure 6.4 Metal removal in first fluidised bed experimental run

It is observed that, at approximately 10 minutes, the onset of fines occurs, and further removal of these fines from solution could not be achieved inside the fluidised bed reactor. This could be because of a high level of homogenous

nucleation. Another source for the high level of fines could be the turbulent conditions established inside the reactor that could result in the attrition of precipitates already adhered to the bed material. This has been shown for the case of nickel carbonate in a fluidised bed reactor (Taty-Costodes et al, 2004).

Conversion in the fluidised bed gave similar results to the batch experiments with approximately 90% and 85% of nickel and cobalt removed respectively. Although the decrease in the cobalt conversion with time was noted, the effect has not been investigated further. It was thought that conditions inside the reactor were of such a nature that the precipitate was an amorphous cobalt sulphide and thus redissolved. Cobalt sulphide (as well as nickel sulphide) occurs in 3 polymorphs (α, β and γ), each having its own solubility. Conditions (especially local conditions at the inlets) could have favoured one of the unstable forms which redissolved before forming the more favoured stable cobalt sulphide.

A statistically designed experimental programme was implemented to optimise operating conditions inside the fluidised bed reactor. Factors were taken from literature sources (Seckler, 1996) as well as the M.Sc dissertations of Guillard (2001) and Peterson (2002). Important factors were the feed flowrate, the metal-sulphide ratio as well as the recirculation ratio.

Peterson (2002) kept a ratio of metal feed to sulphide feed equalling unity. This was largely because of the supersaturation effects caused by high concentration sulphide feeds at lower flowrates. To minimise supersaturation effects at the feed inlet points, lower sulphide concentrations were employed.

For the statistical design, the range of values investigated should be such that the local maximum or minimum would be expected to be found within the region of interest. The next part of the investigation was to conduct scoping studies to find the range of interest for the operation.

The numerous conditions that were investigated are not reported in this investigation merely because of many operational problems experienced during the running of each experiment. Nonetheless, all of the experiments resulted in the formation of particulate fines in the outlet stream. Results for conditions shown in Table 6.3 are plotted in Figure 6.5

Table 6.3 Experimental conditions preceding the statistical design (fresh feed into the reactor)

Variable	value
$[Ni^{2+}]$	2000 ppm
$[Co^{2+}]$	1000 ppm
Metal feed rate	75 ml/min
$[Me^{2+}]:[S^{2-}]$	1:1 *(overall)*
Sulphide feed rate	75 ml/min
Recycle ratio	1

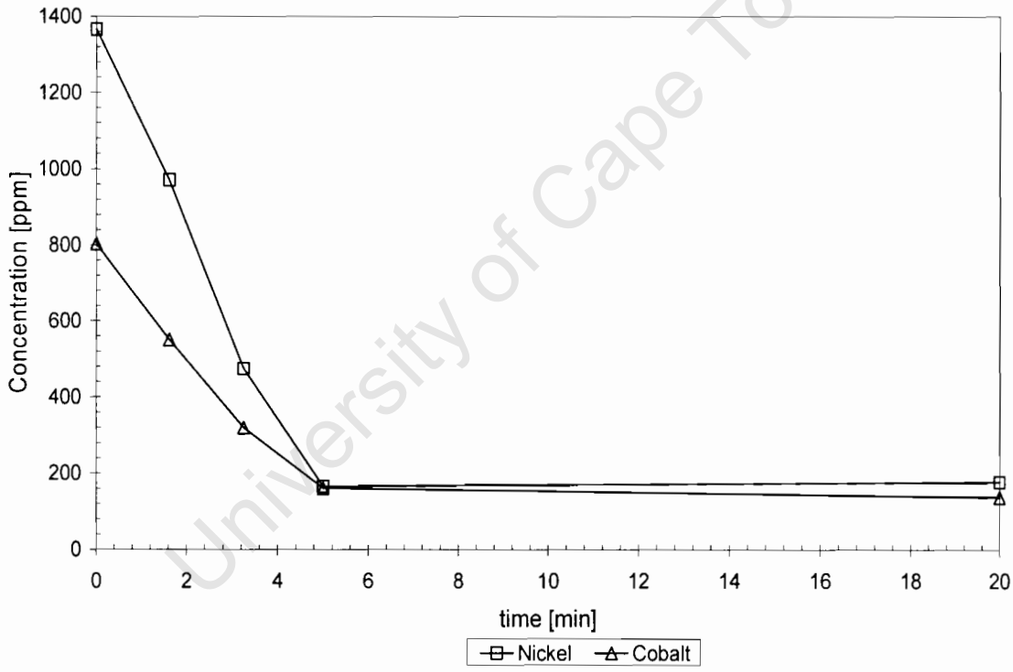

Figure 6.5 Metal conversion versus time for conditions in table 6.3

Under these conditions, the supersaturation for each metal (and assuming that the activity coefficients would not differ greatly) was

$$S_{Ni} = \frac{\gamma_{Ni}[Ni^{2+}]\gamma_S[S^{2-}]}{K_{sp,NiS}} = \frac{0.807*(0.0281)*0.807*(0.041)}{1*10^{-19.4}} = 1.88x10^{16}$$

$$S_{Co} = \frac{\gamma_{Co}[Co^{2+}]\gamma_S[S^{2-}]}{K_{sp,CoS}} = \frac{0.870*(0.0130)*0.869*(0.041)}{1*10^{-21.3}} = 0.807x10^{18}$$

This indicates a higher supersaturation than the initial experiments and it would thus be expected to produce more fines. Preconditioning of the incoming metal stream to dilute it to reduce supersaturation effects was not investigated as the treatment of high concentration streams was the main focus of this investigation.

Conversions of approximately 85% and 82% for nickel and cobalt respectively were achieved. Peterson (2002) in her results showed that the flowrate was less significant than other factors (recycle ratio, feed concentration and metal to sulphide ratio) in optimising the process. Thus the flowrate increase in table 6.3 should have no significant effect in minimising the fines formation.

Omitted from this figure is the total concentration (fines plus dissolved) for each metal. Filtered samples contained particulate fines which were insoluble in HCl. The fines persisted even after allowing them to settle and treating the settled product with HCl. Various references indicate that NiS and CoS both dissolve if treated with concentrated HCl. However this could not be achieved. As stated earlier with the batch results, the possibility of the formation of an insoluble sulphide species might be possible with a mixture of sulphide precipitates in the final product.

It is hypothesised that the conditions inside the fluidised bed reactor are not suitable for high concentration streams, because under any conditions, the supersaturation would be too high and the bed material would be coated immediately, and thus, a thick coating would be formed on the seed. This would significantly increase the potential for loss of the coating due to attrition.

To test if dislodged precipitates would re-attach onto fresh bed material, effluent from the first reactor column was pumped into a second column in series under the same conditions; however, no sulphide was added to the second column. This process was merely a physi-sorption filtering stage and follows a similar set-up investigated by Zhou et al (1999).

A small uptake of the precipitate onto the fresh bed material was achieved. As a further case to highlight attrition inside the fluidised bed reactor, fines exiting the second reactor were much smaller than those entering it. This was evidenced by the fact that samples from the first reactor could be filtered through a 0.45μm nylon filter; however, those from the second reactor could not. This shows that attrition of the coating also leads to significant fines formation.

Under lower flow conditions, higher metal removal was achieved, thus contradicting the work done by Peterson (2002) and showing a dependency of the removal efficiency on the inlet flowrate. However, it should be noted that under lower flowrates, the possibility of the dissolved metal species chemically absorbing to the bed material is also increased because of longer retention times inside the bed. Examples of chemical absorption of metal species onto clay and other sand or mineral deposits are abundant in literature, and could also have played a significant part in the work investigated here. Metal uptake by the bed material has also been reported by Peterson (2002).

Lower flow conditions also lead to reduced turbulence, reduced collisions and thus a reduced tendency for fines formation due to attrition. The lower upflow velocity also reduces fluidisation, resulting in the bed acting as a "combination" of a packed bed and a fluidised bed reactor, with only the lighter particles being fluidised. The packed bed portion would then act as a filtration medium.

6.3 Gaseous H_2S Results

Conditions investigated are reported in table 6.4

Table 6.4 Experimental conditions investigated for gaseous sulphide studies

Experiment number	$[Co^{2+}]$ (ppm)	$[Ni^{2+}]$ (ppm)	Gas flow (l/min)	pH
D1	60.2	130.2	1	6.1 (initial) *not controlled*
D2	108	233.1	1	11.49 (initial) *not controlled*
D3	102.4	218.2	1	5.43 (initial) *$CaCO_3$ buffered*
D4	989.2	1917.2	1	6.78 (initial) *variable*
D5	996	2084.2	1	3.3 (controlled)
D6	1009.7	2051.4	1	7.1 (controlled)

Experiments D1 to D3 were conducted using biogenically produced hydrogen sulphide. The lower concentrations for the metals investigated was because of the small scale of the sulphate reducing bacteria (SRB) reactor. This system was used to characterise the gaseous continuous system (similar to the batch studies previously conducted).

Results for experiments D1 and D2 are presented in Figures 6.6 and 6.7.

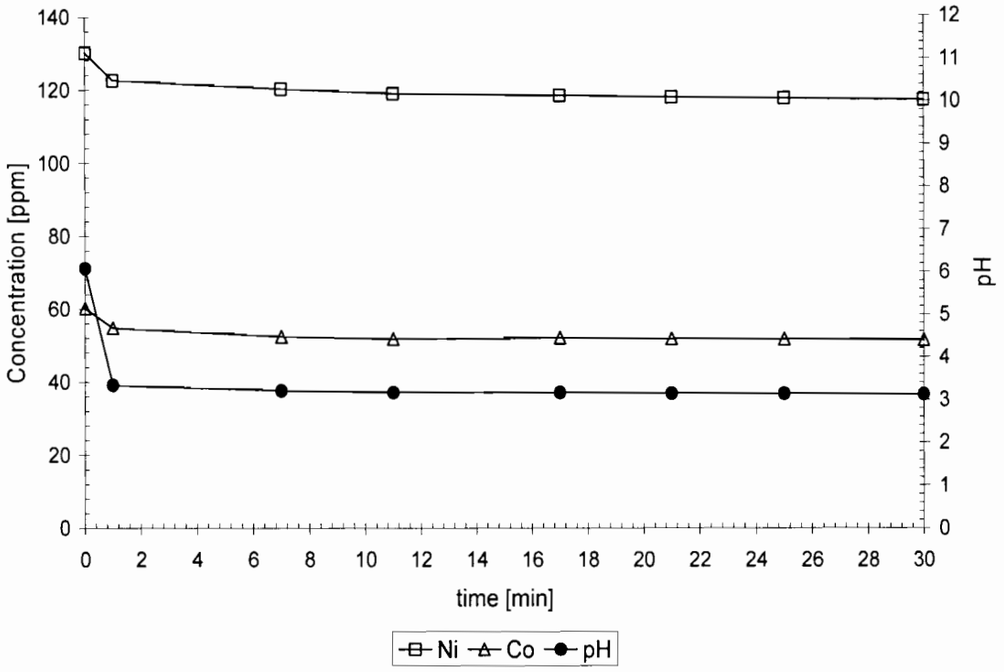

Figure 6.6 Experimental results for experiment D1 (dissolved concentrations)

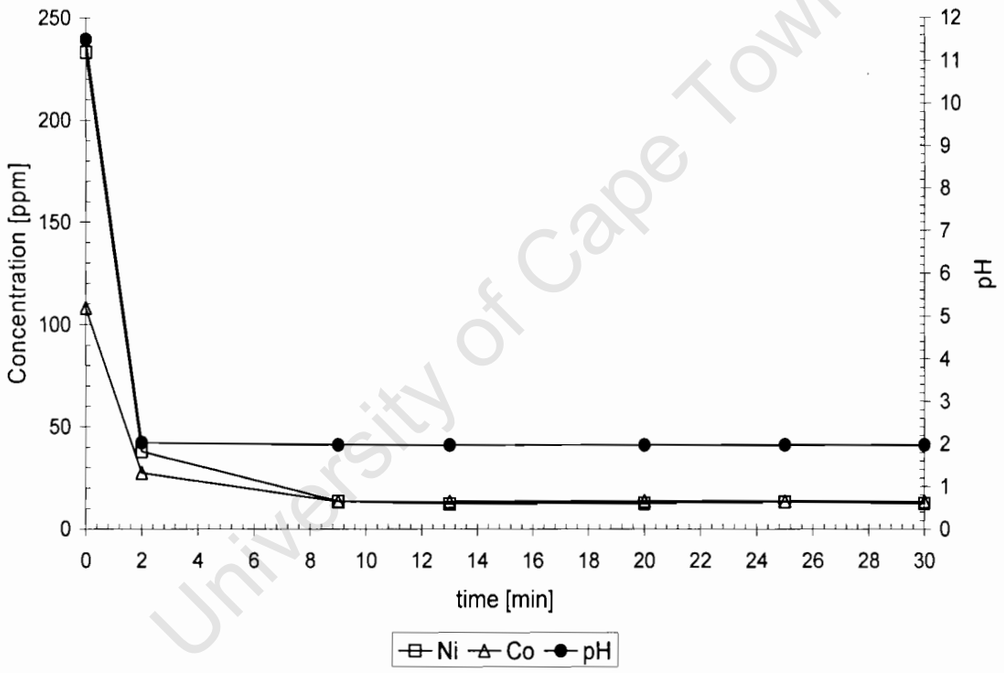

Figure 6.7 Experimental results for experiment D2

The sharp decrease in pH is observed for both experiments due to $Ni^{2+} + HS^{-} \rightarrow NiS + H^{+}$. The decrease in pH to below 7 resulted in the

metal removal dropping to below 15%. This is due to a decrease in the availability of soluble sulphide species at lower pH values (see chapter 4).

The low removal efficiency achieved in experiment D1 was largely due to the low initial pH. At a pH of 6, the dissolution rate of $H_2S(g)$ to $H_2S(aq)$ is too slow, thus very little soluble sulphide is available for precipitation. This allowed most of the H_2S to pass through the system without reacting. Because there is not a constant flow of H_2S from the SRB reactors, the rate is extremely fast in the first minute as the H_2S is introduced. If this initial removal is low, the overall removal over time also tends to remain low.

The high initial pH for experiment D2 resulted in some hydroxide precipitation occurring inside the reactor However, because of the higher reactivity of the sulphide ion, a displacement reaction takes place according to

$$Me(OH)_2 + H_2S \rightarrow MeS + 2H_2O \quad (6.1)$$

This was observed when the precipitate changed colour from the hydroxide gelatinous precipitate to the characteristic black precipitate of metal sulphide precipitates.

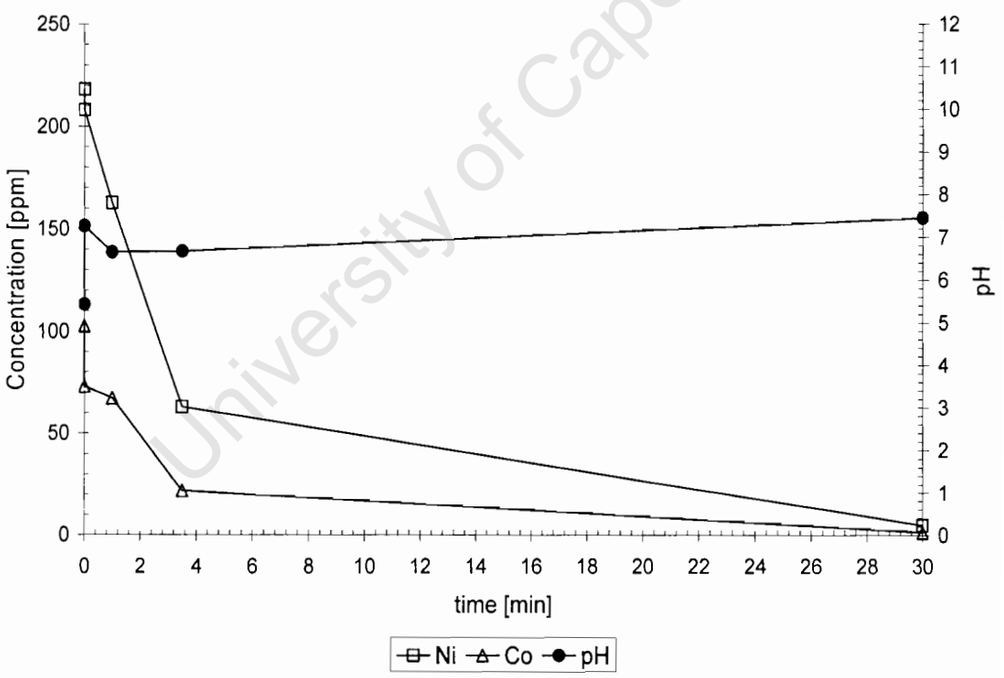

Figure 6.8 Experimental results for experiment D3

Results for experiment D3 are reported in Figure 6.8, where pH control was achieved by $CaCO_3$ addition to the column before starting the experiment. The beneficial effects of pH adjustments on metal removal indicate that pH control would be important for efficient metal removal over time. This was especially observed for experiments D1 and D2 where the initial pH resulted in different removal efficiencies.

Results for experiments D4 to D6 are reported in Figures 6.10 to 6.12. A similar trend is noticed in all the experiments in that there is an initial decrease in the pH before steady-state pH control. This is largely due to the rapid reaction of the sulphide species according to the reaction

$$MeSO_4 + H_2S \rightarrow MeS + H_2SO_4 \qquad (6.2)$$

Figure 6.9 shows the results for experiment D4, highlighting the changing pH results. The sudden rise in pH noticed at approximately 10 minutes could be explained by noting that the liquid residence time in the reactor was approximately 12 minutes per pass. With fast kinetics, a high degree of removal was achieved in less than one pass of the reactor. Because no further reaction occurs, an overdose of hydroxide ions into the system occurs. The NaOH flowrate was adjusted accordingly in the subsequent experiments.

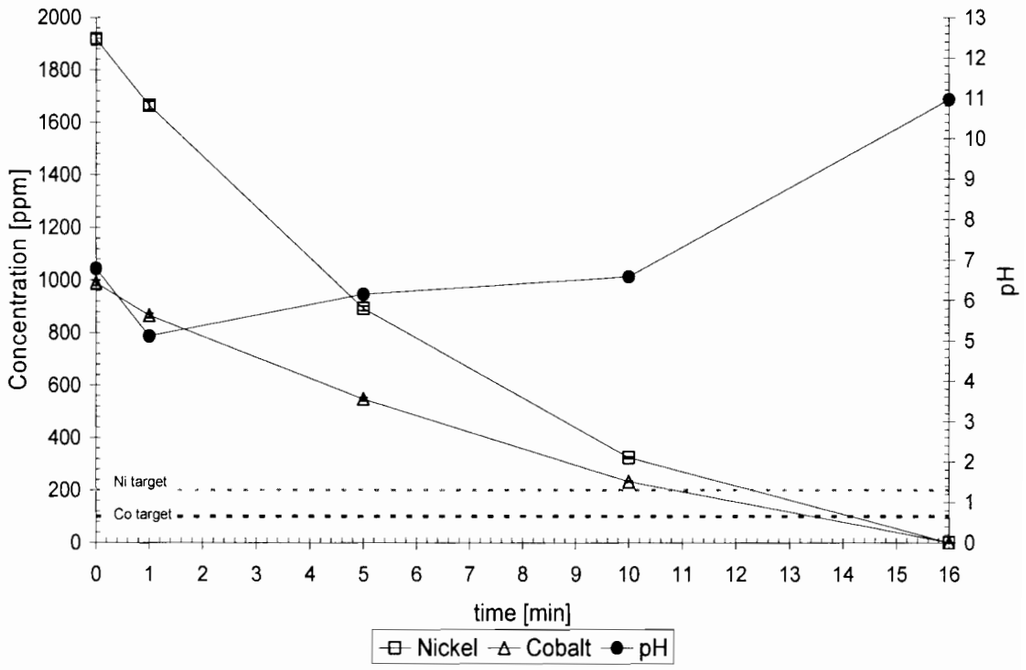

Figure 6.9 Experimental results for experiment D4

Figure 6.10 shows results obtained for experiment D5. The low pH level was maintained to highlight the dependency of the reaction kinetics on pH. Comparing with figure 6.10 where 90% removal of nickel was achieved after approximately 15 minutes, at a lower pH the same removal could only be achieved after approximately 30 minutes.

Upon comparison with figure 6.7, which was at approximately the same pH, the removal efficiency was 9 times higher after 30 minutes. This was as mentioned earlier, where the SRB reactor could not maintain a steady flowrate of H_2S and the only reaction occurred within the first few minutes of operation. This highlighted a disadvantage of using the SRB reactor in batch mode when operating in conjunction with a continuous precipitation reactor.

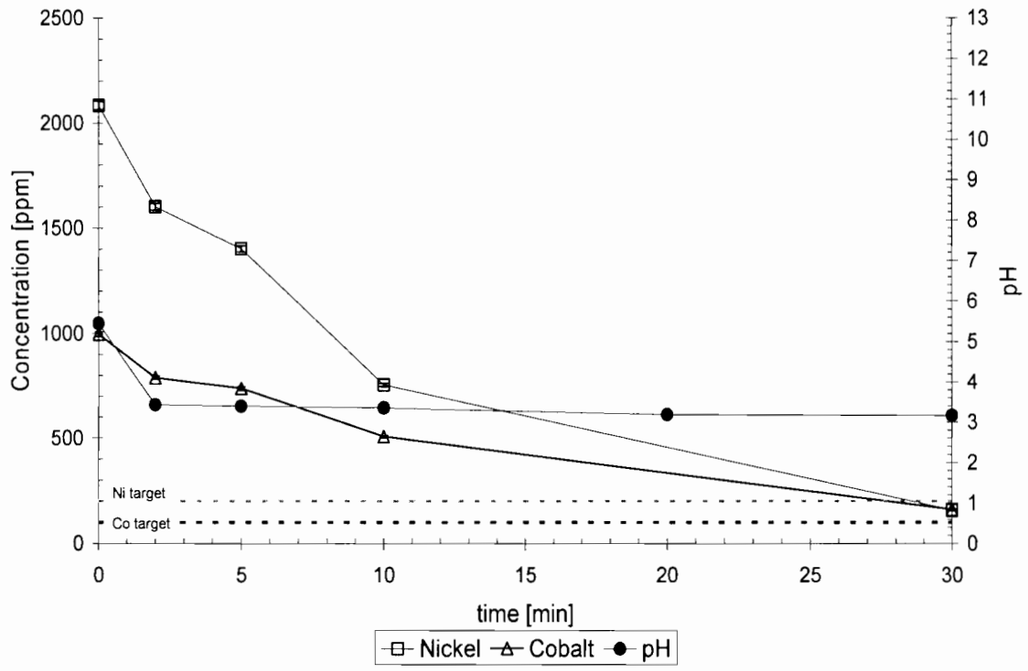

Figure 6.10 Experimental results for experiment D5

Experiment D6 is reported in Figure 6.11. Near complete removal (>99%) was achieved over time with operation at a neutral pH (pH = 7.1).

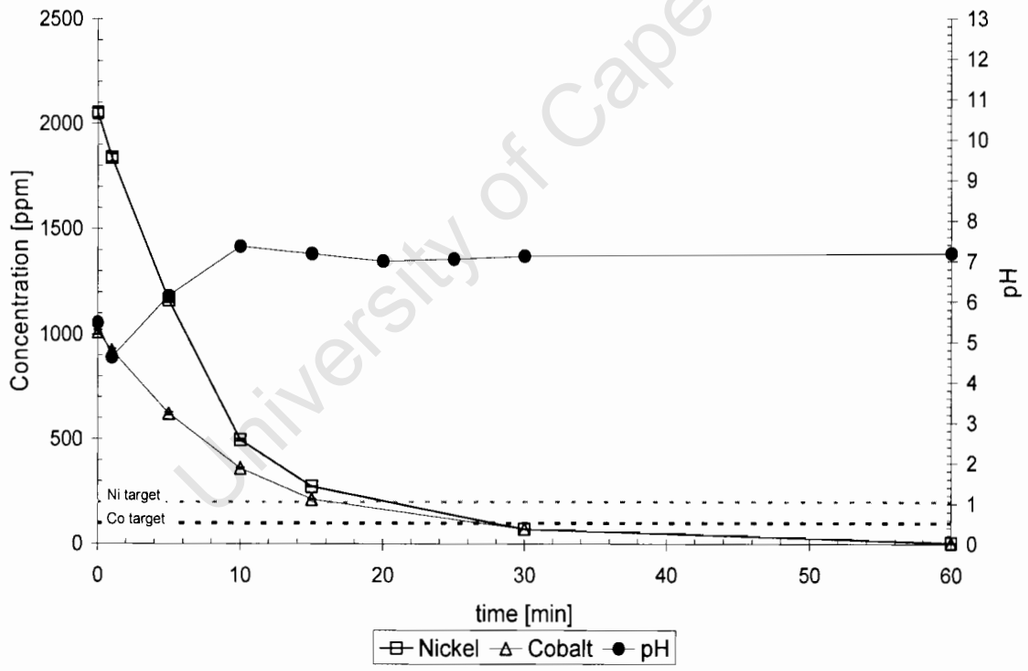

Figure 6.11 Experimental results for experiment D6

It was shown that the pH was a significant factor in metal removal. This was because of the effect of pH on sulphide speciation. As shown in chapter 4, a higher pH favours soluble sulphide species which participate in the precipitation reactions. At lower pH values, the dissolution of gaseous H_2S into solution is extremely slow. This would explain the slow rates achieved at pH = 3.

Although not shown as part of the results, it should be noted that a ***pH-controlled*** environment should be maintained for optimum metal removal. At basic pH values, the sulphide equilibrium shifts towards the more soluble S^{2-} species. In aqueous sulphide precipitation tests, it was shown that this sulphide species leads to high supersaturations. Controlling the pH should minimise the formation of this species and thus indirectly helps in controlling fines formation.

The pH also controls the kinetics of the reaction and this will be discussed separately below.

6.4 Kinetics

6.4.1 Kinetics of batch system

For an equation of the form $Me^{2+} + S^{2-} \rightarrow MeS$, trying to fit an integrated rate law to the batch data would not give very accurate results. A rate law of the form

$$-\frac{d[Me^{2+}]}{dt} = k[Me^{2+}][S^{2-}] \qquad (6.3)$$

could only be fitted to the first two data points as equilibrium is attained extremely rapidly. To increase the model accuracy, more data points have to be taken during the initial precipitation reaction. It was thus decided not to follow this path in determining the reaction kinetics.

Results from experiment A6 indicate slower kinetics and thus it was decided to apply an integrated rate law to it. Although 3 data points are still too few to confidently fit a model, this analysis is presented to demonstrate the method. Upon integration of 6.3, the rate law takes the form

$$\ln\frac{[S^{2-}]}{[Me^{2+}]} = \ln\frac{[S^{2-}]_0}{[Me^{2+}]_0} + ([S^{2-}]_0 - [Me^{2+}]_0)kt \qquad (6.4)$$

$[S^{2-}]$ = sulphide concentration at time t (mol/l)

$[Me^{2+}]$ = metal concentration at time t (mol/l)

$[S^{2-}]_0$ = initial sulphide concentration (mol/l)

$[Me^{2+}]_0$ = initial metal concentration (mol/l)

A linear plot of $\ln\frac{1}{[Me^{2+}]}$ versus time should yield a graph with slope of $([S^{2-}]_0 - [Me^{2+}]_0)k$. This plot is shown in Figure 6.12 which was generated by plotting the change in concentration over the first 5 minutes before equilibrium is reached.

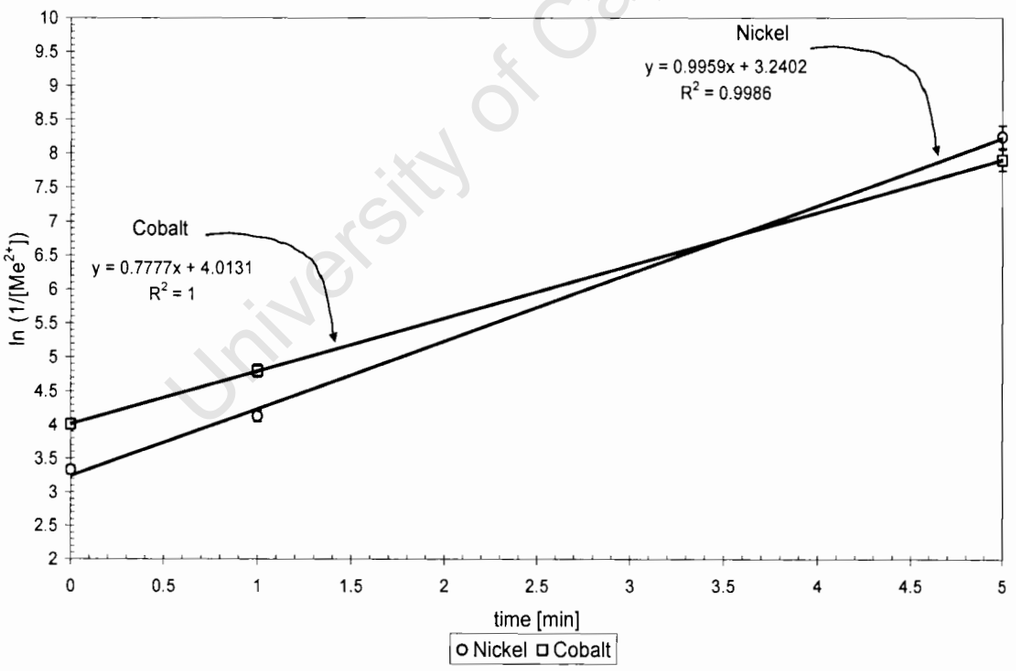

Figure 6.12 Linear plots to determine kinetics (experiment A6)

From calculations (see Appendix 2, Appendix page 16), we find that

$$k_{Ni} = 5.772 \underline{M}^{-1} s^{-1}$$

$$k_{Co} = 2.177 \underline{M}^{-1} s^{-1}$$

The rate constant for nickel precipitation is approximately 2.6 times higher than that of cobalt. This was an interesting observation seeing that Co had a lower K_{sp} value and would thus have expected to generate the higher rate.

A similar trend was observed by Bryson and Bijsterveld (1991) in their precipitation of manganese and cobalt sulphides from a sulphate stream. They observed that cobalt sulphide precipitation exhibited an induction time as well as that the removal was catalysed by the presence of previously precipitated sulphides from the same solution. The nickel sulphide would thus be expected to precipitate first before catalysing the cobalt precipitation.

6.4.2 Kinetics of fluidised bed system

Similar to the calculations of the batch kinetics as above, rate data for the fluidised bed system has also been determined and reported in Figure 6.13

From the figure the slope of the graph was determined to be 0.1375 and 0.1276 for nickel and cobalt respectively, leading to a rate constant of (see Appendix 2, Appendix Page 18)

$$k_{Ni} = 1.04 \underline{M}^{-1} s^{-1}$$

$$k_{Co} = 0.63 \underline{M}^{-1} s^{-1}$$

Lower rates are expected in this system because of the plug flow nature of the fluidised bed reactor. A more accurate measure with the batch system kinetics

would have measurements closer to the sulphide inlet points where high rates of reactions are expected.

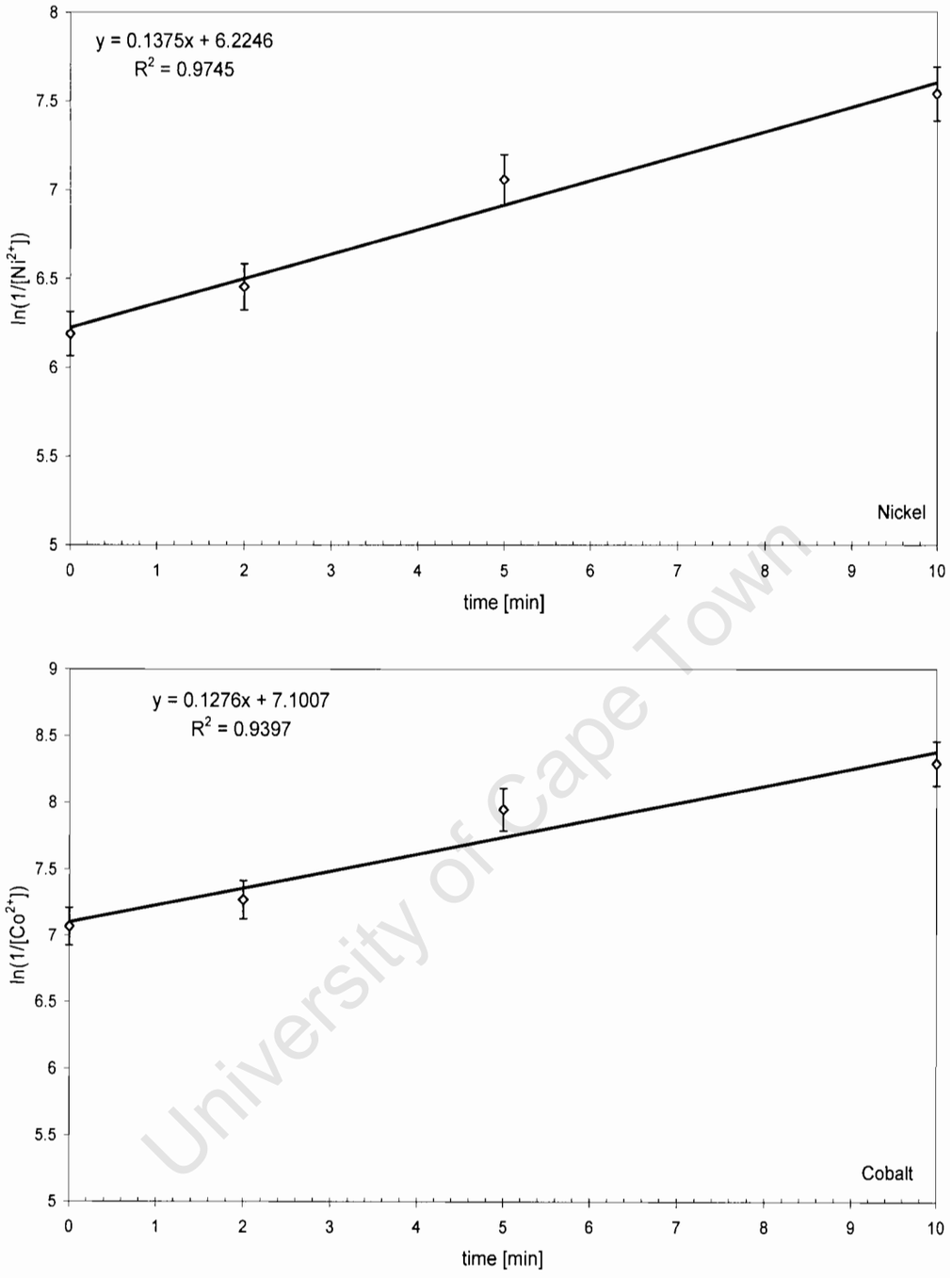

Figure 6.13 Rate kinetics for initial fluidised bed reactor experiments

From precipitation theory, a higher supersaturation results in more homogenous nucleation and consequently the formation of high level of particulate fines. Because the supersaturation in precipitation is generated by a reaction, fast reaction rates would thus imply high supersaturation and increased fines formation.

The fluidised bed reactor in this work has slower reaction kinetics than the batch experiments and thus a lower fines concentration is expected. However, this was not the case as particulate fines from the fluidised bed reactor passed through the filter. This could again be an indication of fines being formed in the reactor due to attrition.

6.4.3 Kinetics of gaseous system

Kinetics for the gaseous system will be discussed by two sets of rate laws. The first discussion will use Higbie's penetration model to determine the mass transfer coefficient. Thereafter, the rate kinetics will be discussed in accordance with the rate laws given in equation 6.3 above.

6.4.3.1 Higbie's Model

Theory has been discussed in chapter 4 and will not be repeated here. Figure 6.14 shows the linear plot for experiment D3.

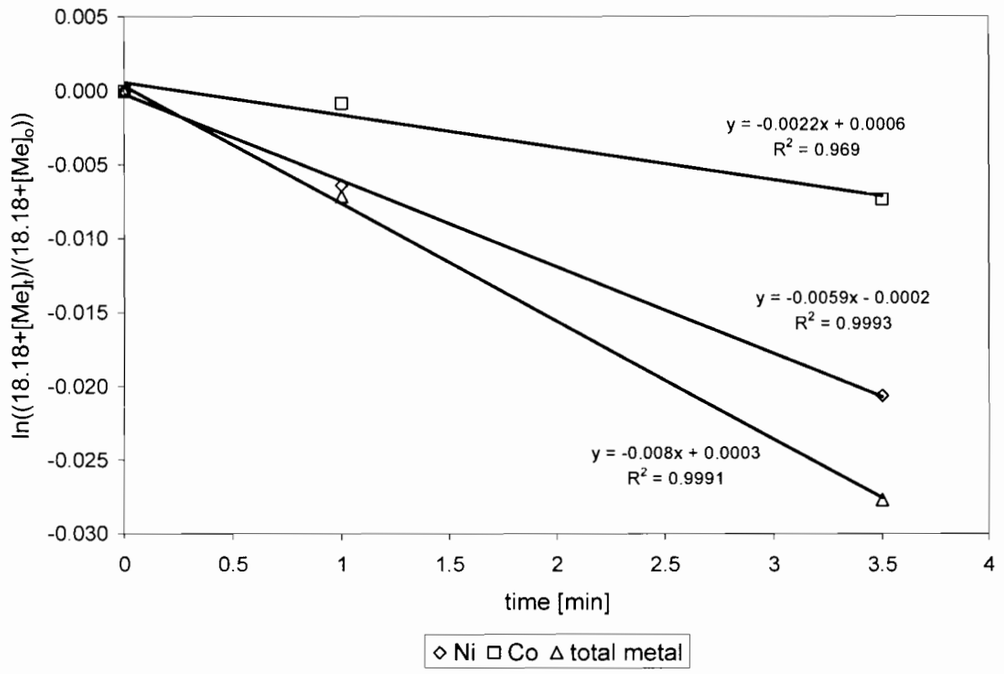

Figure 6.14 Kinetics for pH buffered system

Calculations can be followed in Appendix 2 (from Appendix Page 22). It should be noted that the mass transfer coefficient calculation is dependent on the radius of the bubbles. For ease of comparison, the theoretical prediction for k_L at r = 1mm (arbitrarily chosen) was calculated as reference. The calculated bubble diameter from experimental data was then compared to this reference. The theoretical mass transfer coefficient at r = 1mm is $k_L = 0.000358 m.s^{-1}$.

From data for experiment D3, a slope of $k = 0.008 s^{-1}$ was obtained for the combined metal concentrations. This results in a bubble radius of $r = 1.95 mm$ in comparison to calculations for the theoretical values.

This method of comparison allows two deductions to be made easily. Firstly, the further the calculated diameter deviates from r = 1mm, the less accurate the data in comparison with theory. Secondly, the smaller the bubble diameter, the larger the mass transfer area and thus the faster the rate.

Results for experiments D4 to D6 are reported in Figure 6.15. Appendix 2 (from Appendix Page 25) shows the numerical data for each metal individually.

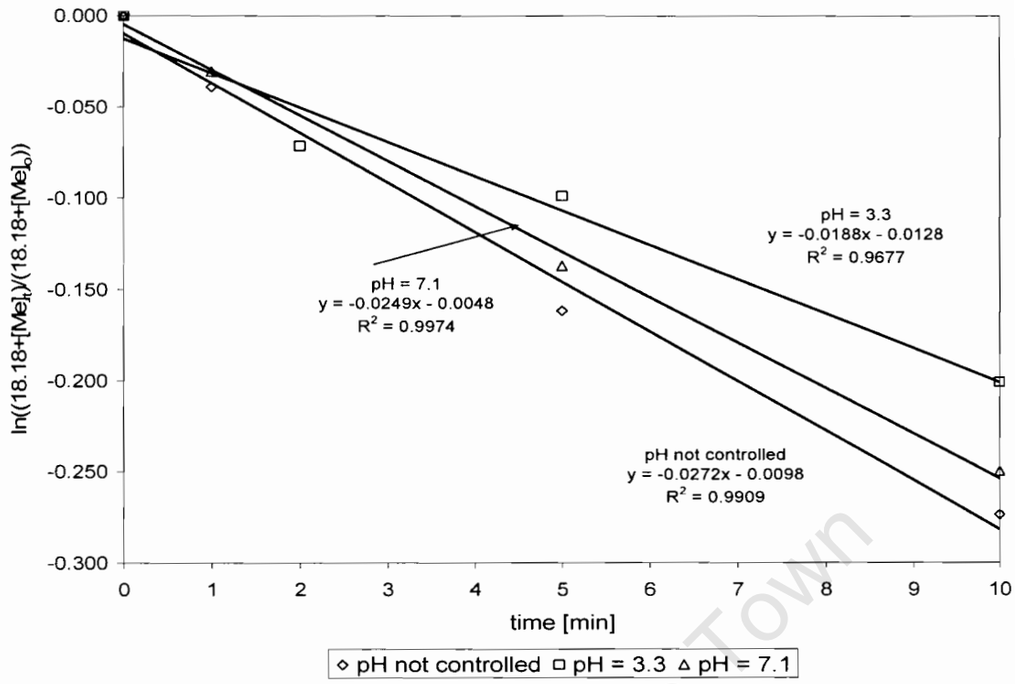

Figure 6.15 Kinetics for the combined metal stream at different pH values

Results for each experimental run with rate determination are reported in Table 6.5

Table 6.5 Kinetics for experiments D4 to D6

Experiment	pH	-k [s^{-1}]	r [mm]
D4	variable	0.0272	0.87
D5	3.3	0.0188	1.10
D6	7.1	0.0249	0.91

For higher pH values, the rate of the reaction increases. This is in accordance with literature (Al-Tarazi et al, 2004; Hammack et al, 1993).

The reaction rate is also dependent on the radius of the bubbles and this is illustrated in figure 6.16.

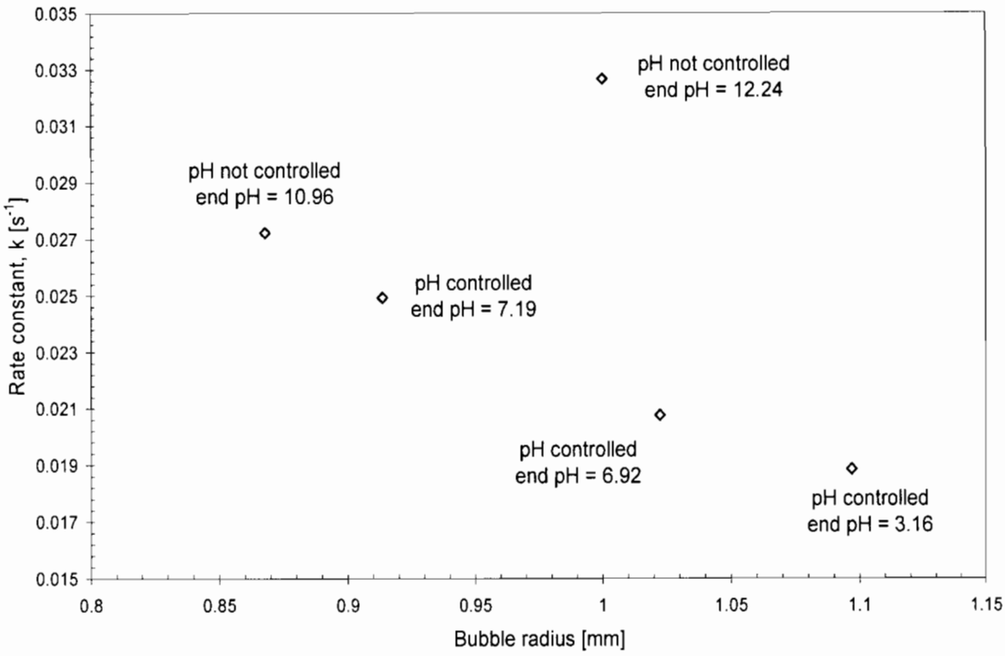

Figure 6.16 Rate constant versus calculated bubble radius

This trend agrees with literature results for any vapour-liquid reactions. The same comparison can also be made with faster kinetics at constant bubble radii. Because all experiments were conducted under the same gas conditions, i.e. G = 1l/min and the same dispersion achieved (all experiments used an air stone for dispersion), it could be assumed that the range of bubble sizes in the experimental runs were consistent.

A comparison for all the calculated k_L values at a constant bubble diameter of r = 1mm is reported in Table 6.6

Table 6.6 Experimental mass transfer coefficient at constant bubble radius (r=1mm)

Experiment	pH	k_L [$m.s^{-1}$]
D4	variable	$4.42*10^{-4}$
D5	3.3	$3.11*10^{-4}$
D6	7.1	$4.10*10^{-4}$

Under these conditions, the effect of pH on the mass transfer coefficient is more pronounced. High mass transfer coefficients, however, could produce

particles of a smaller diameter in comparison with a lower coefficient and slower reactions (Al-Tarazi et al, 2004). This highlights the need for a process optimisation procedure to control pH to produce particles that settle faster and minimise fines.

6.4.3.2 Integrated rate law

An integrated rate equation of the form of equation 6.3 has also been fitted to the data for the gaseous systems. With constant sulphide concentrations in the liquid phase (at a constant pH and assuming that reaction occurs rapidly as soon as the sulphide is absorbed), equation 6.3 can then be rewritten for this case as

$$-\frac{d[Me^{2+}]}{dt} = k'[Me^{2+}] \qquad (6.6)$$

where k' is a pseudo-first order rate constant. Upon integration this yields

$$\ln[Me^{2+}] = \ln[Me^{2+}]_0 - k't \qquad (6.7)$$

A linear plot of $\ln[Me^{2+}]$ versus time should yield a slope equal to the rate constant. Results for experiments D4 to D6 are reported in Figure 6.17

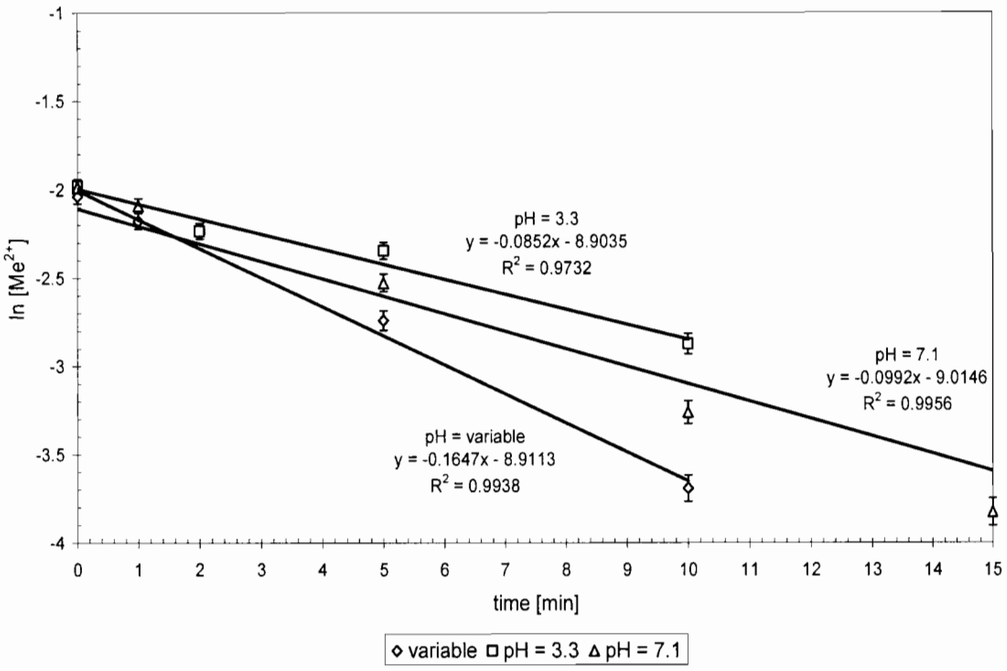

Figure 6.17 Linear plots for calculating the kinetic constant for gaseous systems

Table 6.7 Integrated kinetic constants for the gaseous system

Experiment	pH	-k' [s^{-1}]
D4	variable	0.1647
D5	3.3	0.0852
D6	7.1	0.0992

A similar trend is observed, with an increase in pH resulting in an increase in the rate constant. It should be noted that in equation 6.6, $k' = k[HS^-]$ in accordance with chapter 4. The higher pH favours the formation of HS^- and it should thus be expected to increase the rate constant.

6.5 Settling

6.5.1 Batch system

Precipitate settling rates for the commonly used precipitating agents has also been investigated. Precipitates of hydroxide, carbonate and sulphide were

produced batch wise. The concentrations of each precipitating agent were kept equal at 0.05**M** to investigate these rates.

The settling rates for the precipitates formed are represented in Figure 6.18. In the figure, the ratio h_t/h_o was plotted, where h_t was the volume of solid at time t, and h_o the initial volume of slurry. The decrease in h_t with time is attributed to the settling of the precipitate.

Particulate fines are observed for the liquid sulphide system, where the initial time delay in the settled volume indicates the fines. Observations from these experiments indicate that no clear solid-liquid interface could be detected; however, a settled sludge could be seen at the bottom of the settling cone. A clear reading of the settled volume of precipitate could only be recorded once the fines had settled sufficiently.

This could possibly indicate a broad size distribution for the sulphide system. Since particulate fines would be formed in abundance, the possibility of agglomeration of these fines is high. This would lead to larger particles settling faster (settled volume) as well as fines which still have not settled. These particulate fines present a process problem, seeing that the burden on filters would be increased as well as increased filtration costs due to the acquisition of ultra-fine filters.

Precipitates formed from experiments using gaseous H_2S are also shown on this figure. Discussions for this operation can be followed under the appropriate section in this chapter. Interesting to note is the absence of particulate fines at the beginning, again highlighting the advantage of using a gaseous source of sulphide to minimise fines formation.

These figures also highlight the fact that the sulphide precipitates formed with aqueous sulphide settle faster than any of the precipitates formed with hydroxide and carbonate (if one excluded fines formation). This confirms the literature that the sulphide precipitation method forms precipitates that settle faster.

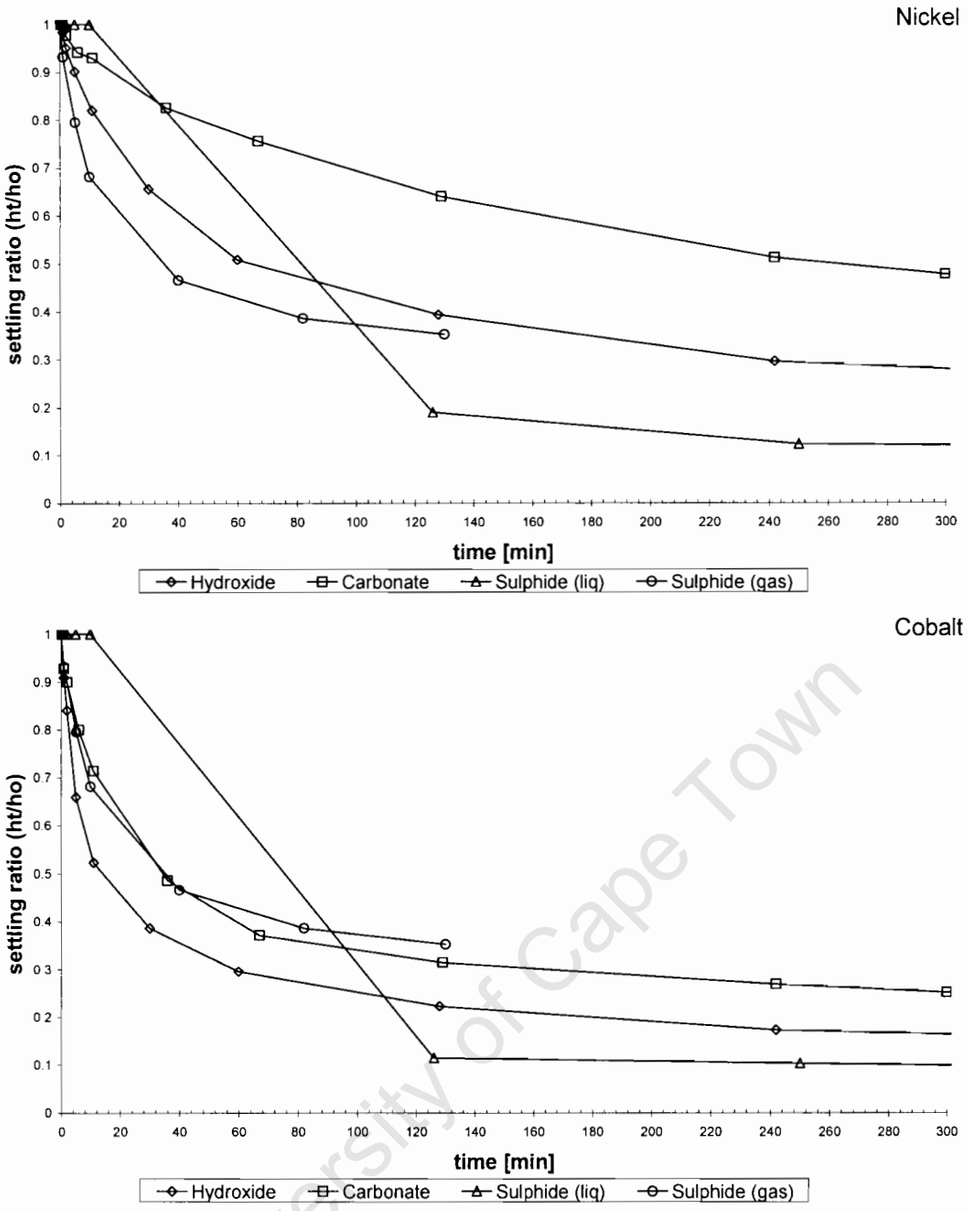

Figure 6.18 Settling rates of different precipitates

The sulphide results are re-plotted on Figure 6.19 together with measurements of the residual metal concentration taken from the same point inside the settling cones, to highlight the fines concentrations.

The decrease in the fines concentration is more pronounced in the cobalt sulphide system, with fines concentration in the liquid decreasing by

approximately 83.3%. Such a sharp decrease was not noticed in the nickel sulphide precipitates formed where fines concentration decreased by 50%.

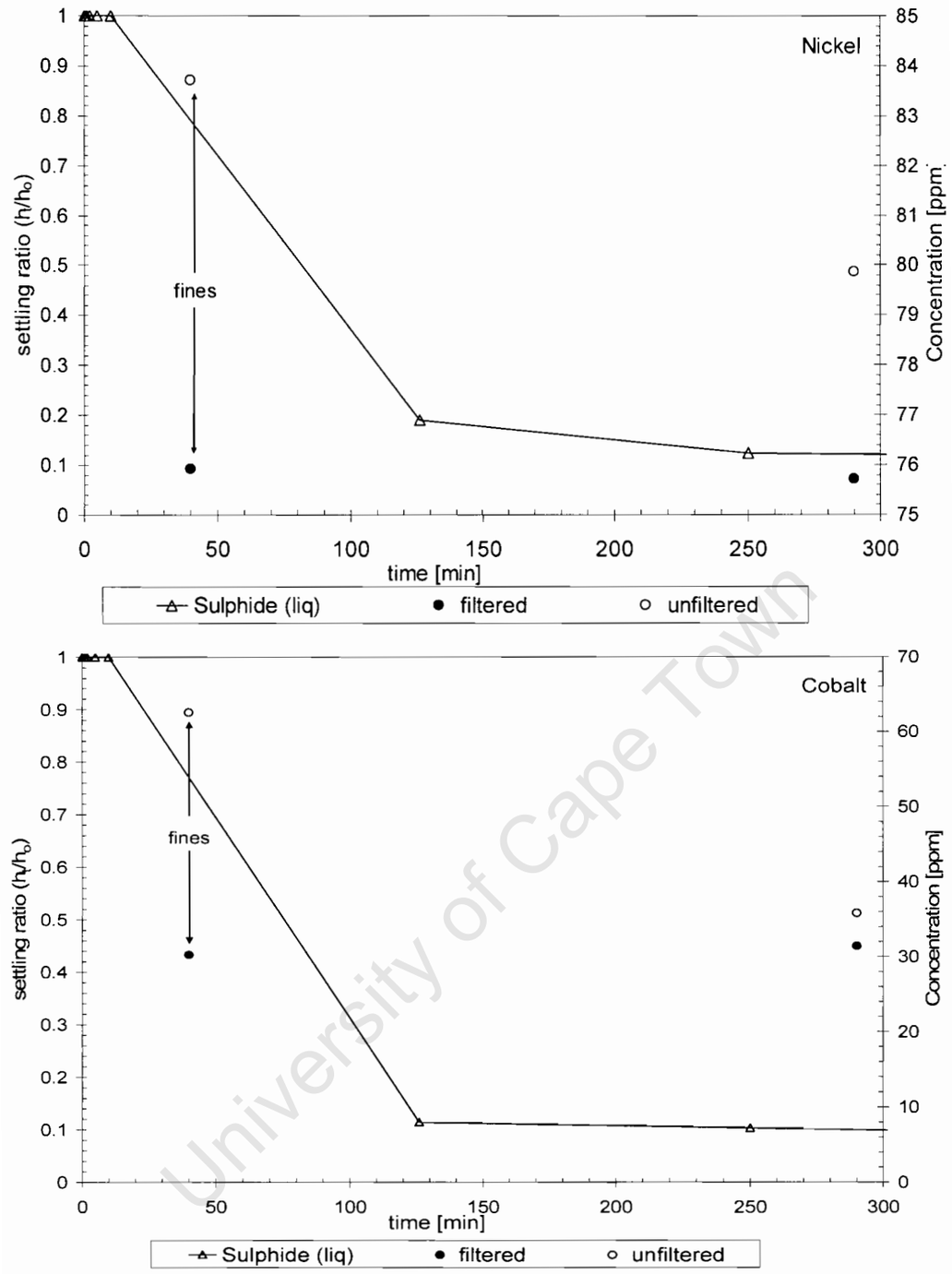

Figure 6.19 Liquid sulphide settling rates showing fines concentrations

6.5.2 Settling rates for gaseous system

Settling rates for sulphide precipitates formed by the use of H_2S are also reported in Figure 6.18. Although there is no clear advantage (the settling rates for the gaseous system are for a mixed sulphide precipitate and not for each individual metal), a review of the other precipitates indicate a difference in the settling rates of the two metals for each precipitate used.

This could imply that for a mixed system of Ni and Co, a precipitate formed could have characteristics of both metals, with a pure Ni and pure Co precipitate forming the boundary limits.

Chapter 7

Conclusions

From the results of the investigation conducted, the following conclusions can be drawn:

- *Sulphide precipitation has very high nucleation rates and fines formation:*
  Because of the low solubility of sulphide precipitates, very high supersaturation is achieved in a precipitation system. Supersaturation is required for both growth and nucleation; however, high supersaturation tends to favour high nucleation rates and slower (compared to the nucleation rates) growth rates. Because of slow growth but high particle formation (nucleation), the tendency for the system to form fines is high.

- *Sulphide precipitation produces a better settling precipitate than hydroxide or carbonate precipitation:*
  Literature suggests that removal of many base and/or heavy metals can be achieved through sulphide precipitation even at low pH. This study has also shown that the removal of Ni and Co from a synthetic stream can be achieved to well within acceptable levels at neutral pH. This does not necessitate the need for post-precipitation treatment as would be required for a hydroxide system.

  The sulphide precipitate also settled much faster than the equivalent hydroxide or carbonate precipitates. Although fines formation is common in sulphide precipitation, control of the local supersaturation by changing the sulphide source, leads to a much denser precipitate with minimal fines formation.

- *The use of a fluidised bed reactor is limited in this configuration for high concentration streams:*

  Although a fluidised bed has been used successfully in previous trials, all of these trials were conducted at low metal concentrations. A fluidised bed reactor offers a lower energy barrier, and favours heterogeneous nucleation; however, the reactor is not suitable for high concentration process streams.

  This is largely due to the high attrition rates experienced inside the reactor. The seed material gets overloaded within the first few minutes of operation and a "heavily" coated seed tend to lose its coating easier than a "lightly" coated seed. Fines formed in this manner also do not adhere to any other seeds.

  The fluidised bed reactor removes metals from solution very efficiently, however overall removal is reduced because of the fines in the outlet stream.

- *The sulphide source determines the level of supersaturation generated:*

  Aqueous sulphide sources lead to high local supersaturation and this again leads to fines formation. A gaseous sulphide source was tested and this reduced the fines formation significantly, leading to the conclusion of reduced local supersaturation.

  A gaseous sulphide source introduces a gas-to-liquid mass-transfer limitation into the generation of supersaturation. Gaseous sulphide also offers a means for controlling the supersaturation because of the sulphide speciation. A direct control of the pH would control the concentration of sulphide into the system.

- *A gaseous sulphide source results in improved removal efficiency in a metal sulphide precipitation system:*

  The overall removal efficiency of the gaseous sulphide system was better than that of the aqueous system. This was largely because of reduced fines in

the outlet stream due to reduced supersaturation. This leads to better product quality, in terms of filterability as well as settleability.

This report also set out to answer a few questions as set out in the introduction. These are:

i. *What are the factors affecting heavy metal removal?*

Although various factors have been investigated in general, all of the results indicate that the dominant factor was the supersaturation. For the gaseous systems, and because of the speciation of the various sulphide species, the pH of the solution also greatly affects the metal removal.

It has been shown that once the supersaturation has been sufficiently reduced to suppress rapid nucleation rates, no fines were detected in the outlet stream. This increased the overall efficiency of the system.

ii. *How does supersaturation affect the product quality?*

The different reactor configurations highlighted that with a reduction in supersaturation, the same conversions could be achieved; however, a product that is easier to handle (in terms of settleability and filterability) is formed.

As stated above, the product quality was greatly improved because of no fines formation.

iii. *Does a gaseous sulphide source greatly affect the removal efficiency and quality?*

Yes it does. The conversion of the gaseous system is comparable to (and sometimes better than) that of a liquid sulphide source; however, because

of no fines forming in the reactor during the experimental runs, the overall efficiency of the system is greatly increased.

Although the particle size has not been measured to determine the quality of the product, the settling rates indicate faster settling rates; thus implying larger sizes and an increased quality.

Recommendations

From the conclusions above, a few recommendations are given should further investigations into this project proceed:

- *Measure the particle size distribution:*
  All results regarding the final product quality were deduced from the settling data. The size distribution of a gaseous system compared to that of an aqueous system should strengthen this conclusion.

- *Data capturing:*
  The instantaneous nature of the precipitation reaction does not allow data to be measured within the first few seconds. Methods for capturing the data within this time frame should be looked at so as to increase understanding within that instant. Whether this is possible analytically is uncertain.

- *Complete system:*
  The gaseous system in this report was batch with respect to the synthetic metal stream. A system with an attached settler/thickener should be investigated, as the current system carried the precipitates out in the outlet stream. Alternatively a system where the formed precipitates could be withdrawn from the reactor should be investigated. A tapered reactor could be used and allow the precipitate to settle inside the reactor.

- *Optimisation:*

Now that the key parameters were identified, the system can be optimised for each. System limitations should also be identified (e.g. is there a limit to the concentration of the H_2S gas?).

APPENDIX 1: Results obtained

Batch results (low concentrations)

	0.1		0.05		0.01		M
Sulphide concentration	*27.25*		*54.50*		*272.48*		*ml*
End Volume	*527.25*		*554.50*		*772.48*		*ml*
time	**conc [ppm]**		**time**	**conc [ppm]**		**time**	**conc [ppm]**	
[min]	**Ni**	**Co**	[min]	**Ni**	**Co**	[min]	**Ni**	**Co**
0	217	108	0	216	109	0	211	107
1	14.91	10.03	1	66.07	35.02	1	21.35	11.74
5	9.38	8.85	5	34.71	24.06	5	16.85	11.86
10	9.94	11.1	10	33.97	25.32	10.5	16.22	12.2
15	9.61	11.8	16	34.04	25.86	15	16.1	12.17
20	11.22	10.8	20	33.62	25.93	20	15.88	12.15
25	9.55	11.3	25	33.6	26.01	30	16.03	12.03
30	9.43	10.85	30	33.24	25.42			
S test 1	0.109	**M**	S test 1	0.069	**M**			
S test 2	0.104	**M**	S test 2	0.064	**M**			
S ave	**0.106**	**M**	**S ave**	**0.067**	**M**			
time	**% removal**		**time**	**% removal**		**time**	**% removal**	
[min]	**Ni**	**Co**	[min]	**Ni**	**Co**	[min]	**Ni**	**Co**
0	0.00	0.00	0	0.00	0.00	0	0.00	0.00
1	93.13	90.71	1	69.41	67.87	1	89.88	89.03
5	95.68	91.81	5	83.93	77.93	5	92.01	88.92
10	95.42	89.72	10	84.27	76.77	10.5	92.31	88.60
15	95.57	89.07	16	84.24	76.28	15	92.37	88.63
20	94.83	90.00	20	84.44	76.21	20	92.47	88.64
25	95.60	89.54	25	84.44	76.14	30	92.40	88.76
30	95.65	89.95	30	84.61	76.68			

volume of sulphide solution added

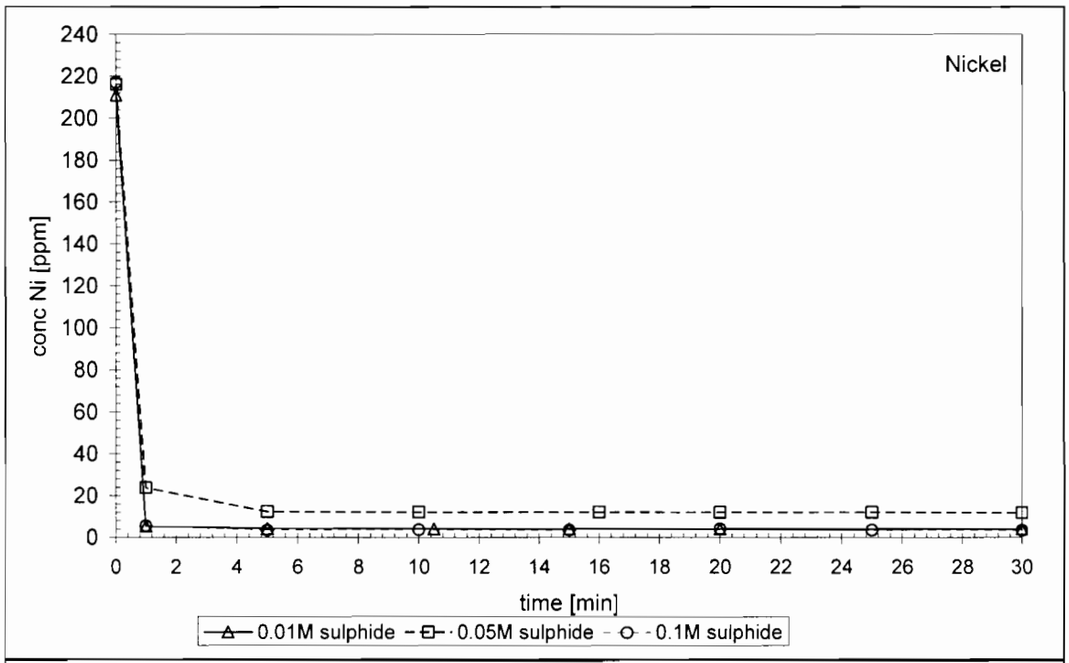

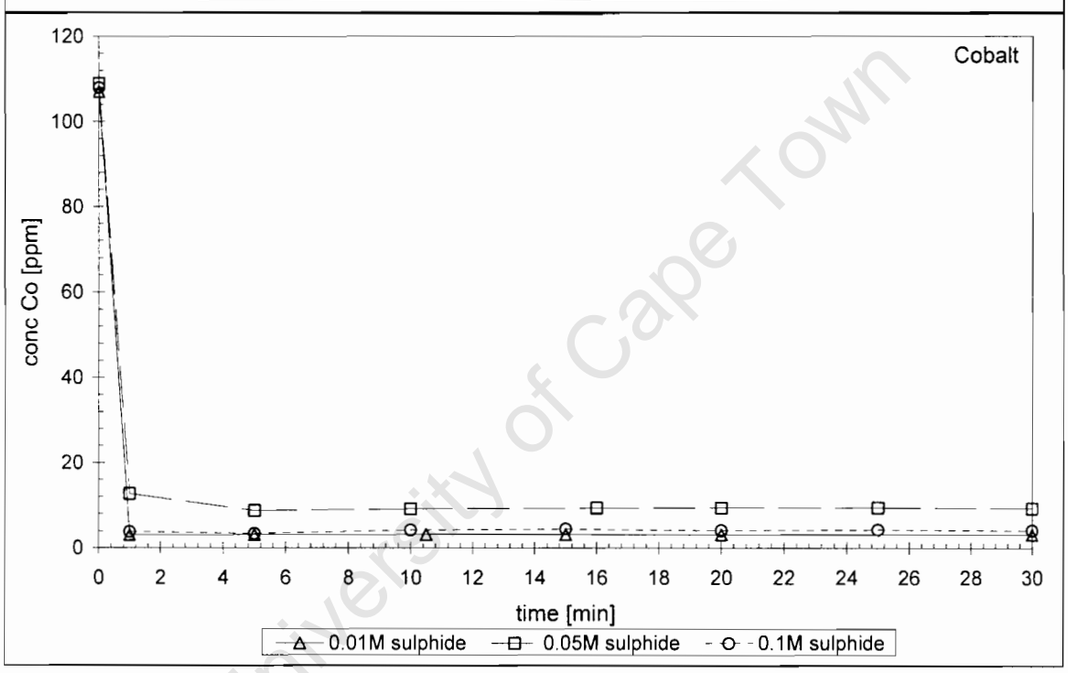

Batch results (high concentrations)

	0.1	0.05	0.01	M
Sulphide concentration	*54.50*	*108.99*	*544.97*	*ml*

volume of sulphide solution added

End Volume *154.50* 208.99 *644.97* *ml*

time	conc [ppm]		time	conc [ppm]		time	conc [ppm]	
[min]	Ni	Co	[min]	Ni	Co	[min]	Ni	Co
0	2170	1080	0	2160	1090	0	2110	1070
1	80.99	117.39	1	102.83	154.7	1	944.58	486.85
5	72.8	151.97	5	89.18	148.33	5	15.47	21.84
10	67.34	151.06	10	91.91	160.16	10	12.74	21.84

time	% removal		time	% removal		time	% removal	
[min]	Ni	Co	[min]	Ni	Co	[min]	Ni	Co
0	0	0	0	0	0	0	0	0
1	96.27	89.13	1	95.24	85.81	1	55.23	54.50
5	96.65	85.93	5	95.87	86.39	5	99.27	97.96
10	96.90	86.01	10	95.74	85.31	10	99.40	97.96

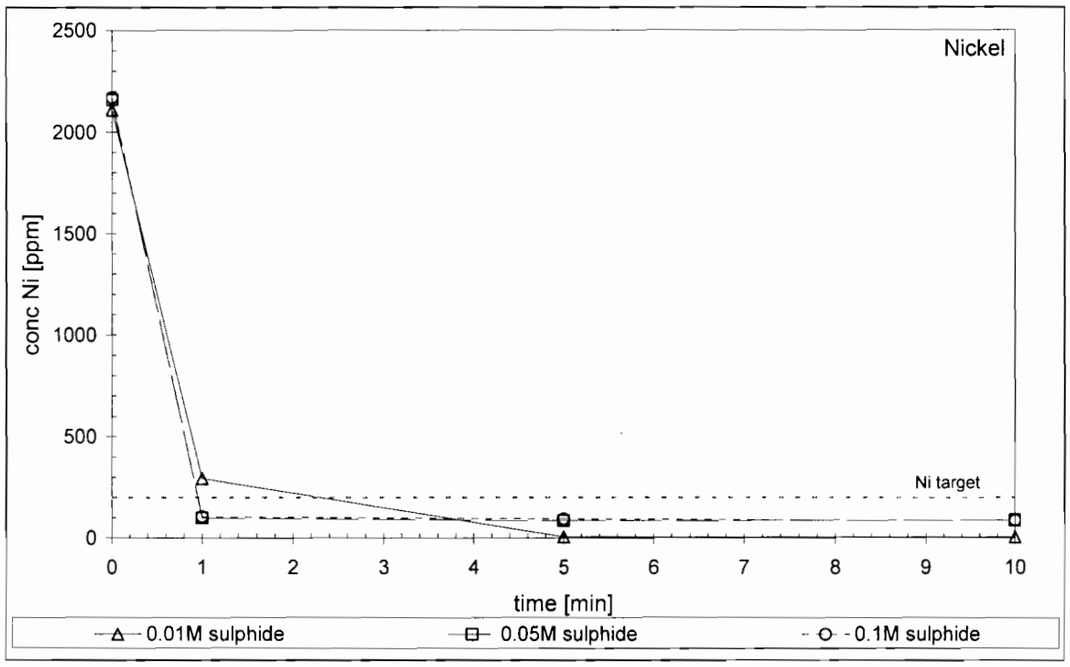

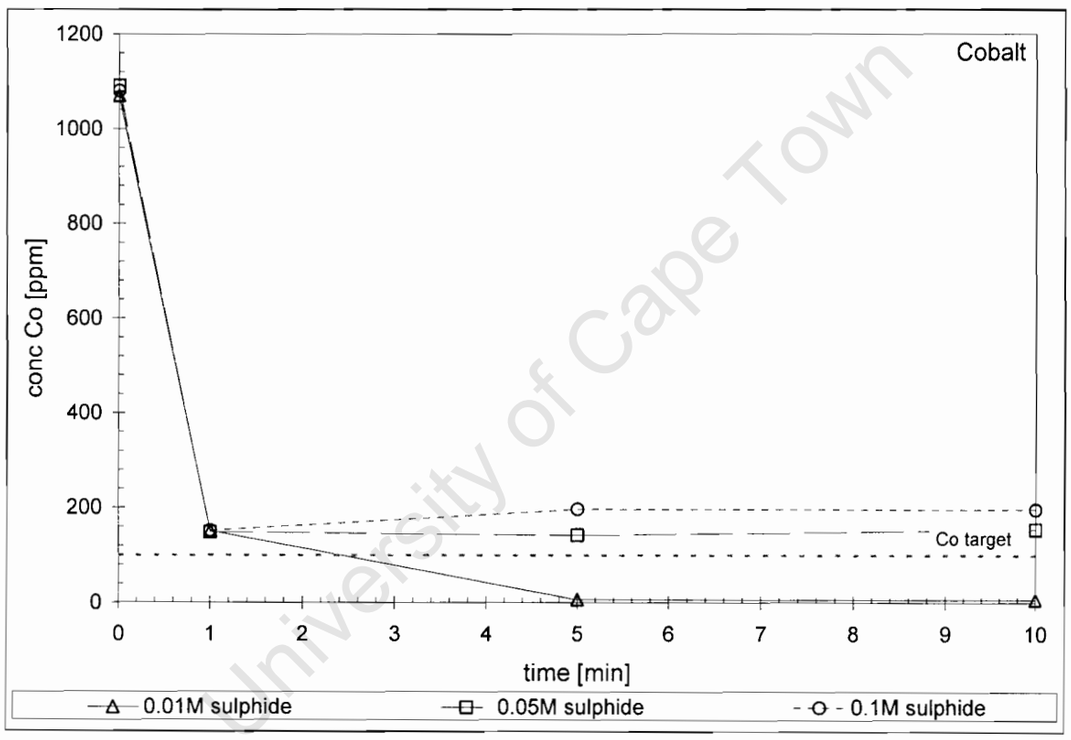

Batch results (20% excess sulphide)

Sulphide concentration 0.05 **M**

time	Ni	Co
0	216.78	109.50
1	1.00	0.60
5	1.00	0.60
10	1.00	0.60

time	% removal	
0	0.00	0.00
1	99.54	99.45
5	99.54	99.45
10	99.54	99.45

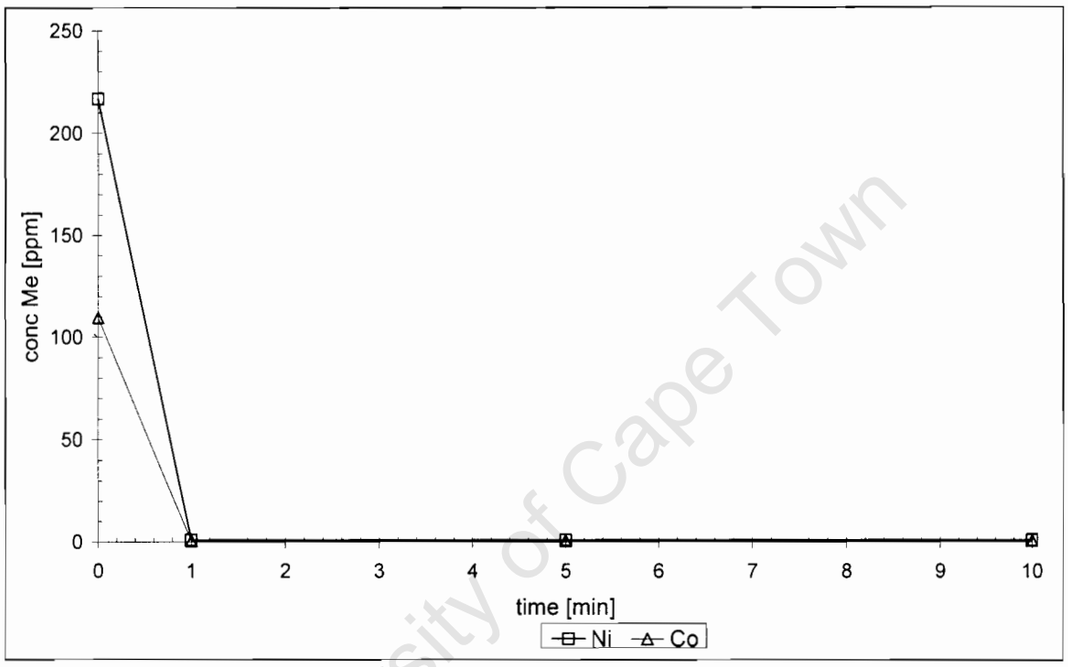

Fluidised Bed results (initial testing)

	Cobalt				Nickel			
time	filtered	unfiltered	conversion	efficiency	filtered	unfiltered	conversion	efficiency
0	50.25	49.6	0.00	0.00	120.3	121.2	0.00	0.00
2	41.1	41.08	18.21	17.18	92.51	93.74	23.10	22.66
5	20.86	20.48	58.49	58.71	50.61	50.87	57.93	58.03
10	14.78	15.14	70.59	69.48	31.29	31.65	73.99	73.89
21	8.92	12.71	82.25	74.38	15.71	21.98	86.94	81.86
32	7.52	13.23	85.03	73.33	11.34	20.63	90.57	82.98
60	8.93	14.72	82.23	70.32	11.79	22.11	90.20	81.76
90	10.74	17.78	78.63	64.15	13.81	26.07	88.52	78.49

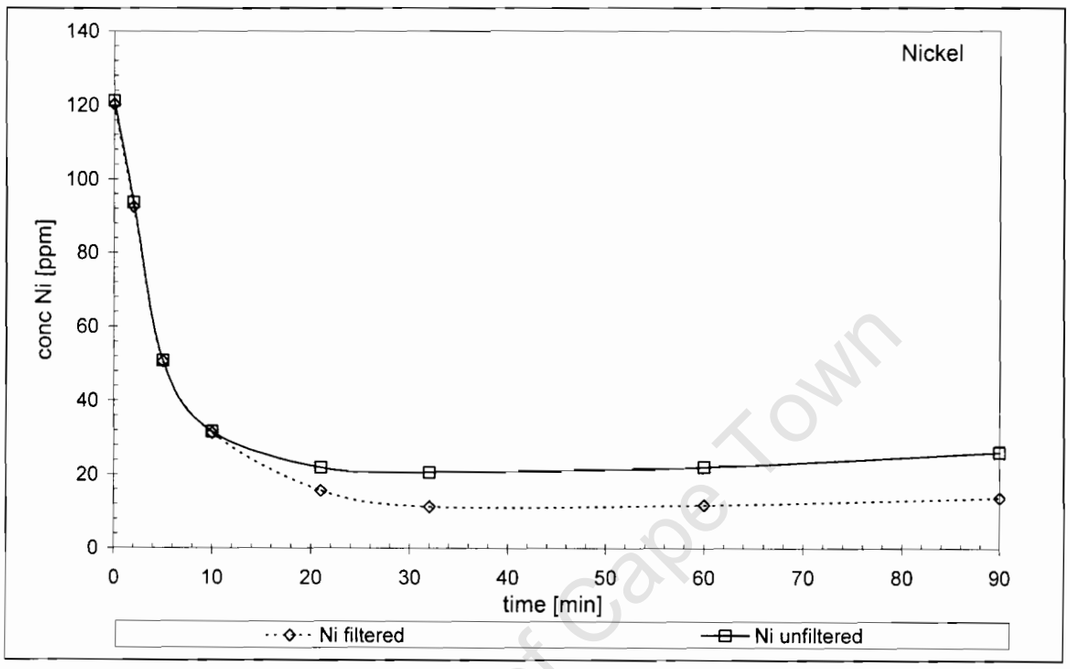

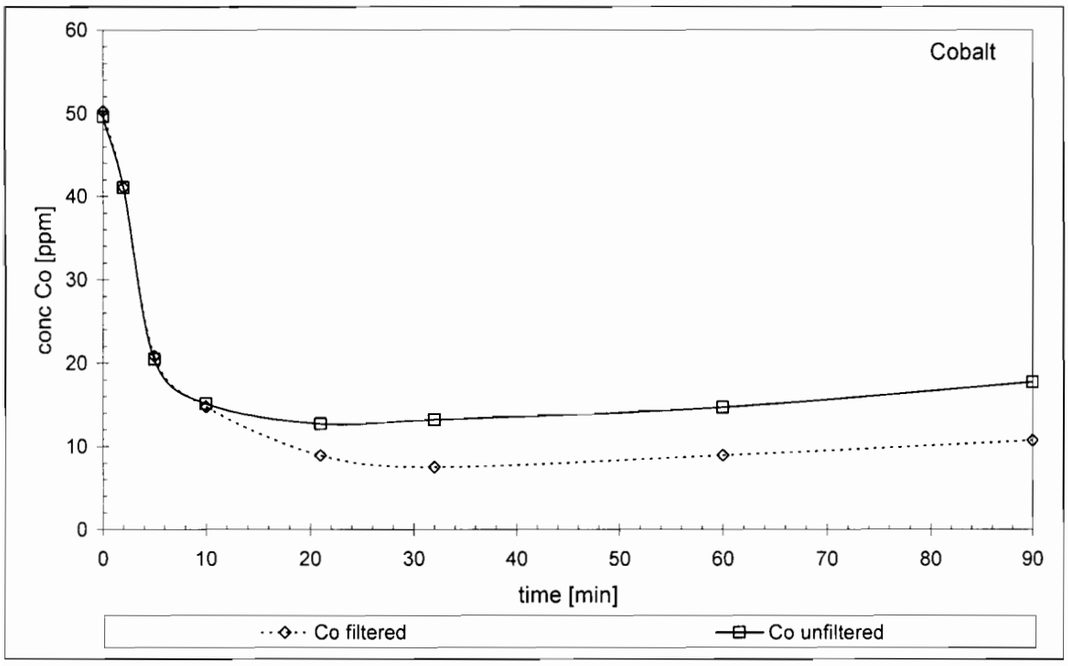

Fluidised bed results (high concentrations)

Nickel

time [min]	pH	conc [ppm]	conversion
0	6.95	1366	0.00
1.62	7.88	970	28.99
3.25	8.1	474	65.30
5	8.36	165	87.92
20		177	87.04

Cobalt

time [min]	pH	conc [ppm]	conversion
0	6.95	803	41.22
1.62	7.88	550	59.74
3.25	8.1	319	76.65
5	8.36	160	88.29
20		137	89.97

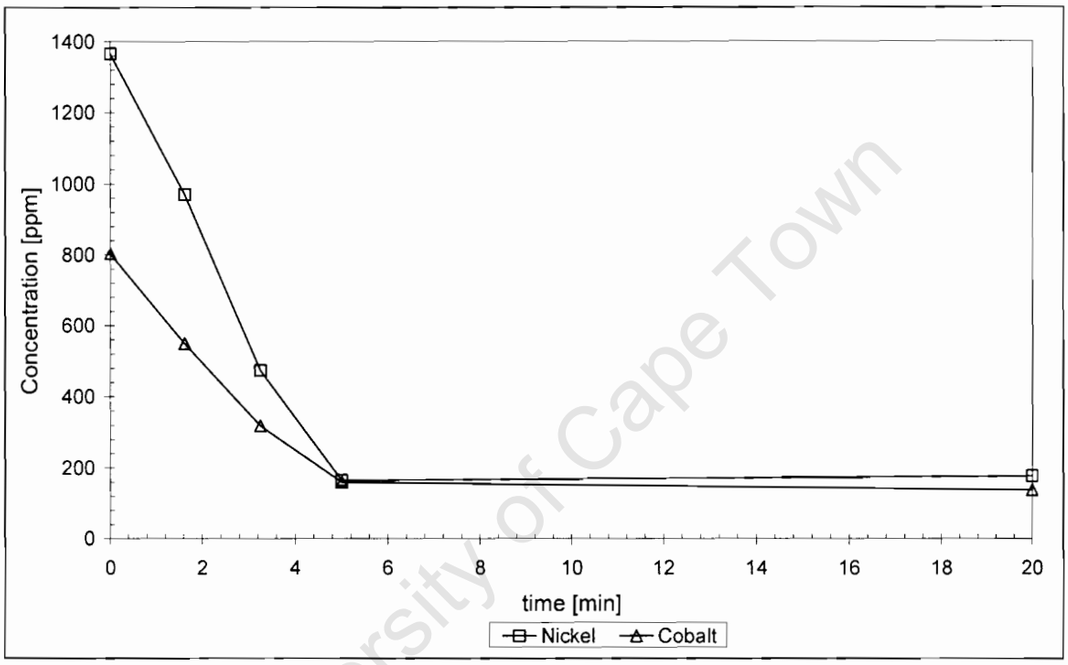

Testing using sulphate reducing bacteria

time	Ni	Co	NaOH trap abs	NaOH trap conc	pH	Conversion Ni	Conversion Co
0	130.16	60.20	0	0.000	6.1	0.00	0.00
1	122.57	54.75	0.027	0.789	3.35	5.83	9.05
7	120.16	52.34	0.545	15.924	3.22	7.68	13.06
11	118.80	51.64	0.41	23.960	3.17	8.73	14.22
17	118.22	51.92	0.518	30.271	3.16	9.17	13.75
21	117.70	51.63	0.286	33.427	3.14	9.57	14.24
25	117.34	51.52	0.318	37.167	3.14	9.85	14.42
30	116.90	51.25	0.14	40.907	3.12	10.19	14.87

time	Ni	Co	NaOH trap abs	NaOH trap conc	pH	Conversion Ni	Conversion Co
0	233.10	108.00		0.000	11.49	0.00	0.00
2	38.00	27.40	0.259	7.568	2.03	83.70	74.63
9	13.50	13.40	2.575	75.240	1.97	94.21	87.59
13	12.30	13.40	0.493	144.051	1.97	94.72	87.59
20	12.60	13.66	0.667	194.892	1.97	94.59	87.35
25	13.20	13.64	0.392	229.079	1.97	94.34	87.37
30	12.50	13.39	0.343	200.444	1.97	94.64	87.60

time	Ni	Co	pH	Conversion Ni	Conversion Co	
0	218.2	102.41	5.43	0.00	0.00	
0	208.00	73.01	7.26	4.67	28.71	due to carbonate precipitation
1	162.60	67.16	6.65	25.48	34.42	
3.5	62.90	21.72	6.67	71.17	78.79	
30	4.77	1.26	7.45	97.81	98.77	

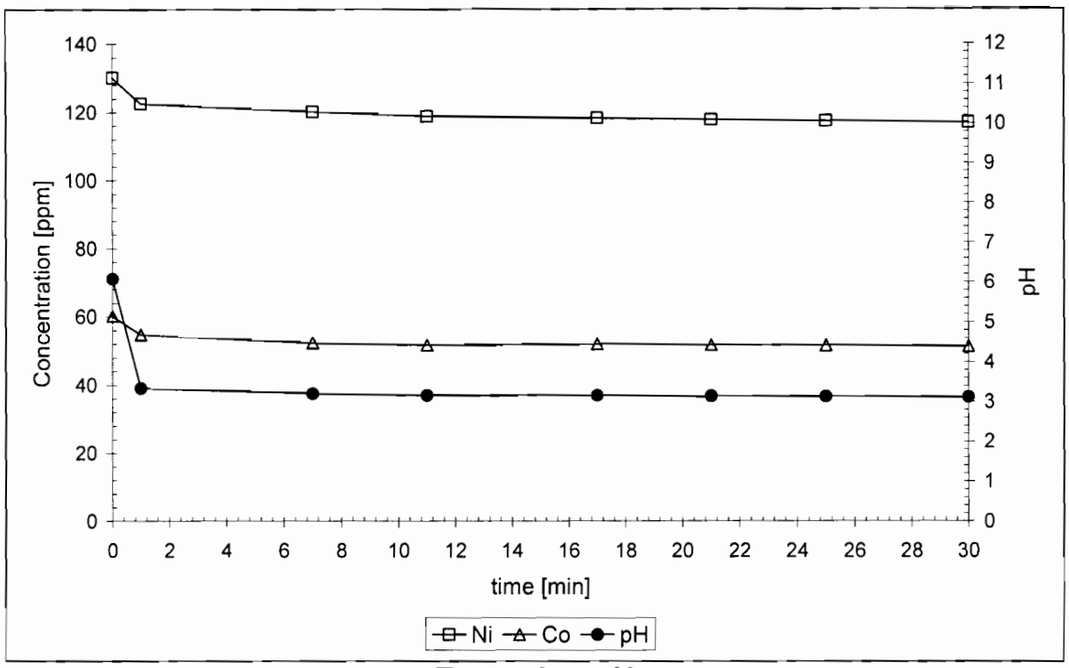

Test at low pH

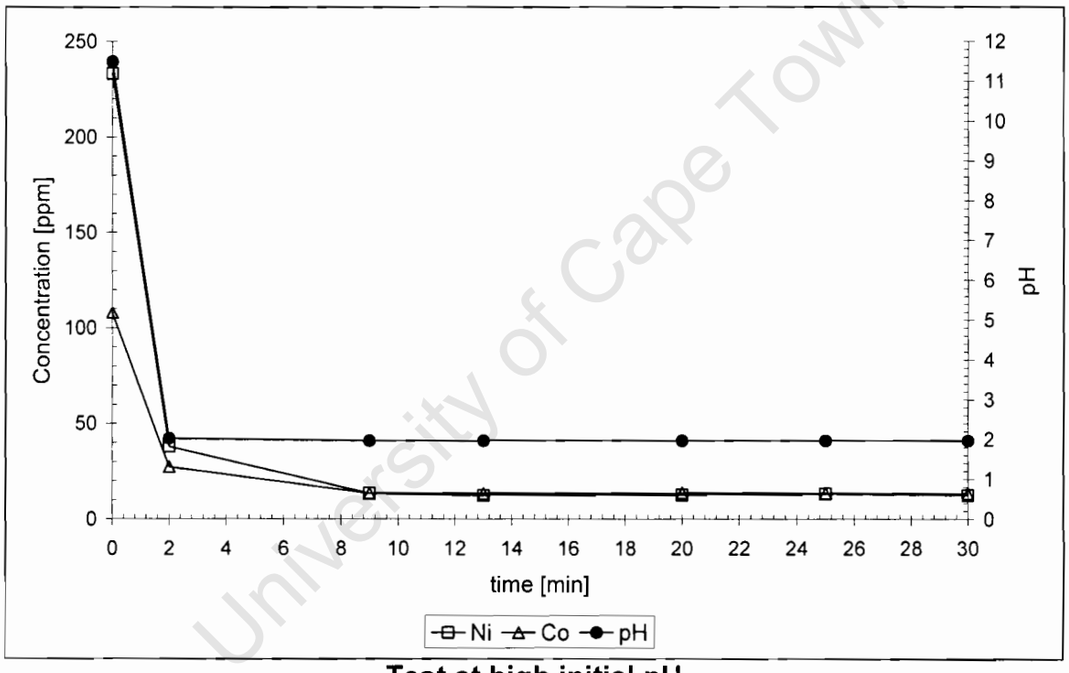

Test at high initial pH

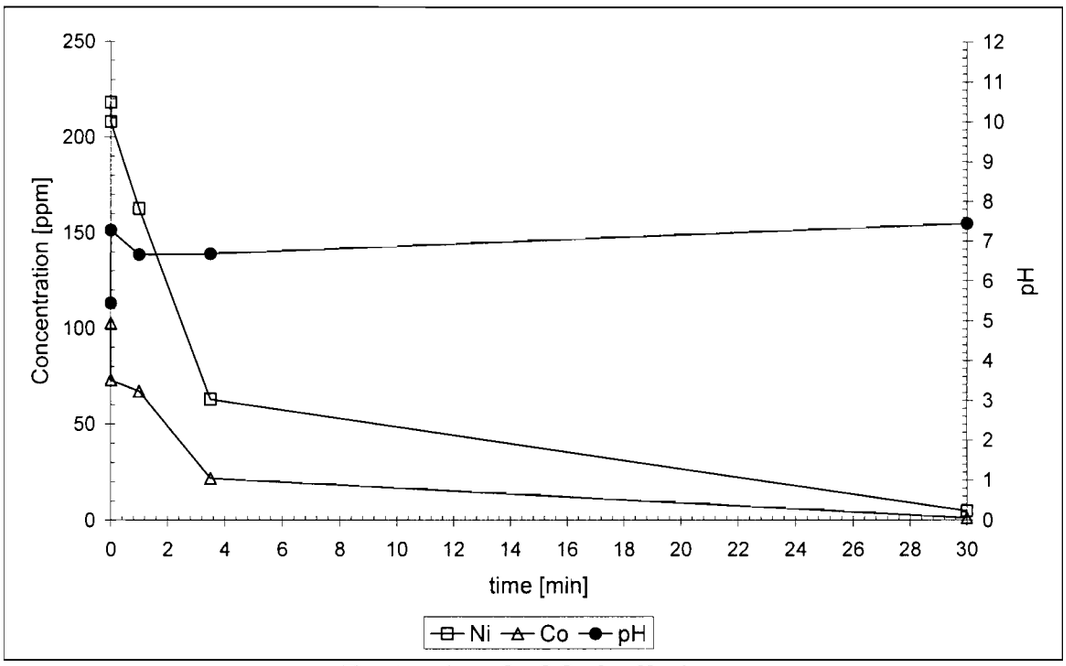

Test using $CaCO_3$ buffering

Testing using bottled gas mixture

first run				Conversion	
time	pH	Ni	Co	Ni	Co
0	5.3	1881.2	955.1	0	0
1	4.87	1381.3	719.2	26.57	24.70
5	6.41	662	388.7	64.81	59.30
10	7.61	2.92	4.93	99.84	99.48
15.5	12.24	0.54	0.23	99.97	99.98

second run				Conversion	
time	pH	Ni	Co	Ni	Co
0	6.78	1917.2	989.2	0	0
1	5.11	1664.2	865.4	13.20	12.52
5	6.15	893.3	547.3	53.41	44.67
10	6.58	324	232.2	83.10	76.53
16	10.96	0.19	0.54	99.99	99.95

third run				Conversion	
time	pH	Ni	Co	Ni	Co
0	5.44	2084.2	996	0.00	0.00
2	3.43	1601.7	789.3	23.15	20.75
5	3.39	1402.2	737.3	32.72	25.97
10	3.35	754.5	507.6	63.80	49.04
20	3.18				
30	3.16	158	161.7	92.42	83.77

fourth run				Conversion	
time	pH	Ni	Co	Ni	Co
0	7	1935.0	979.0	0.00	0.00
3	6.55	1371.8	722.2	29.11	26.23
6	6.88	975.3	589.3	49.60	39.81
10	6.94	602.2	449.7	68.88	54.07
20	6.9				
25	6.62				
30	6.92	48.8	54.9	97.48	94.39
50	6.86				
60	6.92	8.6	9.3	99.55	99.05

fifth run				Conversion	
time	pH	Ni	Co	Ni	Co
0	5.48	2051.4	1009.7	0.00	0.00
1	4.62	1838.2	921.5	10.39	8.74
5	6.15	1162.3	621.1	43.34	38.49
10	7.36	495.1	361.0	75.87	64.25
15	7.18	273.3	213.1	86.68	78.89
20	7				
25	7.05				
30	7.12	70.3	70.4	96.57	93.03
60	7.19	4.2	3.4	99.80	99.66

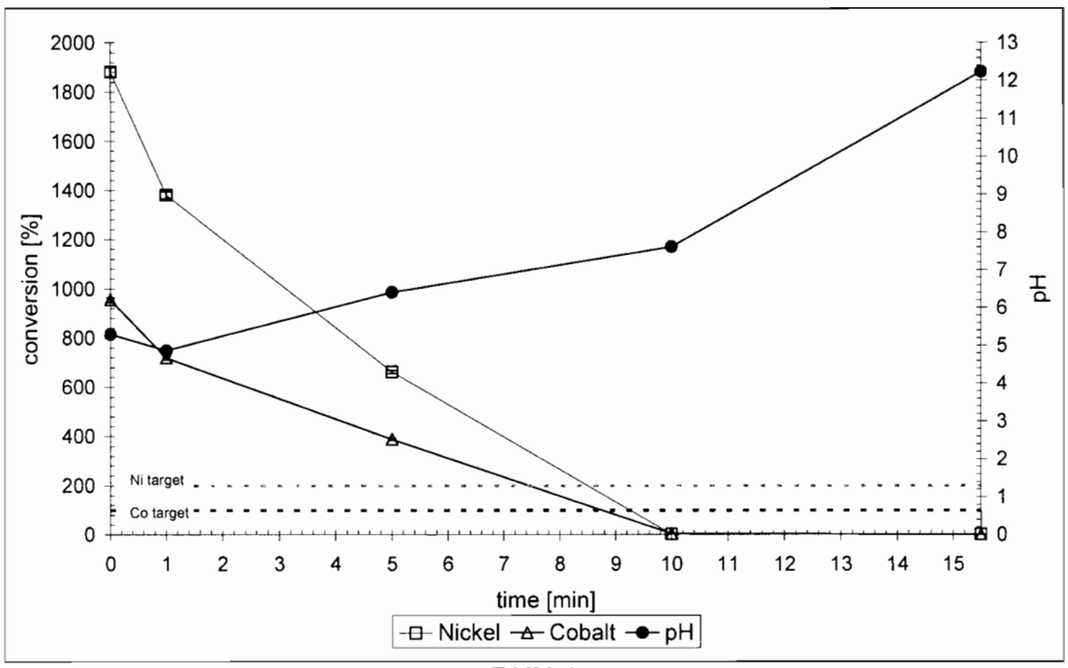

RUN 1

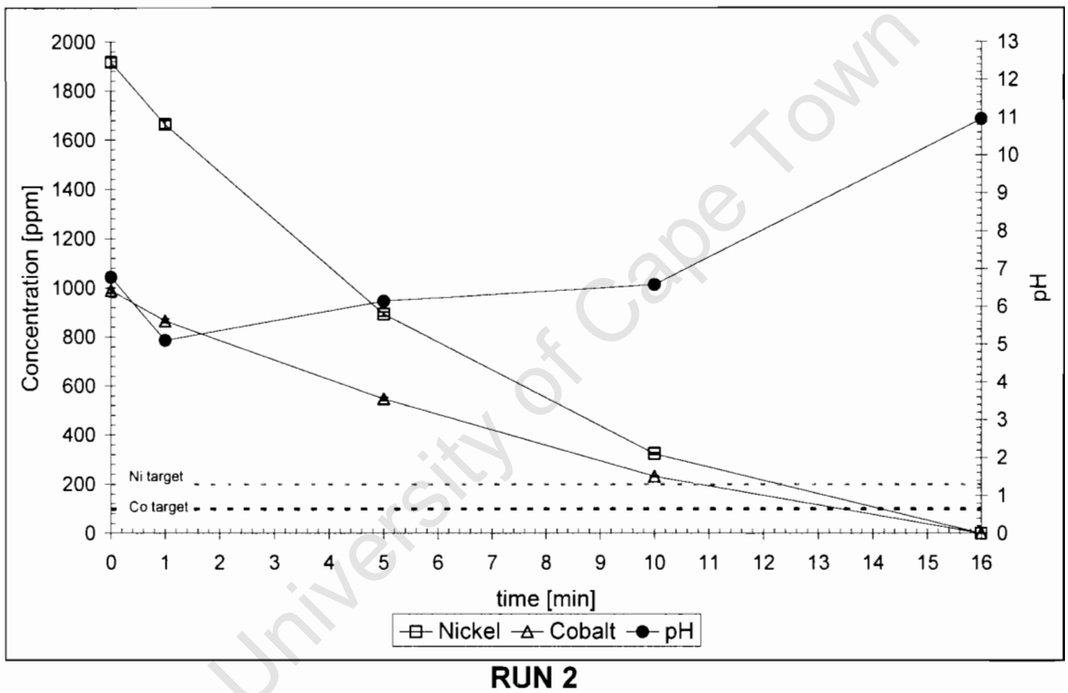

RUN 2

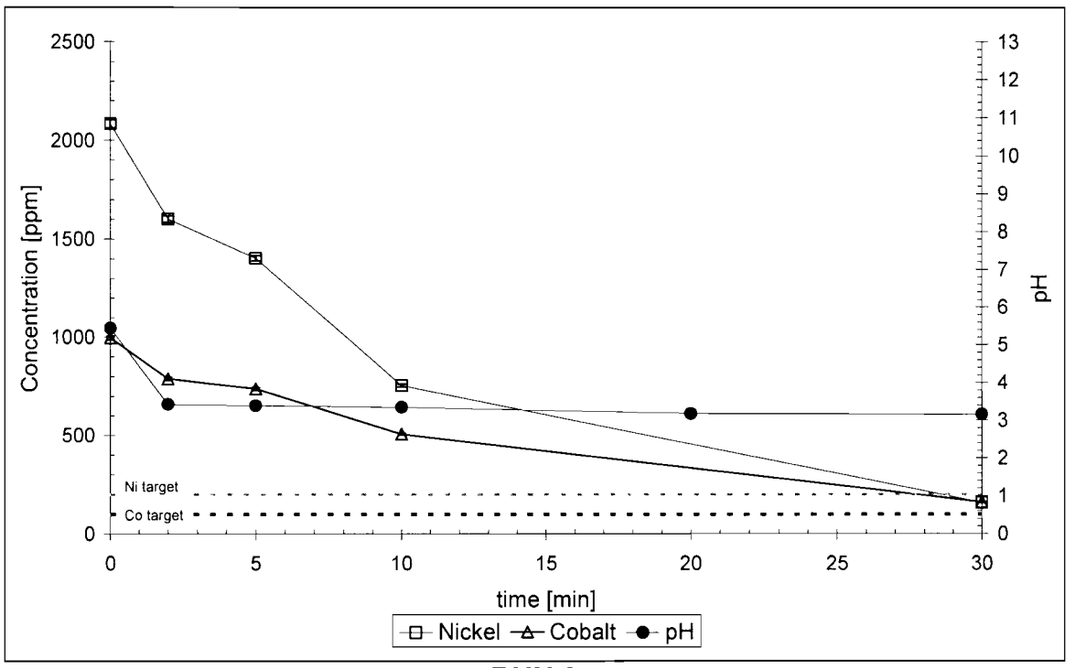

RUN 3

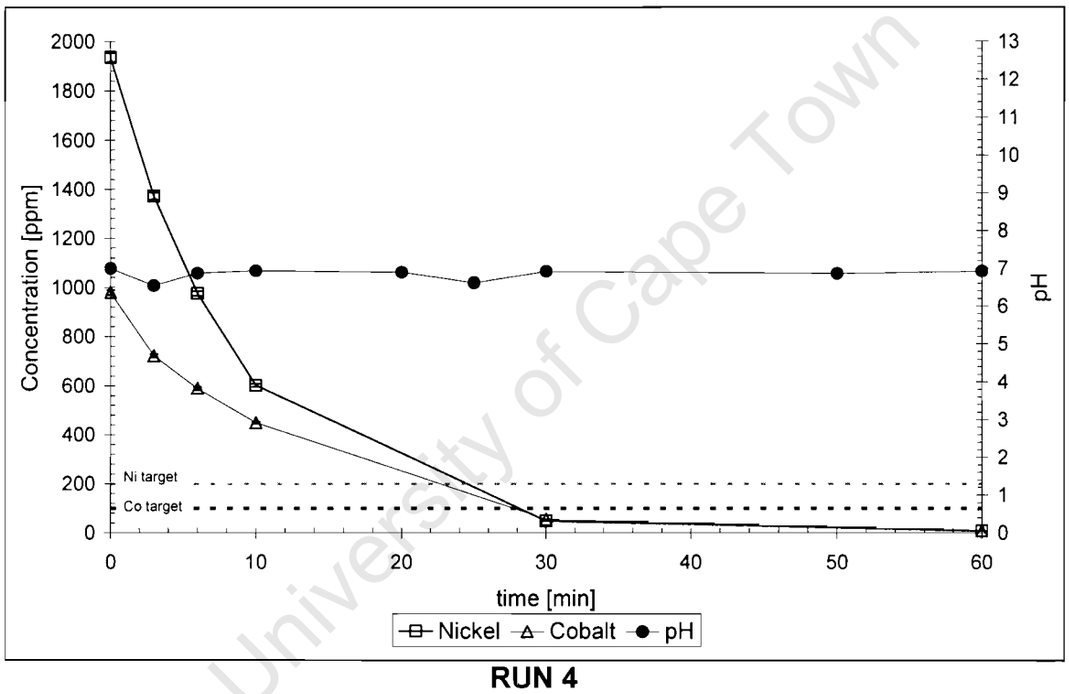

RUN 4

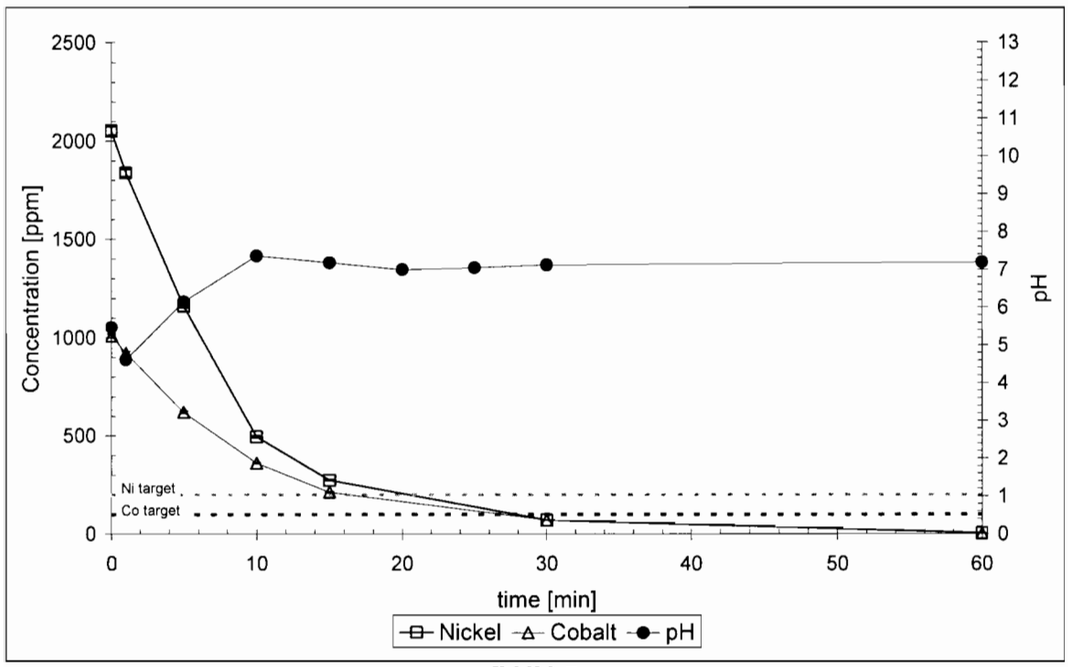

RUN 5

APPENDIX 2: Kinetic calculations

Batch kinetics

0.01		M
544.97		*ml*
time	**conc [ppm]**	
[min]	**Ni**	**Co**
0	2110	1070
1	944.58	486.85
5	15.47	21.84
10	12.74	21.84

Volume added to metal soln

ln (1/[Me^{2+}])	
Ni	Co
3.33	4.01
4.13	4.80
8.24	7.90

slope

Ni	**Co**
0.9959	0.7777

$[Ni^{2+}]_0$	0.0056	**M**
$[Co^{2+}]_0$	0.0025	**M**
$[S^{2-}]_0$	0.0084	**M**
k_{Ni}	5.77	$\mathbf{M}^{-1}min^{-1}$
k_{Co}	2.18	$\mathbf{M}^{-1}min^{-1}$

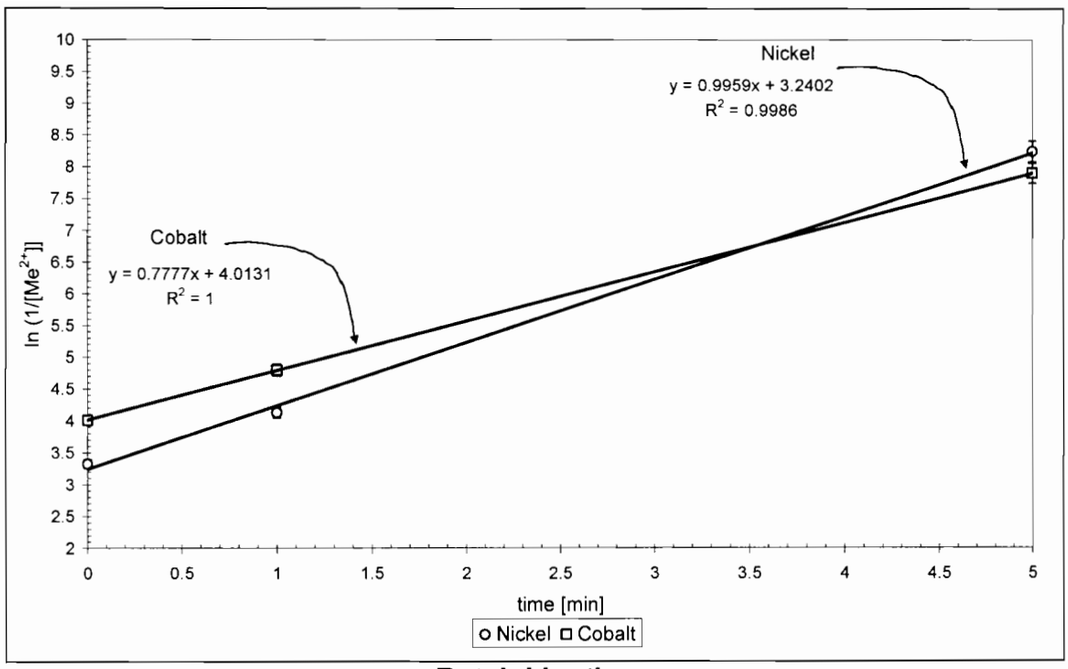

Batch kinetics

Fluidised bed reactor kinetics (low concentrations)

time	Cobalt filtered	Nickel filtered
0	50.25	120.3
2	41.1	92.51
5	20.86	50.61
10	14.78	31.29
21	8.92	15.71
32	7.52	11.34
60	8.93	11.79
90	10.74	13.81

ln(1/[Co])	ln(1/[Ni])
7.067146	6.190087
7.268148	6.452759
7.946323	7.055927
8.290882	7.536777

$[S^{2-}]_o$	4.25E-03	**M**
$[S^{2-}]_o$-$[Ni^{2+}]_o$	2.20E-03	
$[S^{2-}]_o$-$[Co^{2+}]_o$	3.39E-03	
Slope Ni	0.137477	
Slope Co	0.127641	
k Ni	1.04	**M**.s^{-1}
k Co	0.63	**M**.s^{-1}

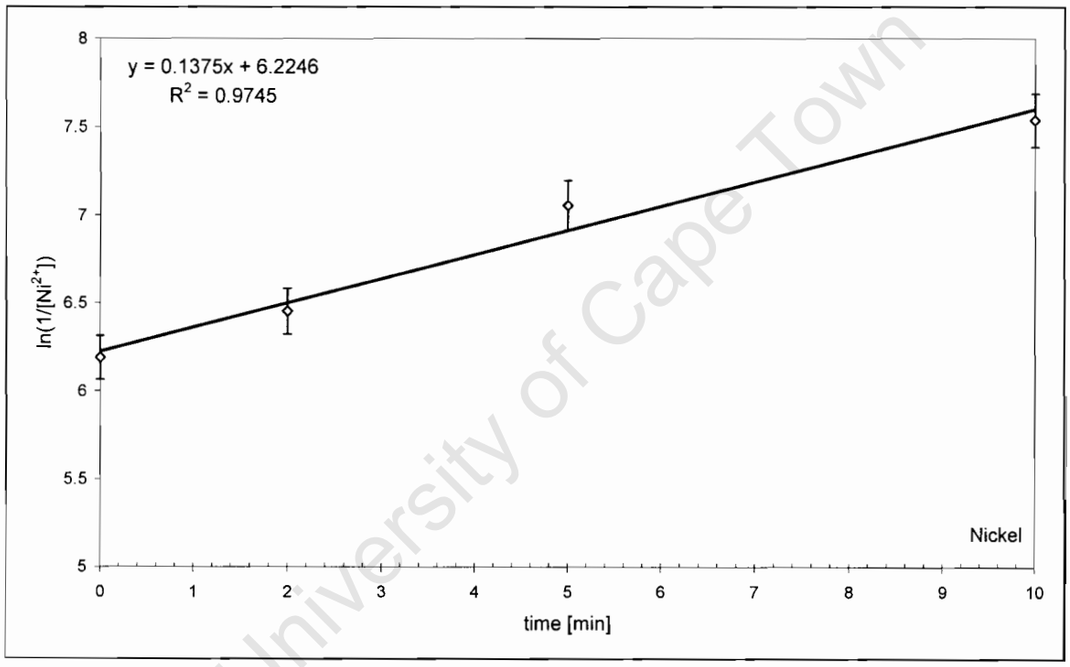

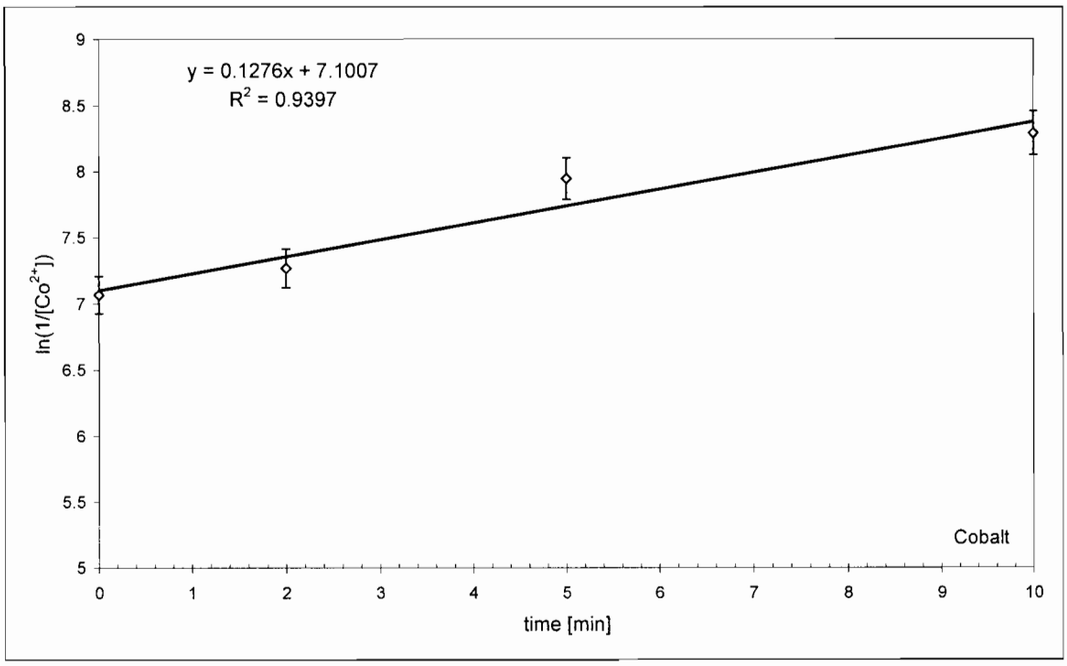

Fluidised bed reactor kinetics (high concentrations)

	Nickel				Cobalt			
time [min]	pH	conc [ppm]		ln(1/[Ni])	pH	conc [ppm]		ln(1/[Co])
0	6.95	1366		3.760434	6.95	803		4.295802
1.62	7.88	970		4.10278	7.88	550		4.674238
3.25	8.1	474		4.818868	8.1	319		5.218965
5	8.36	165		5.87413	8.36	160		5.908983
20		177				137		
	$[Ni^{2+}]_0$	0.0233	**M**		$[Co^{2+}]_0$	0.0137	**M**	
	$[S^{2-}]_0$	0.0553	**M**		$[S^{2-}]_0$	0.0553	**M**	
	k_{Ni}	0.22	$M^{-1}s^{-1}$		k_{Co}	0.13	$M^{-1}s^{-1}$	

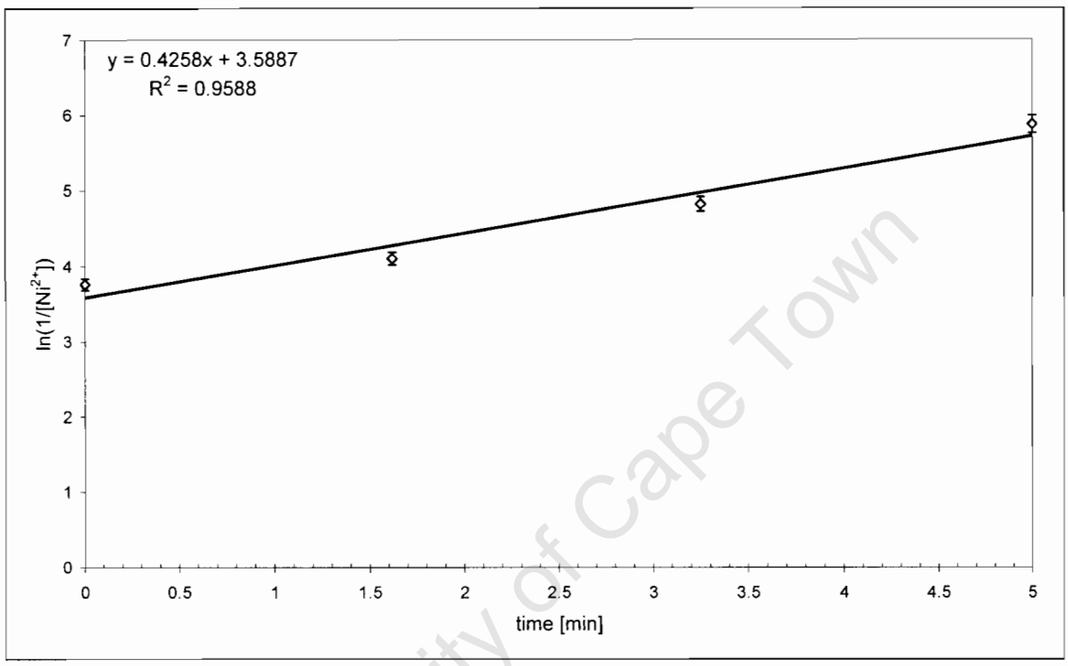

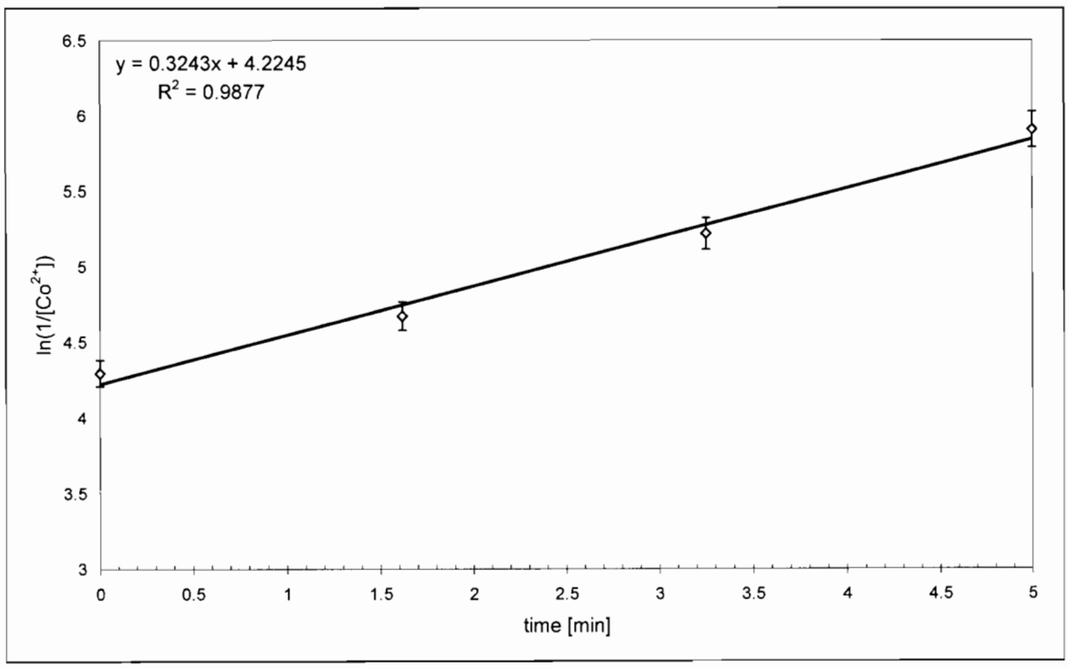

Kinetics using sulphate reducing bacteria

first run						ln ((18.18+Ct)/(18.18+Co))								
time [min]	pH	[Ni] ppm	[Co] ppm	Ni kg/m^3	Co kg/m^3	Ni	Co	Me total			R^2	G	1	l/min
0	6.1	130.16	60.20	0.343	0.158	0.000	0.000	0.000	k_{Ni}	0.000	0.679	h	0.37	m
1	3.352244	122.57	54.75	0.323	0.144	-0.001	-0.001	-0.002	k_{Co}	0.000	0.706	V	0.75	l
7	3.215889	120.16	52.34	0.317	0.138	-0.001	-0.001	-0.003	k_{Me}	0.000	0.692	v_{inf}	0.101026	
11	3.168521	118.80	51.64	0.313	0.136	-0.002	-0.001	-0.003				n	3978.874	
												A_b	0.04578	
												k	0.0002	
												$k_{L\,exp}$	3.28E-06	
												$k_{L\,theo}$	0.000358	

second run						ln ((18.18+Ct)/(18.18+Co))								
time [min]	pH	[Ni] ppm	[Co] ppm	Ni kg/m^3	Co kg/m^3	Ni	Co	Me total			R^2	G	1	l/min
0	11.49	233.10	108.00	0.614	0.284	0.000	0.000	0.000	k_{Ni}	0.002	0.542	h	0.37	m
2	2.027639	38.00	27.40	0.100	0.072	-0.028	-0.012	-0.039	k_{Co}	0.001	0.571	V	0.75	l
9	1.970885	13.50	13.40	0.036	0.035	-0.031	-0.014	-0.044	k_{Me}	0.003	0.552	v_{inf}	0.101026	
13	1.969228	12.30	13.40	0.032	0.035	-0.031	-0.014	-0.045				n	3978.874	
												A_b	0.04578	
												k	0.003	
												$k_{L\,exp}$	4.91E-05	
												$k_{L\,theo}$	0.000358	

third run						ln ((18.18+Ct)/(18.18+Co))								
time [min]	pH	[Ni] ppm	[Co] ppm	Ni kg/m^3	Co kg/m^3	Ni	Co	Me total			R^2	r	1.951758	mm
0	7.26	208.00	73.01	0.548	0.192	0.000	0.000	0.000	k_{Ni}	0.006	0.999	G	1	l/min
1	6.65	162.60	67.16	0.429	0.177	-0.006	-0.001	-0.007	k_{Co}	0.002	0.969	h	0.37	m
3.5	6.67	62.90	21.72	0.166	0.057	-0.021	-0.007	-0.028	k_{Me}	0.008	0.999	V	0.75	l
												v_{inf}	0.141139	
												n	535.1587	
												A_b	0.01679	
												k	0.008	
												$k_{L\,exp}$	0.000357	
												$k_{L\,theo}$	0.000358	

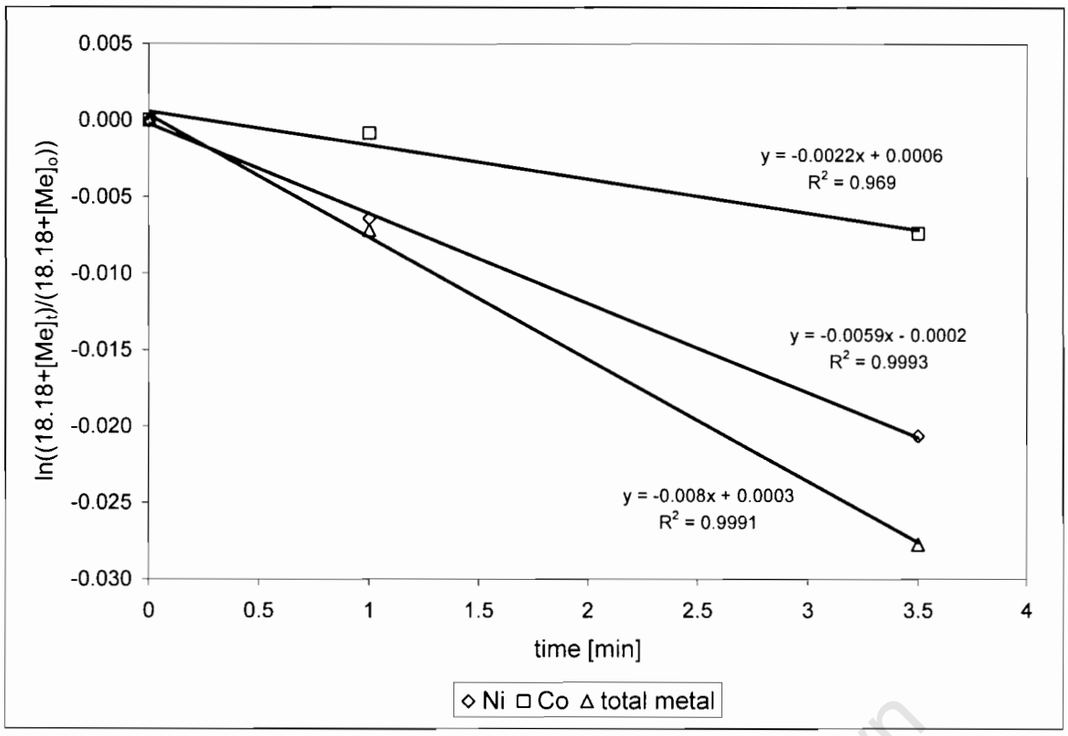

Kinetics using a bottled gas mixture

HIGBIE'S MODEL

first run						ln ((18.18+Ct)/(18.18+Co))								
time [min]	pH	[Ni] ppm	[Co] ppm	Ni kg/m^3	Co kg/m^3	Ni	Co	Me total			R^2			
0	5.3	1881.2	955.1	4.958	2.511	0.000	0.000	0.000	k_{Ni}	0.023	0.972			
1	4.87	1381.3	719.2	3.641	1.891	-0.059	-0.030	-0.079	k_{Co}	0.012	0.980			
5	6.41	662	388.7	1.745	1.022	-0.150	-0.075	-0.203	k_{Me}	0.033	0.980			
10	7.61	2.92	4.93	0.008	0.013	-0.241	-0.129	-0.343						
15.5	12.24	0.54	0.23	0.001	0.001	-0.241	-0.129	-0.344						

												r	1	mm
												G	1	l/min
												h	0.37	m
												V	0.75	l
												v_{inf}	0.101026	
												n	3978.874	
												A_b	0.04578	
												k	0.033	
												$k_{L\ exp}$	0.000541	
												$k_{L\ theo}$	0.000358	

second run						ln ((18.18+Ct)/(18.18+Co))								
time [min]	pH	[Ni] ppm	[Co] ppm	Ni kg/m^3	Co kg/m^3	Ni	Co	Me total			R^2			
0	6.78	1917.2	989.2	5.053	2.601	0.000	0.000	0.000	k_{Ni}	0.020	0.985			
1	5.11	1664.2	865.4	4.386	2.275	-0.029	-0.016	-0.039	k_{Co}	0.010	0.993			
5	6.15	893.3	547.3	2.354	1.439	-0.123	-0.058	-0.162	k_{Me}	0.027	0.991			
10	6.58	324	232.2	0.854	0.610	-0.199	-0.101	-0.274						
16	10.96	0.19	0.54	0.001	0.001	-0.245	-0.134	-0.351						

												r	0.86781	mm
												G	1	l/min
												h	0.37	m
												V	0.75	l
												v_{inf}	0.094112	
												n	6088.155	
												A_b	0.056629	
												k	0.027	
												$k_{L\ exp}$	0.000358	
												$k_{L\ theo}$	0.000358	@ r = 1

third run						ln ((18.18+Ct)/(18.18+Co))								
time [min]	pH	[Ni] ppm	[Co] ppm	Ni kg/m^3	Co kg/m^3	Ni	Co	Me total			R^2			
0	5.44	2084.2	996	5.493	2.618	0.000	0.000	0.000	k_{Ni}	0.015	0.972	r	1.096847	mm
2	3.43	1601.7	789.3	4.221	2.075	-0.055	-0.026	-0.072	k_{Co}	0.006	0.943	G	1	l/min
5	3.39	1402.2	737.3	3.696	1.938	-0.079	-0.033	-0.099	k_{Me}	0.019	0.968	h	0.37	m
10	3.35	754.5	507.6	1.989	1.334	-0.160	-0.064	-0.201				V	0.75	l
30	3.16	158	161.7	0.416	0.425	-0.241	-0.111	-0.324				v_{inf}	0.105805	
												n	3015.244	
												A_b	0.039853	
												k	0.019	
												$k_{L\ exp}$	0.000358	
												$k_{L\ theo}$	0.000358	@ r = 1

fourth run						ln ((18.18+Ct)/(18.18+Co))								
time [min]	pH	[Ni] ppm	[Co] ppm	Ni kg/m^3	Co kg/m^3	Ni	Co	Me total			R^2			
0	7	1935	979	5.100	2.574	0.000	0.000	0.000	k_{Ni}	0.016	0.981	r	1.022424	mm
3	6.55	1371.8	722.2	3.616	1.899	-0.066	-0.033	-0.087	k_{Co}	0.007	0.956	G	1	l/min
6	6.88	975.3	589.3	2.571	1.549	-0.115	-0.051	-0.148	k_{Me}	0.021	0.978	h	0.37	m
10	6.94	602.2	449.7	1.587	1.182	-0.164	-0.069	-0.210				V	0.75	l
30	6.92	48.8	54.9	0.129	0.144	-0.240	-0.124	-0.337				v_{inf}	0.102153	
60	6.92	8.64	9.29	0.023	0.024	-0.246	-0.131	-0.350				n	3722.776	
												A_b	0.044282	
												k	0.021	
												$k_{L\ exp}$	0.000356	
												$k_{L\ theo}$	0.000356	

fifth (and final) run						ln ((18.18+Ct)/(18.18+Co))							r	0.913527	mm
time [min]	pH	[Ni] ppm	[Co] ppm	Ni kg/m^3	Co kg/m^3	Ni	Co	Me total			R^2		G	1	l/min
0	5.48	2051.4	1009.7	5.407	2.654	0.000	0.000	0.000	k_{Ni}	0.019	0.997		h	0.37	m
1	4.62	1838.2	921.5	4.845	2.423	-0.024	-0.011	-0.031	k_{Co}	0.009	0.992		V	0.75	l
5	6.15	1162.3	621.1	3.063	1.633	-0.105	-0.050	-0.137	k_{Me}	0.025	0.997		v_{inf}	0.09656	
10	7.36	495.1	361	1.305	0.949	-0.191	-0.085	-0.250					n	5219.11	
15	7.18	273.3	213.1	0.720	0.560	-0.222	-0.106	-0.299					A_b	0.052432	
30	7.12	70.3	70.4	0.185	0.185	-0.250	-0.126	-0.347					k	0.025	
60	7.19	4.2	3.4	0.011	0.009	-0.260	-0.136	-0.366					$k_{L\,exp}$	0.000358	
													$k_{L\,theo}$	0.000358	@ r = 1

INTEGRATED RATE LAW

RUN 1

ln[Ni]	ln[Co]	ln[Me]
-2.47	-3.16	-2.06
-2.78	-3.44	-2.36
-3.52	-4.05	-3.06
-8.94	-8.42	-7.95
-10.63	-11.49	-10.27

RUN 2

ln[Ni]	ln[Co]	ln[Me]
-2.45	-3.12	-2.04
-2.59	-3.25	-2.18
-3.22	-3.71	-2.74
-4.23	-4.57	-3.69
-11.67	-10.63	-10.33

RUN 3

ln[Ni]	ln[Co]	ln[Me]
-2.37	-3.11	-1.98
-2.63	-3.35	-2.23
-2.77	-3.41	-2.34
-3.38	-3.79	-2.87
-4.95	-4.93	-4.25

RUN 4

ln[Ni]	ln[Co]	ln[Me]
-2.44	-3.13	-2.04
-2.79	-3.44	-2.37
-3.13	-3.64	-2.66
-3.61	-3.91	-3.06
-6.12	-6.01	-5.37
-7.85	-7.79	-7.13

RUN 5

ln[Ni]	ln[Co]	ln[Me]
-2.38	-3.10	-1.99
-2.49	-3.19	-2.09
-2.95	-3.59	-2.53
-3.81	-4.13	-3.26
-4.40	-4.66	-3.83
-5.76	-5.76	-5.07
-8.58	-8.79	-7.99

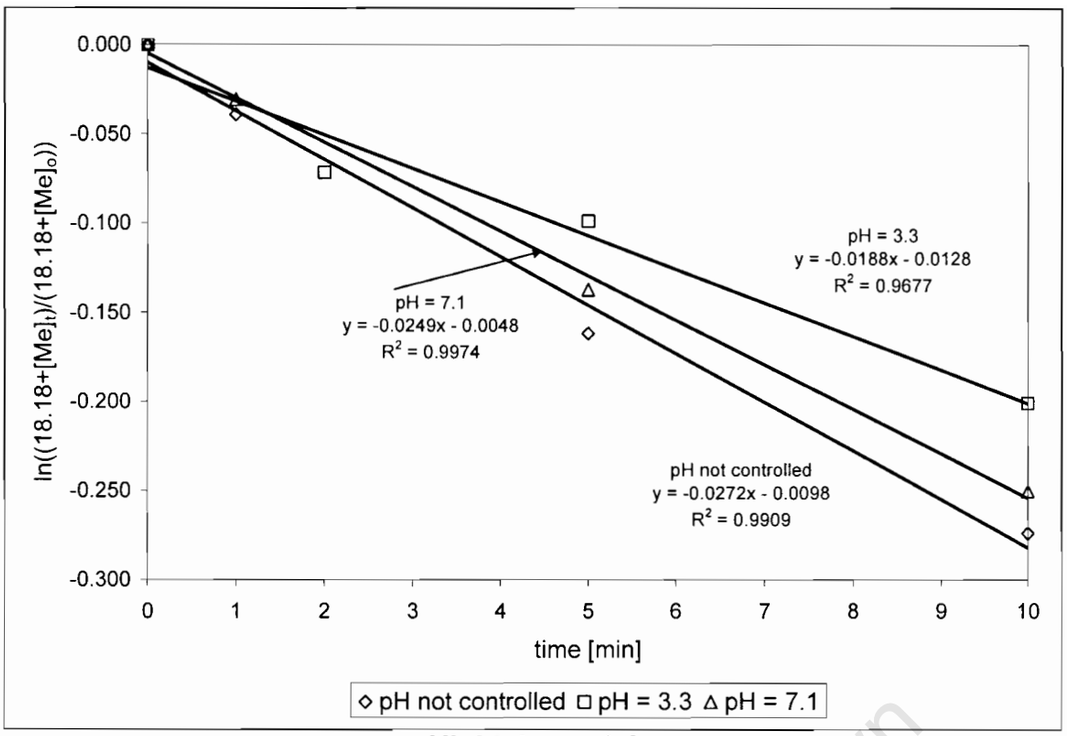

Higbie's model

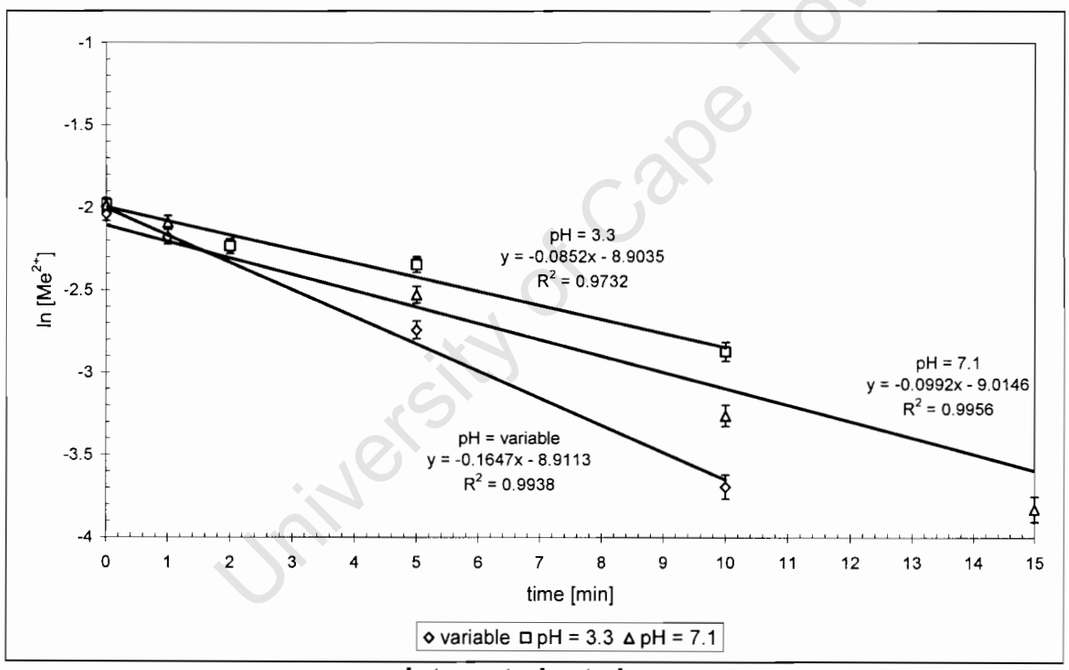

Integrated rate law

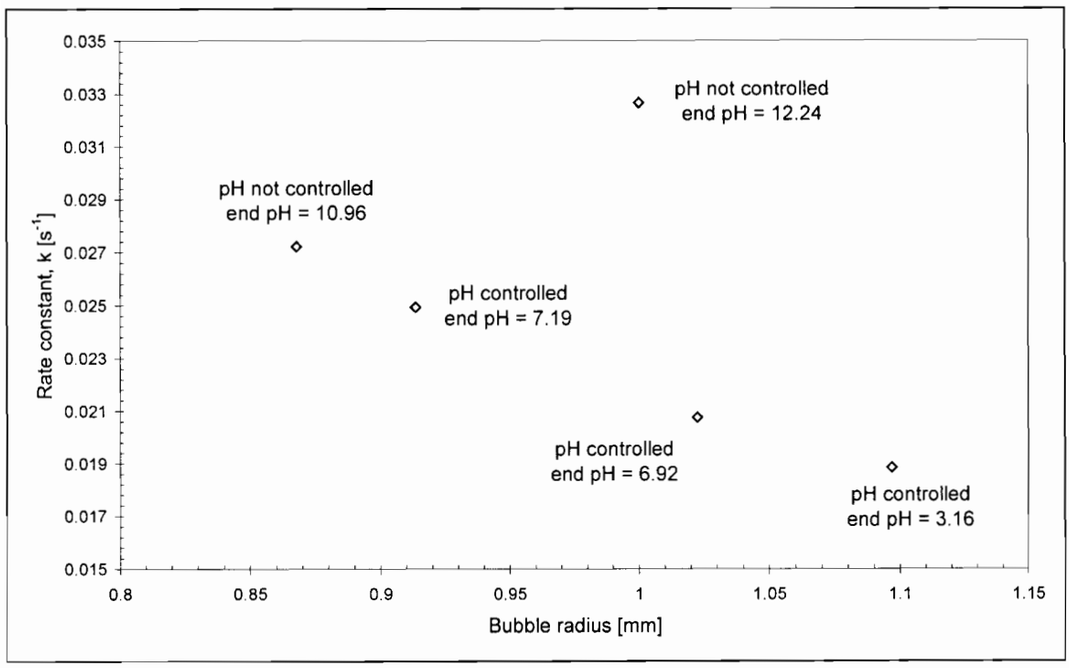

APPENDIX 3: Settling rates

NaOH precipitate

time (min)	*volume (ml)*		*ratio h_t/h_o*	
	Ni	Co	Ni	Co
0	610	440	1.00	1.00
1	600	400	0.98	0.91
2	580	370	0.95	0.84
5	550	290	0.90	0.66
11	500	230	0.82	0.52
30	400	170	0.66	0.39
60	310	130	0.51	0.30
128	240	98	0.39	0.22
242	180	76	0.30	0.17
302	170	72	0.28	0.16
1266	70	58	0.11	0.13

Na_2CO_3 precipitate

time (min)	*volume (ml)*		*ratio h_t/h_o*	
	Ni	Co	Ni	Co
0	430	350	1.00	1.00
1	430	325	1.00	0.93
2.00	420	315	0.98	0.90
6	405	280	0.94	0.80
11	400	250	0.93	0.71
36	355	170	0.83	0.49
67	325	130	0.76	0.37
129	275	110	0.64	0.31
242	220	94	0.51	0.27
300	205	88	0.48	0.25
1284	130	68	0.30	0.19

Na_2S precipitate

time (min)	*volume (ml)*		*ratio h_t/h_o*	
	Ni	Co	Ni	Co
0	440	350	1.00	1.00
1	440	350	1.00	1.00
2	440	350	1.00	1.00
5	440	350	1.00	1.00
10	440	350	1.00	1.00
126	440	40	1.00	0.11
250	54	36	0.12	0.10
318	52	34	0.12	0.10
1261	48	32	0.11	0.09

H_2S precipitate		
time (min)	***volume (ml)*** Ni/Co co-precipitate	***ratio h_t/h_o*** Ni/Co
0	880	1.00
1	820	0.93
5.17	700	0.80
10	600	0.68
40	410	0.47
82	340	0.39
130	310	0.35

Supernatant concentrations

filtered samples

NaOH precipitate			**Na_2CO_3 precipitate**			**Na_2S precipitate**		
time (min)	*conc (ppm)*		*time (min)*	*conc (ppm)*		*time (min)*	*conc (ppm)*	
	Ni	Co		Ni	Co		Ni	Co
0	2003	1004	0	2006	1005	0	2002	1004
60	0.24	2.9	242	186.81	128.8	250	6.79	16.17
242	2.07	1.8	1284	187.63	90.4	1261	15.72	18.7
1266	0.5	3.2						

unfiltered samples

NaOH precipitate			**Na_2CO_3 precipitate**			**Na_2S precipitate**		
time (min)	*conc (ppm)*		*time (min)*	*conc (ppm)*		*time (min)*	*conc (ppm)*	
	Ni	Co		Ni	Co		Ni	Co
0	2003	1004	0	2006	1005	0	2002	1004
60	0.75	5.4	242	264	203.9	250	15.61	19.33
242	4.11	1.7	1284	209.37	100.3	1261	8.63	25.15

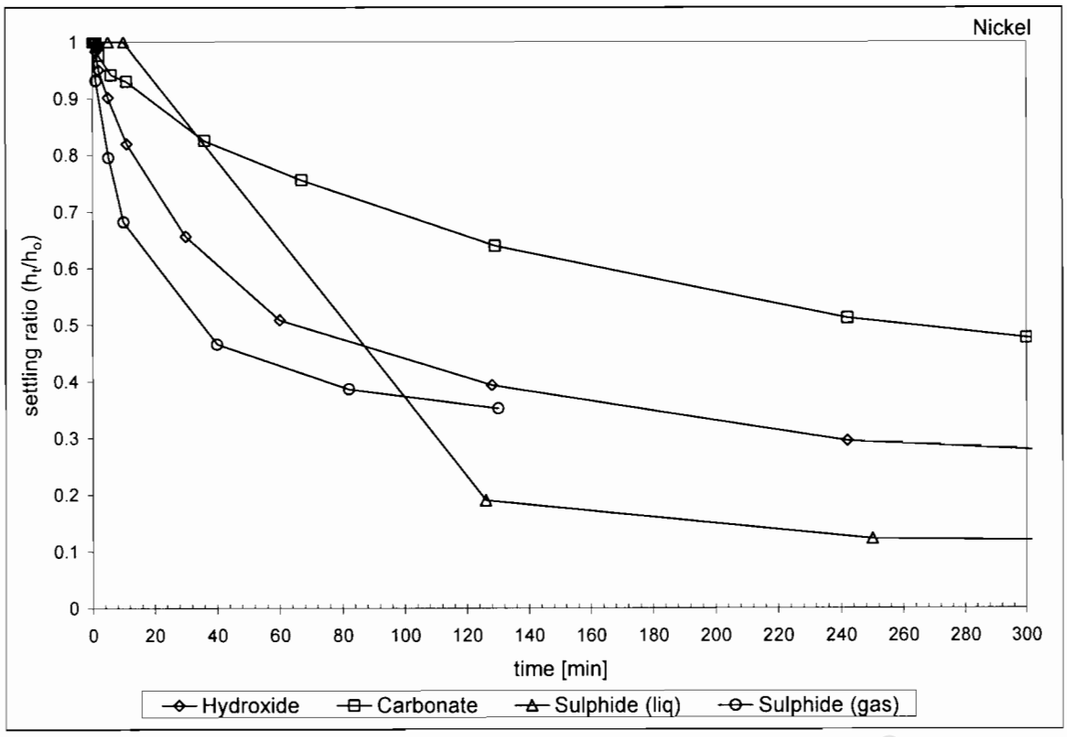

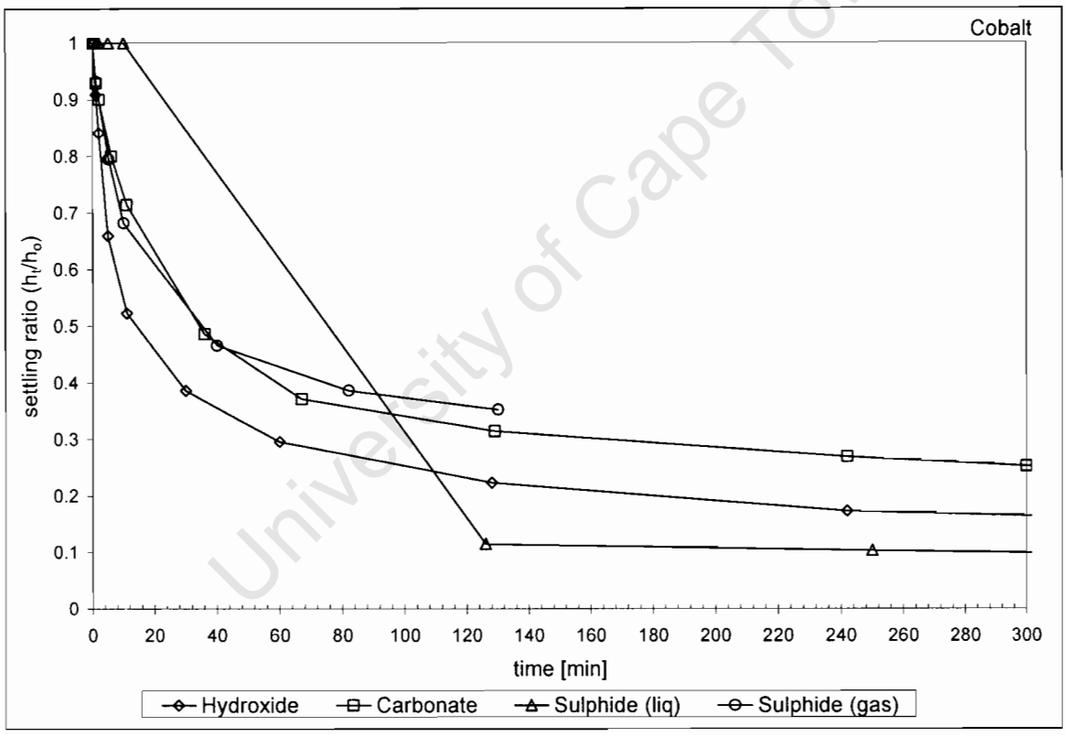

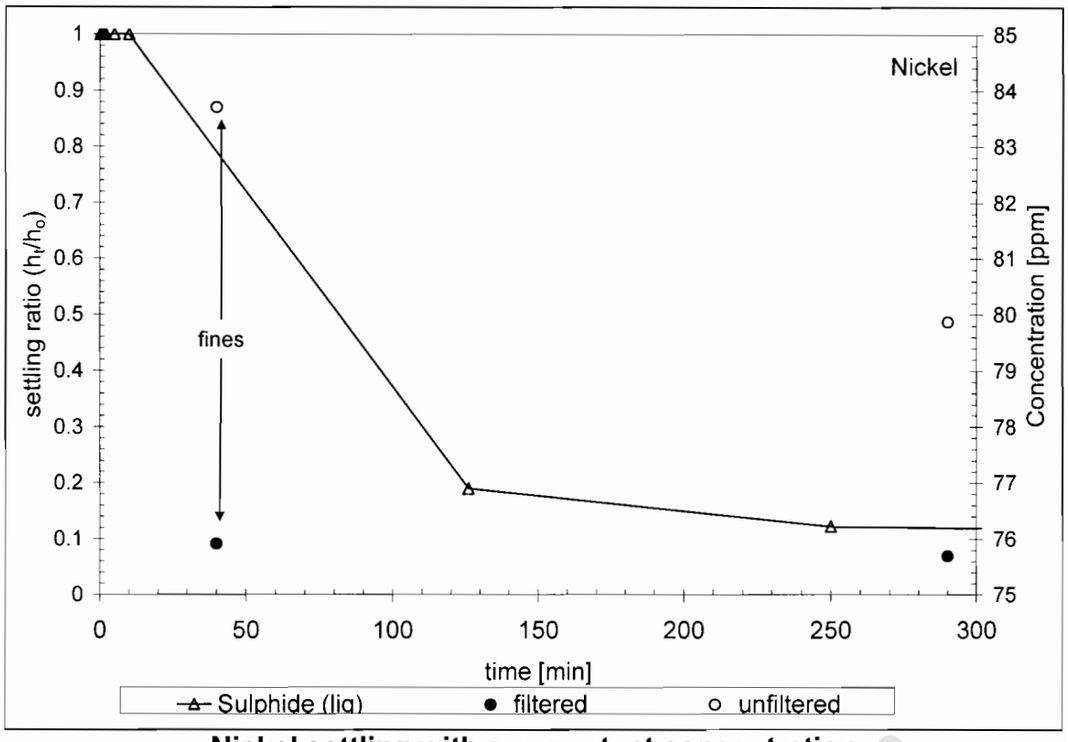

Nickel settling with supernatant concentration

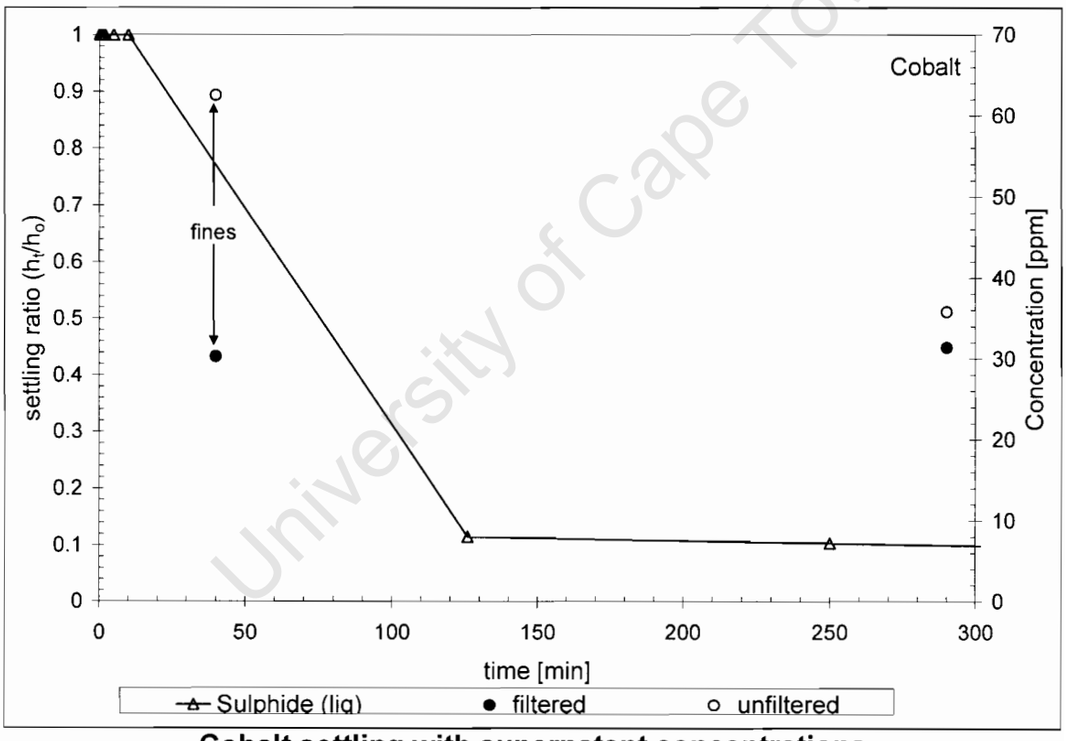

Cobalt settling with supernatant concentrations